Fall 12-14-2011

Functional Analysis of Host Cell Proteins and Stress Responses that Inhibit West Nile Virus Infection

Sean C. Courtney

FUNCTIONAL ANALYSIS OF HOST CELL PROTEINS AND STRESS RESPONSES THAT INHIBIT WEST NILE VIRUS INFECTION

by

SEAN CHRISTOPHER COURTNEY

Under the direction of Margo A. Brinton

ABSTRACT

Resistance to flavivirus-induced disease is conferred by a single gene that encodes oligoadenylate synthetase (Oas) 1b (Oas1b). Oas1b is not a functional synthetase suggesting its anti-flavivirus mechanism is RNase L-independent and that it may be mediated by interactions with other host cell protein(s). A yeast two-hybrid screen was used to identify host cell binding partners of Oas1b. Candidate partners were confirmed by yeast co-transformation and co-immunoprecipitation analyses. Oxysterol binding protein-related 1L (ORP1L) and ATP binding cassette subfamily F 3 (ABCF3) were found to interact with Oas1b. RNAi knockdown studies suggested that ORP1L and ABCF3 form a tripartite complex with Oas1b that is critical for the flavivirus-induced disease resistance mechanism.

Stresses including oxidation, nutrient starvation, and viral infections often induce the formation of stress granules (SGs) in eukaryotic cells. In response to stress, eIF2α kinases phosphorylate eIF2α leading to stalled 48S pre-initiation complexes and SG formation. West Nile virus (WNV) Eg101 infections were previously shown not to induce the formation of SGs. Infections with viruses of other natural WNV strains, as well as a WNV lineage 1/2-based infectious clone (W956IC) were analyzed and only W956IC infections were found to induce SGs. eIF2α kinase knockout MEFs were used to show that the W956IC-induced SGs were PKR-dependent. WNV chimeras were made by inserting Eg101 genes into the W956IC backbone. Chimeras replacing NS5 or NS1 and NS5 or NS1 and NS3 and NS4a reduced SG formation as well as early viral RNA synthesis similar to Eg101 infections. W956IC infections but not Eg101 infections were shown to produce exposed viral dsRNA at early times after infection. The data suggest that natural WNV infections evade the cell SG response by suppressing the amplification of viral RNA until cytoplasmic membranes have been remodeled to protect replication complexes from detection.

It was previously reported that WNV Eg101 infections inhibited the formation of arsenite-induced SGs. The ability of other natural WNV strain infections to inhibit SG formation by arsenite (HRI), DTT (PERK), W956IC co-infection (PKR), and heat shock treatments was assessed. WNV infections only inhibited arsenite-induced SG formation suggesting that WNV infections specifically suppress the response to oxidative intermediates.

INDEX WORDS: West Nile virus, 2′-5′ Oligoadenylate synthetase 1b (Oas1b), Oxysterol binding protein-related protein 1L (ORP1L), ATP binding cassette subfamily F 3 (ABCF3), Small hairpin RNA (shRNA), Stress granule, eIF2α, PKR, Chimera.

FUNCTIONAL ANALYSIS OF HOST CELL PROTEINS AND STRESS RESPONSES THAT INHIBIT WEST NILE VIRUS INFECTION

by

SEAN CHRISTOPHER COURTNEY

A Dissertation Submitted in Partial Fulfillment of the Requirements for the Degree of

Doctor of Philosophy

in the College of Arts and Sciences

Georgia State University

2011

FUNCTIONAL ANALYSIS OF HOST CELL PROTEINS AND STRESS RESPONSES THAT INHIBIT WEST NILE VIRUS INFECTION

by

SEAN CHRISTOPHER COURTNEY

Committee Chair: Margo A. Brinton

Committee: John Houghton

Irene Weber

Electronic Version Approved:

Office of Graduate Studies

College of Arts and Sciences

Georgia State University

December 2011

DEDICATION

I dedicate this dissertation to my family and loved ones. To my parents, Chris and Donna Courtney, who have always pushed me to work hard and never give up in order to achieve my life goals. With your unconditional love you have always provided me the environment, opportunity and passion to be the best at anything I attempt. To my sister Jill and her family, Jason, Taylor and Brooks, I want to thank you all for always finding a way to make me laugh. You all bring so much joy to my heart. To my dearest friends, Montez Bynum and Ryan Butts, you have both been integral to my journey and I love you each dearly. Thank you all for being there for me when times were tough and always finding a way to keep me focused. Without every one of you none of this would have been possible and I want to personally thank you each of you because your support has been truly amazing. I love you all.

"Some people drink from the fountain of knowledge...others just gargle."

~Robert Anthony

"Stay thirsty my friends!"

~The Most Interesting Man in the World (Dos Equis)

ACKNOWLEDGEMENTS

I would like to extend my sincerest gratitude to my principle advisor, Dr. Margo A. Brinton. Thank you for the experiences you have provided me within this lab, along with your support, patience, expert advice and trust. I would also like to thank my committee members Dr. John Houghton and Dr. Irene Weber for your skillful assistance and knowledgeable suggestions. The three of you have given me the utmost confidence to succeed as a scientist. I would especially like to thank Dr. Svetlana Scherbik for all of her assistance and patience, but even more for her great friendship. Lastly, I would like to thank all of the members of the Brinton lab, past and present, for all of their support and camaraderie through the years.

TABLE OF CONTENTS

LIST OF TABLES

LIST OF FIGURES

LIST OF ABREVIATIONS

Dengue virus (DEN)

Yellow fever virus (YFV)

Japanese encephalitis virus (JEV)

West Nile virus (WNV)

Sindbis virus (SinV)

Vesicular stomatitis virus (VSV)

Open Reading Frame (ORF)

Endoplasmic Reticulum (ER)

Envelope (E)

Membrane (prM, M)

Capsid (C)

Nonstructural Protein (NS)

RNA-binding domain (RBD)

Virus-like particles (VLPs)

Interferon (IFN)

Nucleoside triphosphatase (NTPase)

RNA triphospatase (RTPase)

Methyltransferase (MTase)

RNA-dependent RNA polymerase (RdRp)

Oligoadenylate synthetase (OAS)

Oligoadenylate synthetase 1b (Oas1b)

Truncated Oas1b (Oas1bt)

Oas1b with a deletion of the C-terminal Transmembrane domain (Oas1bΔTM)

Oxysterol binding protein-related protein 1L (Orp1L)

ATP binding cassette (ABC)

ATP binding cassette subfamily F 3 (Abcf3)

Mouse embryofibroblasts (MEFs)

Baby Hampster Kidney (BHK)

Viral RNA (vRNA)

Multiplicity of infection (MOI)

Late endosomes (LEs)

Rab7-interacting lysosomal protein (RILP)

Vesicle associated membrane protein (VAMP)-associated protein (VAP-A)

Eukaryotic translation initiation factor 2α (eIF2α)

Protein Kinase R (PKR)

PKR-like ER-associated eIF2α kinase (PERK)

Heme-regulated initiation factor 2α (HRI)

General control nondepressible 2 (GCN2)

T cell intracellular antigen 1 (TIA-1)

TIA-1-related (TIAR)

Ras GAP SH3 domain binding protein (G3BP)

Stress granules (SGs)

Processing bodies (PBs)

Internal ribosome entry site (IRES)

Double-strand RNA (dsRNA)

Lineage 2/1-based WNV infectious clone virus (W956IC)

2-Aminopurine (2-AP)

Pathogen recognition receptor (PRR)

CHAPTER 1

INTRODUCTION

Classification and Clinical Significance of Flaviviruses

The family *Flaviviridae* contains three genera, *Flavivirus*, *Pestivirus,* and *Hepacivirus*, and the unclassified hepatitis G viruses. The genus *Flavivirus* consists of about 60 viruses and includes human pathogens such as dengue virus (DEN), yellow fever virus (YFV), Japanese encephalitis virus (JEV), and West Nile virus (WNV) (Lindenbach, 2007). West Nile virus was first isolated in Uganda in 1937 and the majority of the more than 70 strains have been classified into two distinct lineages based on sequence homology. Lineage 1 WNV strains are endemic in northern Africa, Europe, India, the Middle East, Asia and North America, while lineage 2 WNV strains are typically found in sub-Saharan Africa (Bakonyi et al., 2006; Hayes et al., 2005; Knipe, 2007; Lanciotti et al., 2002). As of late 2006, the Centers for Disease Control (CDC) had reported over 23,000 cases of human WNV infection within the United States (Sejvar, 2007).

WNV is arthropod-borne and its transmission cycle in nature is usually between *Culex* mosquito species and birds; however, transmission of WNV to horses and humans by mosquitoes occurs occasionally (Brinton, 2002). WNV infectious particles present in the salivary glands of infected mosquitoes are transmitted to vertebrate hosts during a blood meal. Initially, the virus replicates at the site of infection and then moves to the regional lymph nodes. Once in the lymph nodes, the virus can disseminate into the vascular system, spread to peripheral organs and in some cases, cross the blood brain barrier. WNV is part of the Japanese encephalitis serocomplex and is known to attack the central nervous system, particularly the medulla of the brainstem (Brinton, 2002). WNV infection usually produces asymptomatic or mild disease with symptoms that can include fever, headache, body rash, muscle fatigue, and disorientation (Brinton, 2002).

About 1 in 150 or fewer infected individuals develop more severe diseases such as encephalitis, hepatitis and polio-like syndromes (Brinton, 2002). The infection usually clears within about 3-6 days; however, about 10% of those with severe illness can have a fatal outcome with older and immunocompromised individuals having a higher incidence of mortality.

Flavivirus Replication Cycle

WNV replicates in a wide range of cell cultures including primary chicken, duck, and mouse embryo cells and continuous cell lines from monkeys, humans, pigs, rodents, amphibians, and insects (Brinton, 1986). The life cycle of flaviviruses occurs entirely within the cytoplasm of infected cells (Figure 1.1). Entry of the virion into cells is mediated through the interaction of the E protein with an unknown receptor(s). The virion is endocytosed at clatherin-coated pits, transported to prelysosomal vesicles, and low pH-induced fusion of the virion and vesicle releases the viral nucleocapsid (Chu et al., 2006; Chu and Ng, 2004; Heinz and Allison, 2000; Heinz et al., 2004). After release, the viral genome acts as a messenger RNA (mRNA) and immediately begins translation of the single open reading frame (ORF) to produce the viral polyprotein. The viral polyprotein is cleaved co- and post-translationally by both cellular and viral proteases (Lindenbach, 2007). Replication of the viral genome occurs within vesicular invaginations of the ER membrane that open to the cytoplasm through a small pore (Kim et al., 2004; Welsch et al., 2009). The nascent viral genomic RNA exits these vesicle structures and is either translated by neighboring ribosomes or bound to capsid proteins attached to opposing ER membrane which also contain viral envelope (E) and membrane (prM) proteins. The capsid protein encapsidates the viral genome and produces the immature virion within the lumen of the ER (Welsch et al., 2009). Immature virions traverse the ER and trans-Golgi network,

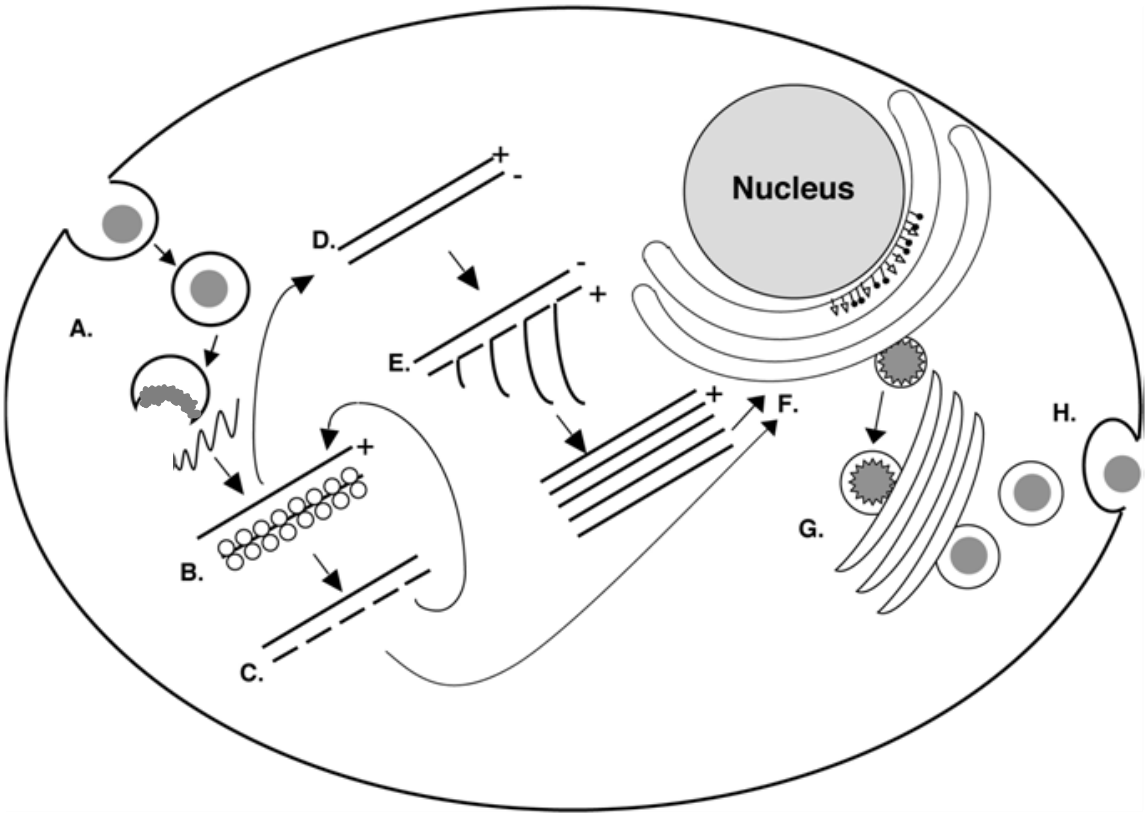

Figure 1.1. Flavivirus Replication Cycle. (A) Virion attachment, entry, and fusion and uncoating of the viral genome RNA. **(B)** Translation of the viral RNA. **(C)** Proteolytic processing of the viral polyprotein into the individual viral proteins. **D)** Synthesis of the complementary viral minus strand RNA. **(E)** Synthesis of the genome RNA from the template minus strand RNA. **(F)** Encapsidation and assembly of immature virions in the ER. **(G)** Processing of prM to M to produce mature virions in the trans-Golgi network. **(H)** Fusion of virion-containing vesicles and the plasma membrane resulting in release of infectious virus particles from the cell. Modified figure and legend adapted from (Brinton, 2008).

concurrently maturing via the cleavage of prM to M (Plevka et al., 2011). Mature virions are approximately 50 nm in diameter, spherical and enveloped. WNV virions are transported in vesicles to the plasma membrane and released by fusion of the vesicle with the plasma membrane (Brinton, 2002).

Flavivirus Genome

The flavivirus genome is a positive-sense, single-strand RNA (+ssRNA) with a capped 5' end but no 3' poly (A) tail. Flavivirus genomes are unique among mammalian positive-sense RNA viruses in the lack of a 3' poly (A) tail (Brinton, 2002). The flavivirus genome is about 11 kb in length and contains one open reading frame that encodes three N-terminally located viral structural proteins, capsid (C), membrane (prM/M), and envelope (E), followed by seven C-terminal nonstructural proteins, NS1, NS2a, NS2b, NS3, NS4a, NS4b, and NS5 (Figure 1.2) (Brinton, 2002). The ten mature viral proteins are generated via proteolytic processing of the polyprotein by both viral and cellular proteases (Brinton, 2002). The majority of the nonstructural proteins are multi-functional and all seven appear to be involved in viral RNA synthesis (Brinton, 2002; Mackenzie et al., 1996).

Structural Proteins

WNV virions are ~50 nm in diameter, spherical and enveloped. They are made up of three structural proteins: E, prM/M and capsid (C). The E and M proteins compose the exterior surface of the virion (Lindenbach, 2007). The E glycoprotein is required for receptor recognition and fusion of the virion for entry into cells; however, the cellular protein used as the WNV entry receptor has yet to be determined. Immature virions have trimers of prM and E heterodimers on

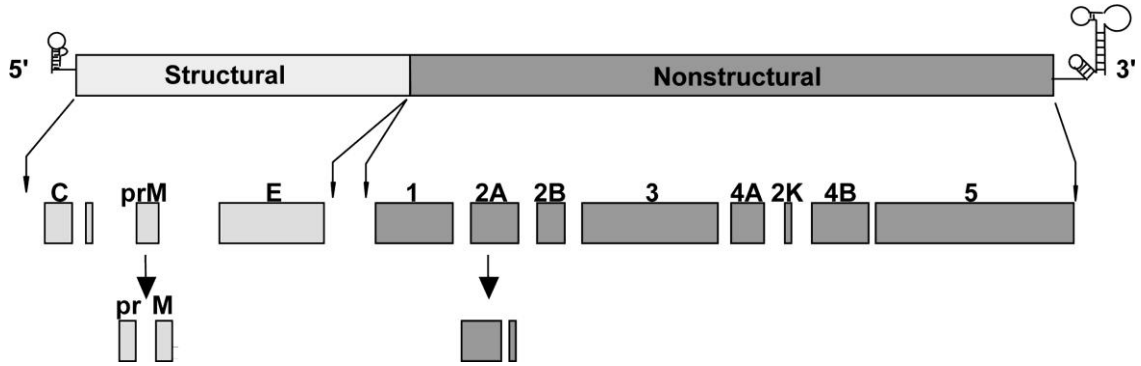

Figure 1.2. Schematic representation of the WNV polyprotein. The WNV genome is translated into a single polyprotein that is processed co- and post-translationally by both host and viral proteases into 10 viral proteins. Three structural proteins (E, prM/M, and C) are encoded in the N-terminus while seven nonstructural proteins (NS1, NS2a, NS2b, NS3, NS4a, NS4b, and NS5) are encoded in the C-terminus. Figure and modified legend adapted from (Brinton, 2002).

their surface that create spikes. The M protein is cleaved from prM by the host protease furin in the trans-Golgi network, which leads to a conformational change and rearrangement of the E proteins so that they lie flat against the envelope and form an icosahedrom shell on the outside of the virion (Kuhn et al., 2002).

The mature virion particles that contain a smooth surface with icosahedral symmetry made up of 90 head-to-tail homodimers of E (Brinton, 2008; Kuhn et al., 2002). The virion capsid is about 30 nm in diameter and has no discernable geometric symmetry inside virions. RNA-binding domains (RBD) are found at both the N- and C-termini of the C protein and are separated by a hydrophobic domain that tethers the protein to the lipid bilayer membrane. Flavivirus-infected cells have been reported to release non-infectious virus-like particles (VLPs) that are composed of the E and M proteins but lack capsid and viral RNA (Ferlenghi et al., 2001; Takahashi et al., 2009). These data suggest that C dimers are essential for the recruitment of viral RNA for the formation of infectious virions; however, no encapsidation signal has yet been identified in the genome RNA (Brinton, 2008). The C dimers have very high net positive charges, suggesting that the interaction between C dimers and the viral genomic RNA is nonspecific.

Viral Nonstructural Proteins (NS)

The WNV genome encodes seven nonstructural proteins, NS1, NS2a, NS2b, NS3, NS4a, NS4b and NS5. Each of these viral nonstructural proteins is suggested to be required for replication of the viral genome; however, the precise function(s) of each of these proteins within viral replication complexes is not known.

The WNV NS1 protein is a ~46 kDa glycoprotein that localizes to the ER membrane and cell surface, and is secreted from infected cells (Avirutnan et al., 2011; Brinton, 2008; Falgout and Markoff, 1995; Smith and Wright, 1985; Somnuke et al., 2011; Wilson et al., 2008). A correlation between the levels of secreted NS1 in the blood and disease severity has been observed in a hamster model (Macdonald et al., 2005). Secreted NS1 proteins from different flavivirus members have been reported to attenuate the antimicrobial complement pathway by directly binding to various complement proteins including regulatory protein H, C4, C4b binding protein and C1s (Avirutnan et al., 2011; Chung et al., 2006; Somnuke et al., 2011). For example, NS1 binding to regulatory protein H inhibits complement activation and decreases the deposition of complement attack complexes on infected cells (Chung et al., 2006). Secreted NS1 has also recently been reported to inhibit the establishment of an antiviral state by blocking TLR3-mediated activation of IFN regulatory factor 3 and production of interleukin 6 (Wilson et al., 2008). The precise intracellular functions of NS1 are currently unknown; however, it has been suggested to be involved in virus replication and has been reported to co-localize with viral replication complexes, likely through interactions with NS4a (Lindenbach and Rice, 1999; Mackenzie et al., 1996). Studies delivering NS1 protein by trans-complementation resulted in the recovery of virus containing a defective yellow fever virus genome and the recovery of these trans-complemented viruses suggested a role for NS1 in the initial synthesis of the viral minus strand RNA (Lindenbach and Rice, 1997). The NS1 protein contains two or three N-linked glycosylation sites and studies have shown that there is a reduction in viral RNA synthesis when these sites are mutated (Muylaert et al., 1996). Within the Japanese encephalitis virus serogroup of flaviviruses, a longer NS1 protein, referred to as NS1′, is produced. NS1′ is suggested to form by the presence of a slippery sequence near the NS1-NS2a junction that causes a -1 ribosomal

frameshift to occur due to a downstream psuedoknot structure (Melian et al., 2010). NS1′ was suggested to function in viral neuroinvasion by studies showing that removal of the pseudoknot structure inhibited the production of NS1′ and mice subsequently injected intraperitoneally with the virus produced greater than 80% survivial of encephalitis compared to mice injected with wildtype virus (Melian et al., 2010).

Infected cells contain both a ~22 kDa full length NS2a protein and a C-terminally truncated ~20 kDa protein (Chambers et al., 1990a; Nestorowicz et al., 1994). Again, the precise function(s) of NS2a in flavivirus replication is unknown but it is suggested to be a transmembrane protein that is involved in virus assembly and has been reported to localize with replication complexes and interact with NS3, NS5 and the 3′ UTR (Kummerer and Rice, 2002; Lindenbach, 2007; Mackenzie et al., 1998). NS2a was also shown to act as a suppressor of interferon-β (IFN-β) signaling when it was exogenously expressed in cells infected with Newcastle disease virus (NDV) and rescued the replication of the IFN-sensitive NDV (Munoz-Jordan et al., 2003). The ~14 kDa NS2b protein is also membrane associated. Currently, NS2b has only been identified as a cofactor of NS3 required for viral polyprotein processing (Lindenbach, 2007). Both NS2a and NS2b are suggested to be transmembrane proteins that aid in anchoring the soluble viral NS3 protease to the replication complex.

The ~70 kDa flaviviral NS3 protein possesses numerous enzymatic functions. NS3 functions as the viral serine protease and this activity is contained within an N-terminal domain of NS3. NS2b functions as a cofactor for the NS3 protease activity (Bessaud et al., 2006; Chambers et al., 1990b; Miller et al., 2006). The NS2b-NS3 protease complex cleaves the NS2a/2b, NS2b/NS3, NS3/NS4a, and NS4b/NS5 junctions of the viral polyprotein (Assenberg et al., 2009; Brinton, 2008; Lindenbach, 2007). The remainder of the NS3 sequence contains

homologies to RNA helicase, nucleoside triphosphatase (NTPase), and RNA triphosphatase (RTPase) motifs. The RNA helicase domain is a supergroup 2 RNA helicase (Gorbalenya et al., 1989) and is proposed to hydrolyze ATP to unwind the secondary structures of the viral RNA (Wengler, 1991, 1993). Mutational studies specifically abolishing the RNA helicase activity of NS3 further confirmed the necessity of the functionality of this domain for virus growth (Matusan et al., 2001). The C-terminal RTPase domain is proposed to dephosphorylate the 5′ end of the genome to allow capping (Wengler, 1993). When overexpressed alone, the flavivirus NS3 protein induces apoptosis in a pathway involving both caspases-8 and -3; however, this is not the case during an infection. NS3 also contains the main antigenic peptide determinant of MHC class-II molecules important for the antiviral CD8+ cytotoxic T cell response (Lobigs et al., 1994; Ramanathan et al., 2006).

NS4a (~16 kDa) and NS4b (~27 kDa) are both small hydrophobic proteins and are connected by a 2K peptide. The precise function(s) of these proteins in viral replication is currently unknown but both have been shown to colocalize with the viral replication complexes (Mackenzie et al., 1998; Miller et al., 2006). The 2K peptide is removed by both host and viral proteases and a mutation at the 9^{th} residue (Val to Met) of the 2K peptide has been reported to confer resistance to lycorine, a flavivirus inhibitor, as well as rescuing viral growth in Oas1b-expressing cells (Mertens et al., 2010; Zou et al., 2009). It has been reported that the cleavage of the 2K peptide is an important step for membrane rearrangement, likely essential for replication complex formation (Miller et al., 2007; Roosendaal et al., 2006). Overexpression of recombinant NS4a protein alone was shown to induce membrane rearrangement that slightly differed from virus-induced membrane rearrangements, suggesting that NS4a is the main viral protein involved in this function but other cell factors may also be involved in inducing membrane rearrangement

during flavivirus infections (Roosendaal et al., 2006). Similar to NS2a, NS4a and NS4b were both shown to act as IFN signaling antagonists, with NS4b being the most suppressive (Munoz-Jordan et al., 2005; Munoz-Jordan et al., 2003). In addition, the co-expression of NS2a, NS4a and NS4b was shown to completely inhibit IFN signaling (Munoz-Jordan et al., 2003).

NS5 is the largest flavivirus nonstructural protein (~103 kDa) and is also multifunctional, containing both methyltransferase (MTase) and RNA-dependent RNA polymerase (RdRp) activities. The N-terminus of NS5 contains extensive sequence homology to S-adenosyl-methionine (SAM)-dependent MTases (Koonin, 1993). *In vitro* studies confirmed the MTase activity by demonstrating that a purified MTase domain of NS5 could transfer methyl groups from SAM to RNA substrates (Egloff et al., 2002). Mutagenesis studies showed that the MTase activity was essential for flavivirus replication (Hanley et al., 2002). The RdRp of flaviviruses is structurally similar to the RdRps of many other positive-strand RNA viruses (Brinton, 2008; Koonin, 1991; Malet et al., 2007; Rice et al., 1985). Mutating amino acids in the highly conserved GDD motif of the NS5 RdRp completely ablates RNA synthesis activity, confirming the requirement of an intact RdRp domain for viral RNA replication (Kim et al., 2007). Other functions have been identified for NS5 in addition to the MTase and RdRp activities. NS5 contains two nuclear localization signals and has been reported to localize NS5 to the nucleus of infected cells depending on its phosphorylation status (Pryor et al., 2007). However, NS5 nuclear localization has been shown to vary depending on cell type and virus strain. The mechanism controlling NS5's nuclear localization is unknown but it has been suggested to be involved in regulating virus production as well as in mediating the antiviral response to infection by regulating IL-8 production (Pryor et al., 2007). Similar to the NS2a, NS4a and NS4b, NS5 was also shown to interfere with IFN signaling by binding to the intracellular side of IFN receptor

complexes and inhibit the phosphorylation of downstream effector molecules, such as STAT1 (Best et al., 2005).

Host Genetic Resistance/Susceptibility to Virus-Induced Disease

Viruses are intracellular pathogens that must intimately interact with a host cell to replicate. This interaction between host and virus is typically parasitic since viruses use host cell machinery for synthesis of their products. This relationship is usually detrimental to the host when a virus first infects a previously uninfected species. Viruses typically co-evolve with their host over time and it is likely that many of the host species populations currently resistant to a particular virus infection were selected due to virus-induced morbidity or mortality over time. The interactions between host and virus are complex, commonly involving both the innate and adaptive immune responses. However, resistance or susceptibility to virus-induced diseases can sometimes be controlled by a single gene. There have been approximately 30 examples of this phenomenon identified to occur naturally in mice and a few identified in humans (Lee et al., 2003). Resistance genes are first identified when individuals of a given host species vary in their response to infection with a single virus or members of a virus family. Mapping analyses are subsequently used to identify the chromosome and then the gene(s) associated with the disease response phenotype. There are three main stages of a virus infection at which host resistance mechanisms have been shown to function: entry of viruses, intracellular stages of virus replication, or recognition and destruction of infected cells by immune cells (Lee et al., 2003).

Genetic Resistance due to Blocking Viral Entry

Host resistance to virus-induced disease is most commonly observed to occur at the stage of virus entry into the cell and defines viral tropism. Examples of viruses for which this has been shown to be the case are mouse hepatitis virus (MHV) and human immunodeficiency virus (HIV) (Lee et al., 2003). Disease resistance to MHV is conferred by variation in *Caecam1*, the MHV receptor. CEACAM1a is expressed in susceptible BALB/c mice while CAECAM1b is expressed in resistant SJL/J mice (Tan et al., 2002). Differences in susceptibility were determined to be due to a dramatic difference in MHV binding to these two receptors due to substitutions at six residues in an exposed loop of the amino-terminal immunoglobulin-like domain where the MHV spike proteins bind (Boyle et al., 1987; Dveksler et al., 1991; Ohtsuka et al., 1996; Rao et al., 1997). An example of genetic resistance to virus-induced disease in humans was observed during HIV-1 virus infections. Disease resistance is conferred in a subset of individuals that express a 32 bp deletion in their CCR5 gene. CCR5 is a co-receptor for M-tropic HIV-1 viruses (Berger et al., 1999; Dean et al., 1996; Liu et al., 1996; Samson et al., 1996; Zimmerman et al., 1997). Individuals homozygous for this deletion are completely resistant to M-tropic HIV-1 infections while heterozygous individuals display delayed progression to the onset of AIDS (Berger et al., 1999; Dean et al., 1996).

Genetic Resistance due to Intracellular Effectors

Other host genetic resistance mechanisms are mediated intracellularly during viral infections. Viruses that are affected by this type of genetic resistance include orthomyxoviruses (i.e. influenza A virus and Thogoto virus), vesicular stomatitis virus (VSV), murine leukemia virus and members of the genus Flavivirus (Lee et al., 2003). During influenza A virus

infections, disease resistance in A2G mice is mediated by the product of the *Mx1* dominant allele (Haller and Kochs, 2002; Kolb et al., 1992). Susceptible mice, such as CBA/J and BALB/c, do not express a functional Mx1 protein due to either a non-sense mutation or a large deletion within the allele, respectively (Staeheli et al., 1988). The Mx1 protein is classified as a GTPase, homologous to dynamin proteins and is localized within the cell nucleus. It was suggested that the Mx1 protein of mice confers resistance to influenza A virus infections by binding the viral polymerase and sequestering it to promyelocytic leukemia protein nuclear bodies, thereby inhibiting replication of the virus (Geoffroy and Chelbi-Alix, 2011; Haller and Kochs, 2002; Stranden et al., 1993). Mice also express an Mx2 protein that is localized to the cytoplasm. This protein has been shown to inhibit the replication of viruses such as Thogoto virus (Haller and Kochs, 2002). Mx2 proteins interact with Thogoto virus nucleocapsid proteins and prevent their translocation into the nucleus which is required for virus replication (Haller and Kochs, 2002). The human genome encodes MxA and MxB proteins. Only the MxA protein has been defined as having antiviral activity (Haller and Kochs, 2002). In contrast to the mouse Mx1 and Mx2 proteins that function in separate compartments of the cell, the antiviral activity of human MxA functions regardless of the intracellular location and affects numerous other viruses (Haller and Kochs, 2002).

Some inbred mouse strains show differential susceptibility to flavivirus-induced disease (Perelygin et al., 2002; Urosevic et al., 1999; Webster and Johnson, 1941). It was shown that an allele of a single gene, *Flv*, conferred differential susceptibility specific to flavivirus infection in mice and that resistance is inherited as a dominant Mendelian trait (Groschel and Koprowski, 1965; Sabin, 1952; Sangster et al., 1993; Sangster and Shellam, 1986). A positional cloning approach identified Oas1b as the Flv^r gene (Perelygin et al., 2002). When the resistant allele,

Flv^{r}, was subsequently "knocked in" to a susceptible mouse strain replacing the susceptible allele, *Flv*^{s}, the mice generated displayed the flavivirus resistance phenotype (Scherbik et al., 2007a). These results proved that resistance/susceptibility to flavivirus-induced disease is mediated by a single gene.

OAS proteins are upregulated by interferons that are produced in response to a viral stimulus (Sarkar and Sen, 2004). Typically, the antiviral activity of OAS proteins is mediated by the recognition of viral dsRNA during infection, which activates the OAS proteins to synthesize 2′-5′ linked oligo As (2-5 As) from ATP. The 2-5 As then activate latent RNase L to degrade viral or cellular ssRNA, thereby inhibiting infection (Figure 1.3). Eight duplicated copies of the Oas1 gene exist in mice (Oas1a-h) and are encoded in a 210 kb genomic region on chromosome 5; however, only Oas1a and Oas1g are functional synthetases (Kakuta et al., 2002). A full-length Oas1b protein is expressed by the *Flv*^{r} allele in resistant mice, while a truncated Oas1b protein is expressed in susceptible mouse strains from the *Flv*^{s} allele (Figure 1.4). The truncated form of Oas1b (Oas1bt) is the result of a premature stop codon produced by a C820T transition within the fourth exon, yielding a protein that is 30% shorter (Perelygin et al., 2002). Both the full-length and truncated Oas1b proteins have a four amino acid deletion in their N-terminal P-loop motif as well as a deletion in their C-terminal CFK motif. The CFK motif and the P-loop motif are critical for 2-5 OAS activity and the CFK motif is essential for multimerization.

Genetic Resistance due to Recognition and Destruction by Immune Cells

Alleles that confer disease resistance are sometimes involved in the recognition and removal of the virus by immune cells. Some examples of viruses that are susceptible to these alleles include Friend leukemia virus and murine cytomegalovirus (MCMV) (Britt and Chesebro,

1980; Farrell et al., 1997; Lee et al., 2003). In the case of MCMV, resistance is observed in C57BL/6 mice and is mediated by the product of the *Cmv1*^{r} allele, which encodes the Ly49H activating receptor expressed by natural killer (NK) cells that can recognize the MCMV m157 antigen expressed on the surface of infected cells and mediate their killing (Brown et al., 2001; Daniels et al., 2001; Lee et al., 2001). This is in contrast to susceptible DBA/2 mice that possess the *Cmv1*^{s} allele that does not encode the Ly49H receptor, but instead encodes the Ly49I inhibitory receptor on NK cells that also recognizes and binds to m157 but does not result in infected cell killing by NK cells (Arase et al., 2002). The m157 antigen mimics MHC class I molecules and are recognized by Ly49I leading to inhibitory signaling that downregulates MHC class I expression in infected cells (Adams et al., 2007). Due to these differences, resistant mice are able to control the infection by removing the MCMV-infected cells through NK cell mediated killing, whereas susceptible mice are unable to efficiently activate their NK cell response to stop the MCMV infection, resulting in higher viral titers in infected mouse tissues (Scalzo et al., 1990).

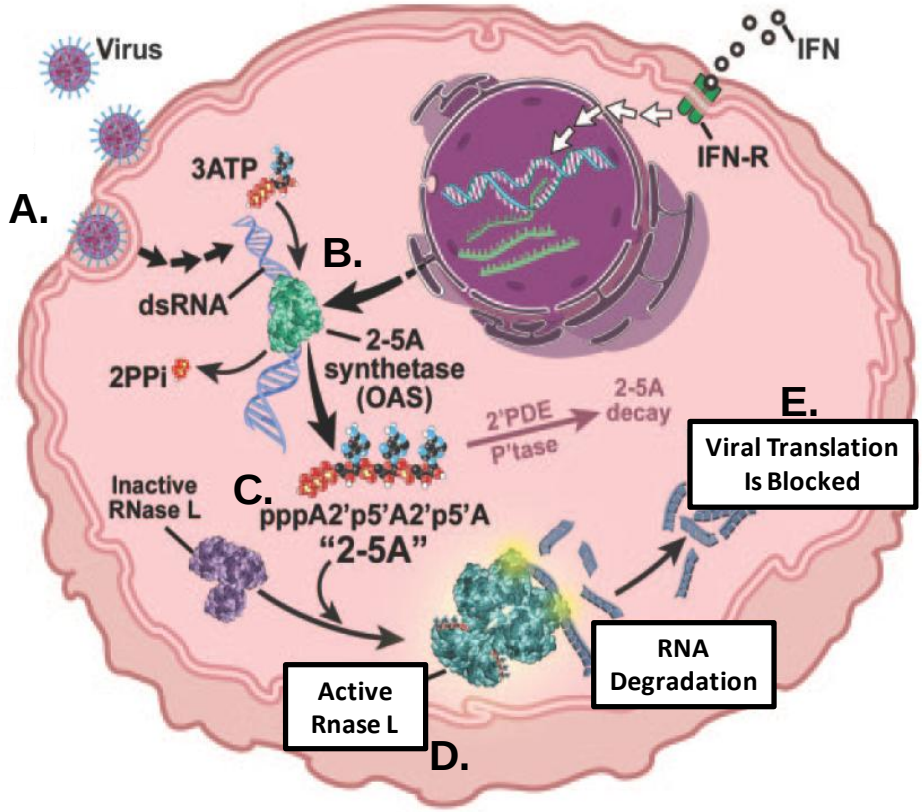

Figure 1.3. Schematic representation of the OAS-RNase L innate immune response pathway. (A) During RNA virus infections, **(B)** dsRNA is produced that is sensed by OAS proteins. **(C)** Upon recognition of dsRNA, these OAS proteins synthesize short 2′ – 5′ linked oligo As from ATP. **(D)** The oligo As activate latent RNase L, which can then degrade cellular and viral RNAs, **(E)** thereby blocking cell and viral translation.
Modified figure and legend adapted from (Silverman, 2007).

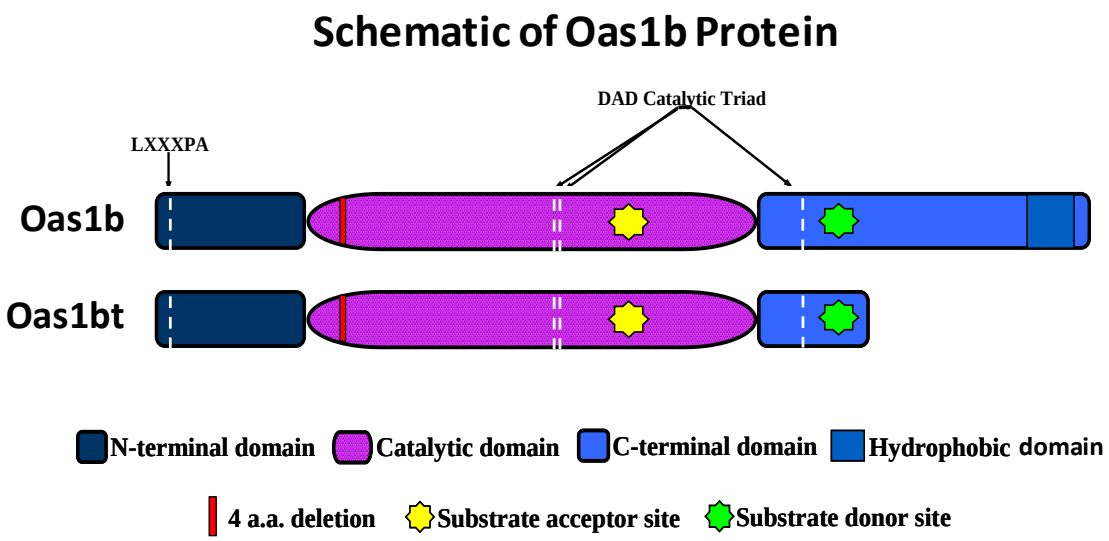

Figure 1.4. Schematic representation of full lenth and truncated Oas1b. Full length Oas1b is generated from the *Flv*^{r} resistance allele while truncated Oas1b (Oas1bt) is generated from the *Flv*^{s} susceptibility allele. Oas1bt is ~30% shorter due to a premature stop codon within the 4th exon. Image adapted with permission from Dr. Husni Elbahesh.

Stress Granules

Translation initiation starts with the formation of the 43S complex of the small 40S ribosome subunit, eIF2-GTP-$tRNA_i^{Met}$, and eIF3 (Pestova et al., 2001). The 43S subunit then associates with other initiation factors (i.e. eIF4F, eIF4A, eIF4B, eIF1A and poly A binding protein) and scans the 5′ UTR of the mRNA until it locates the initiator codon and forms the 48S pre-initiation complex (Anderson and Kedersha, 2002b). eIF2-bound GTP in the 48S pre-initiation complex is then hydrolyzed by eIF5, resulting in the release of some initiation factors and allowing the binding of the large 60S ribosomal subunit to produce the complete 80S ribosome (Anderson and Kedersha, 2002b; Pestova et al., 2001). The 80S ribosome can then continue the translation of the nascent protein by moving down the mRNA and allowing other 80S ribosomes to form at the beginning of the mRNA, creating a polysome. Environmental stresses such as oxidation, UV irradiation, heat, and viral infection lead to the transient formation of discrete cytoplasmic foci known as stress granules (SGs) (Anderson and Kedersha, 2002a, 2006, 2007, 2008; Emara and Brinton, 2007; Gilks et al., 2004; Kedersha and Anderson, 2002; Kedersha et al., 2002; Kedersha et al., 1999). Stress granules were first discovered in chicken embryo fibroblast cells maintained at 45ºC (Collier and Schlesinger, 1986). In response to stress, the alpha subunit of eIF2 (eIF2α) is phosphorylated by one of four eIF2α kinases, protein kinase R (PKR), PKR-related endoplasmic reticulum localized kinase (PERK), general control nonrepressed 2 kinase (GCN2), or heme-regulated inhibitor kinase (HRI) (Anderson and Kedersha, 2002a, 2008). Phosphorylation of the alpha subunit of the eIF2αβγ ternary complex converts it to a competitive inhibitor of eIF2B and renders it unable to load initiator $tRNA_i^{Met}$ to the ribosome for the initiation of protein synthesis. The decreased amounts of available eIF2-GTP-$tRNA_i^{Met}$ then allows the binding of RNA-binding proteins such as T cell intracellular

antigen 1 (TIA-1), TIA1-related (TIAR) or Ras GTPase-activating protein-binding protein (G3BP) to 48S pre-initiation complexes (Gilks et al., 2004; Kedersha and Anderson, 2002). These proteins can self aggregate to form SGs. Binding of these proteins to 48S pre-initiation complexes leads to the stalling of mRNA translation (translational arrest) and results in dissociation of the polysomes through run off of ribosomes (Figure 1.5A-C) (Anderson and Kedersha, 2002a). However, global translation is not completely silenced since the translation of stress-response proteins including the heat shock proteins still occurs (Anderson and Kedersha, 2008; Kedersha et al., 2002). Other components of SGs include translation initiation factors (eIF4E, eIF3, eIF4A, and eIFG), PABP, and other RNA-binding proteins involved in mRNA splicing, transcription, signaling and development (Anderson and Kedersha, 2007, 2008). In two recent reviews by Anderson et al. (Anderson and Kedersha, 2006, 2008), lists of proteins shown to co-localize to SGs by fluorescent microscopy are provided (Anderson and Kedersha, 2006, 2008). It is thought that numerous species of SGs exist with varying protein components and that SGs are dynamic, rather than static in nature (Kedersha et al., 2000). Messenger RNAs sequestered in SGs can subsequently either be released for reinitiation of translation (Figure 1.5D) or moved to processing bodies (PBs) for degradation (Figure 1.5E) (Anderson and Kedersha, 2006, 2007; Beckham et al., 2007; Sheth and Parker, 2003).

Virus-Induced Stress Granule Formation

Virus infections can induce SG formation; however, not all virus infections induce the formation of SGs. Formation of SGs during viral infections is typically mediated by PKR, which senses double-stranded viral RNA, and/or by PERK, which is activated in response to the accumulation of unfolded proteins in the ER. Many types of viruses induce the formation of SGs

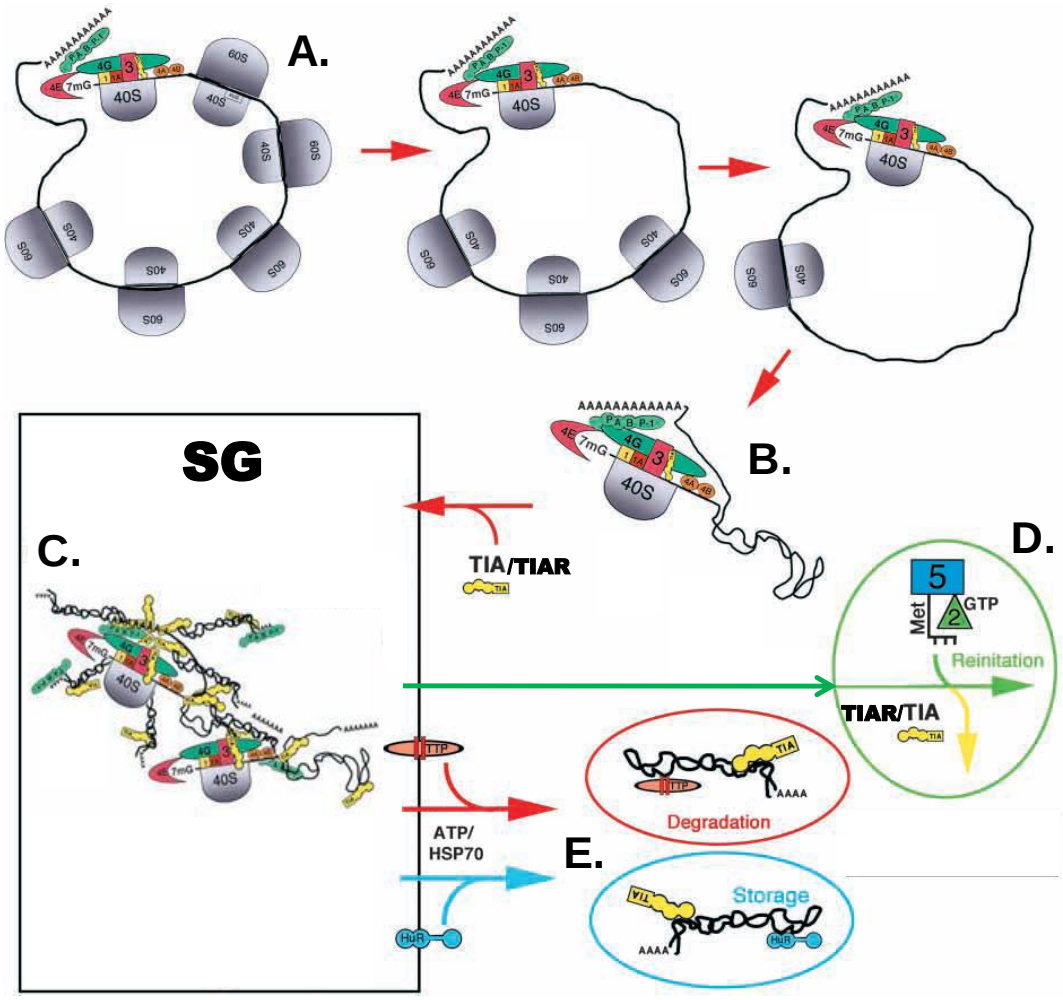

Figure 1.5. Canonical pathway for the formation of stress granules. (A-C) Once 48S pre-initiation complexes stall, the polysomes begin to dissociate through ribosome run off and the stalled pre-initiation complexes are then bound to SG-nucleating proteins such as TIA-1 and TIAR forming SGs. **(D)** After recovery from stress, mRNAs bound in these SGs can reinitiate translation. **(E)** If stress is not relieved, the mRNAs in SGs can be sent to processing bodies for degradation. Modified figure and legend adapted from (Anderson and Kedersha, 2002a).

but some also actively suppress SG formation (Ariumi et al., 2011; Dauber et al., 2011; Dougherty et al., 2011; Hanley et al., 2010; Khong and Jan, 2011; Legros et al., 2011; Lindquist et al., 2011a; Lindquist et al., 2011b; McInerney et al., 2005; Montero et al., 2008; Piotrowska et al., 2010; Querec et al., 2009; Rojas et al., 2010; Simpson-Holley et al., 2011; White et al., 2007). For example, infections with Semliki Forest virus (SFV) and some strains of reoviruses shut down host translation and induce the formation of SGs. SGs form in SFV-infected cells but SFV encodes a translation enhancer that works downstream of eIF2α phosphorylation and is involved in disassembling SGs located in close proximity to the viral positive-sense genome RNA, thus allowing the translation of SFV viral proteins but not most host proteins (McInerney et al., 2005). Reovirus c8 and c87 strain infections inhibit host protein translation, whereas infections by the Dearing reovirus stain do not. The inhibition of host protein translation during c8 and c87 reovirus infections induces the formation of SGs but allows the selective translation of reovirus proteins (Smith et al., 2006). The precise mechanism by which these reovirus strains selectively translate viral proteins in the presence of SGs is unknown; however, it was reported that the expression of ATF4, a transcription factor important for cellular recovery from stress, was required for the increased replication efficiency of these strains (Smith et al., 2006). Poliovirus infections have also been shown to induce the formation of SGs early after infection (Dougherty et al., 2011; Mazroui et al., 2006; Piotrowska et al., 2010; White et al., 2007). As the infection continues, SGs disassemble due to the cleavage of the SG protein G3BP by the viral 3C protease (White et al., 2007). However, recent studies have shown that although G3BP-positive SGs disassembled in poliovirus-infected cells, TIA-1-containing SGs did not disassemble (Piotrowska et al., 2010). Recently, infection of BHK cells with the highly attenuated yellow fever virus vaccine, YF-17D, was reported to efficiently induce the formation of SGs (Querec et

al., 2009). This is in contrast to previous studies done in our lab showing that infections by other members of the genus Flavivirus, WNV and dengue virus, did not induce SGs and inhibited the formation of SGs induced by oxidative stress (Emara and Brinton, 2007).

Although rotavirus infections have been reported to induce the phosphorylation of eIF2α at early times after infection which leads to host cell shut off via the activation of PKR, SGs do not form in these infected cells (Montero et al., 2008; Rojas et al., 2010). The mechanism by which rotavirus infections prevent SG formation in infected cells is currently unknown, but studies have shown that infected cells dramatically relocalize host SG proteins to different compartments (i.e. poly A binding protein relocates from the cytoplasm to the nucleus) suggesting the possibility that these proteins are being used for the benefit of virus replication (Montero et al., 2008). Human T cell leukemia virus (HTLV)-1 infections have also been shown to inhibit the formation of SGs (Legros et al., 2011). The HTLV-1 Tax protein was initially described as a viral oncoprotein, but has also been shown to translocate from the nucleus to the cytoplasm during different stresses of infected cells (Gatza and Marriott, 2006; Suzuki et al., 1996). Studies showed that cytoplasmic Tax was capable of inhibiting the formation of SGs during infection through its interaction with histone deacytelase 6 (HDAC6) (Legros et al., 2011). The exact mechanism by which the Tax-HDAC6 interaction inhibits SG formation is currently unknown but this study represents the first example of a virally encoded protein responsible for specifically inhibiting SG formation in infected cells. Future studies will likely identify other unique pathways utilized by viruses to inhibit SG formation during infection.

GOALS OF THIS DISSERTATION

Specific Aim 1: To identify and characterize unique cellular binding partners of Oas1b and to analyze the involvement of selected Oas1b interaction partners in the West Nile virus infection cycle.

Viruses use host cell proteins to facilitate their replication in infected cells. Resistance specific to flavivirus-induced disease in mice is conferred by the *Flv* gene, which was identified as the enzymatically inactive *2'*-5' oligoadenylate synthetase 1b (Oas1b) (Scherbik et al., 2007a). The only known antiviral activity associated with Oas proteins is through the activation of RNaseL; however, Oas1b was shown to be a non-functional synthetase, suggesting that Oas1b mediates its antiflaviviral activity through an OAS-RNaseL-independent pathway. Experiments were proposed to identify cellular protein(s) interaction partners of Oas1b and to analyze the function of those candidate proteins in the WNV replication cycle to gain insights about the mechanism by which Oas1b specifically reduces the efficiency of flavivirus replication

Specific Aim 2: To analyze the formation of virus-induced stress granules during infection of BHK cells with a WNV lineage 2-based infectious clone.

Previous work in the lab showed that infections with the natural WNV strain Eg101 do not induce the formation of SGs in BHK cells (Emara and Brinton, 2007). However, recent studies showed that infections with a chimeric WNV lineage 2/1 infectious clone (W956IC) did induce the formation of SGs. Studies were performed to identify the kinase responsible for SG formation in W956IC-infected cells and to analyze the mechanism of differential SG formation by infections with natural WNV strains and W956IC.

CHAPTER 2

Specific Aim 1: To identify and characterize unique cellular binding partners of Oas1b and to analyze the involvement of selected Oas1b interaction partners in the West Nile virus infection cycle.

INTRODUCTION

The genus *Flavivirus* consists of about 60 viruses and includes human pathogens such as dengue virus, yellow fever virus, Japanese encephalitis virus, and West Nile virus (WNV) (Lindenbach, 2007). West Nile virus was first isolated in Uganda in 1937 and has been endemic in Africa, southern Europe, Australia, and southern Asia (Brinton, 2002). Recently, it emerged in the United States with over 23,000 cases reported as of late 2006 (Brinton, 2008; Sejvar, 2007). WNV is arthropod-borne and its transmission cycle in nature is usually between *Culex* mosquito species and birds, but virus transmission to horses and humans by mosquitoes occurs occasionally (Brinton, 2002). WNV infection of humans is usually asymptomatic but can sometimes result in mild disease with symptoms such as fever, headache, body rash, muscle fatigue, and disorientation (Brinton, 2002). About 1 in 150, or fewer, infected individuals develop more severe diseases such as encephalitis, meningoencephalitis, paralysis, poliomyelitis-like paralysis or hepatitis (Brinton, 2002).

The flavivirus genome is a positive-sense, single-stranded RNA with a capped 5' end but no 3' poly (A) tail. These features are unique among mammalian positive-sense RNA viruses (Brinton, 2002). The 11 kb flavivirus genome encodes one open reading frame that contains three N-terminal viral structural proteins, capsid (C), membrane (prM, M), and envelope (E), followed by seven nonstructural proteins, NS1, NS2A, NS2B, NS3, NS4A, NS4B, and NS5

(Brinton, 2002). The ten mature viral proteins are generated by proteolytic processing of the polyprotein by viral and cellular proteases (Brinton, 2002). The majority of the non-structural proteins are multi-functional and all seven appear to be involved in viral RNA synthesis (Brinton, 2002; Mackenzie et al., 1996).

The 2'-5' oligoadenylate synthetase (2-5 OAS)/RNase L pathway is one of the innate host defenses against viral infections. OAS gene expression is up-regulated by interferons produced by cells in response to a viral infection (Sarkar and Sen, 2004). Viral double-stranded RNA (dsRNA) activates OAS causing it to polymerize adenosine triphosphate (ATP) into short 2'-5'-linked oligomers (2-5A) (Justesen et al., 2000). These oligomers then bind to and activate latent endoribonuclease L (RNase L) that is constitutively expressed in cells. Activated RNase L cleaves viral and cellular single-stranded RNAs, thereby reducing viral translation (Kakuta et al., 2002). Eight duplicated copies of the OAS1 gene (Oas1a-h) are clustered within a 210 kb genomic region on mouse chromosome 5 (Kakuta et al., 2002). Previous breeding studies with mice displaying differential susceptibility to flavivirus-induced disease showed that the alleles of a single Mendelian dominant gene, *Flv*, controlled this phenotype (Webster and Clow, 1936; Webster and Johnson, 1941). Oas1b was identified by a positional cloning strategy as the *Flv* gene (Perelygin et al., 2002). A full-length Oas1b protein is expressed by the Flv^r allele in resistant mice, while a truncated Oas1b (Oas1bt) protein is expressed from the Flv^s allele in susceptible mice. The resistant allele, Flv^r, was "knocked in" to a susceptible mouse strain, C57BL/6 (B6), replacing the susceptible allele, Flv^s, to generate C57BL/6-Oas1bKI (KI) mice that display the flavivirus resistance phenotype (Scherbik et al., 2007a). Among the eight Oas1 genes in mice only Oas1a and Oas1g have been reported to be functional synthetases (Elbahesh

et al., 2011a; Kakuta et al., 2002). Therefore, Oas1b does not mediate its antiviral activity through the canonical OAS-RNase L pathway (Elbahesh et al., 2011a; Scherbik et al., 2006).

As one means of gaining insights into the mechanism by which Oas1b specifically reduces the efficiency of flavivirus replication, cellular protein interaction partners of Oas1b were identified and their involvement in the Oas1b-mediated flavivirus resistance mechanism was analyzed. Results from the current study identified peptides from ORP1L and ABCF3 as Oas1b interaction partners in a yeast two-hybrid analysis. These interactions were confirmed by *in vitro* yeast co-transformation and co-immunoprecipitation assays, as well as by immunoprecipitation studies in mammalian cells using full length proteins. RNAi knockdown of ORP1L resulted in decreased replication of the flavivirus WNV as well as of other RNA viruses and this effect did not require the presence of Oas1b. Knockdown of ORP1L was recently reported to cause increased endosomal movement (Vihervaara et al., 2011) and this could explain the observed effect on the replication of multiple viruses that enter cells by endocytosis. Knockdown of ABCF3 increased WNV replication but not Sindbis virus replication and this effect was only observed in Oas1b-expressing cells. The results provide new insights about the Oas1b-mediated flavivirus resistance mechanism.

RESULTS

Identification of putative Oas1b binding partners in a yeast two-hybrid screen

Although Oas1b was identified as the only gene needed to confer resistance to flavivirus-induced disease in mice (Scherbik et al., 2007a), it was shown to mediate its flavivirus-specific antiviral activity by an RNase L-independent mechanism (Elbahesh et al., 2011a; Scherbik et al., 2006). A yeast two-hybrid screen was used to identify candidate cell protein Oas1b binding

partners that might participate in the Oas1b-mediated anti-flaviviral mechanism. In initial experiments, a pre-transformed Mouse Brain cDNA library was screened as described in Materials and Methods against a full length Oas1b bait; however, no viable yeast colonies were detected on the selection plates. Yeast two-hybrid screens are unable to detect interactions with proteins containing a transmembrane domain that tethers them to cytoplasmic membranes preventing their translocation to the nucleus to act as transcription factors (Iyer et al., 2005). None of the members of the OAS family so far analyzed have previously been reported to have a transmembrane domain. However, analysis of the Oas1b sequence using the PredictProtein software (www.predictprotein.org) predicted a short transmembrane domain starting 23 amino acids from the C-terminus (Figure 2.1A). To determine whether the predicted transmembrane domain of Oas1b was able to tether it to a cytoplasmic membrane, a vector expressing a GST-tagged full length Oas1b protein was transiently transfected into BHK cells and the localization of the protein was detected by confocal microscopy. Oas1b colocalized with the endoplasmic reticulum (ER) marker calnexin, but not with the mitochondrial marker CoxIV (Figure 2.1B). Oas1b was shown to remain localized to the ER after WNV infection of these cells (Figure 2.1B). In contrast, transient expression of a GST-tagged truncated Oas1b (GST-Oas1bt) or a GST tag alone resulted in a diffuse protein distribution throughout the cell with no ER colocalization (Figure 2.1B). These results confirmed the presence of a transmembrane tail on the full length Oas1b protein that anchors Oas1b to the ER membrane. The sequence of the Oas1b transmembrane domain was BLASTed against the GenBank database but no matches were found. The origin of this domain and the mechanism by which it was acquired by Oas1b are currently not known.

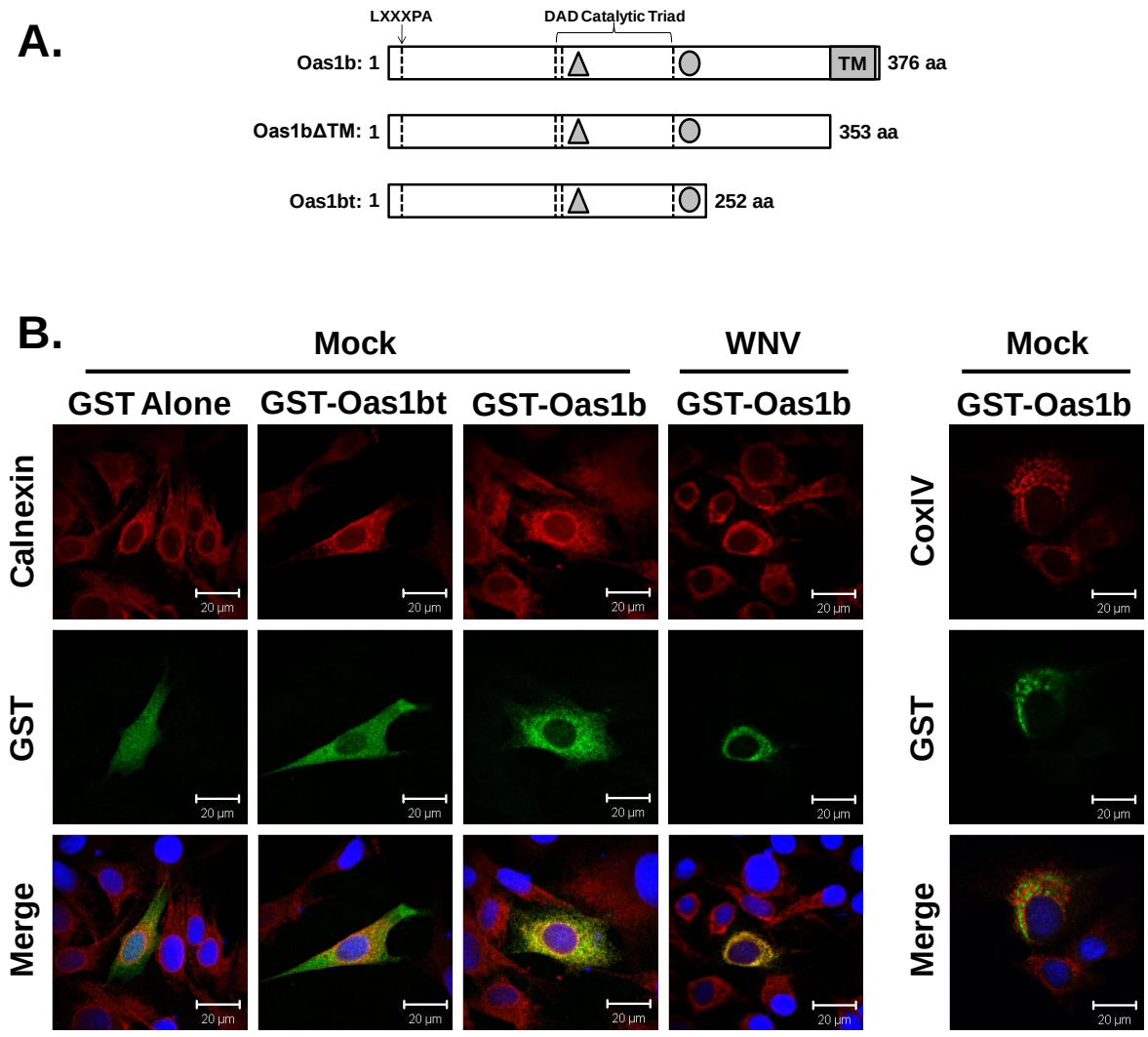

Figure 2.1. Full length Oas1b contains a transmembrane domain that localizes it to the ER membrane. (A) The full length Oas1b protein expressed in resistant cells is predicted to contain a C-terminal transmembrane domain. The Oas1bΔTM truncation mutant lacks the C-terminal transmembrane tail.. The truncated Oas1b (Oas1bt) expressed in susceptible cells is generated by a premature stop codon in exon 4. **(B)** Plasmids expressing GST, GST-Oas1bt, or GST-Oas1b were transiently transfected into BHK cells. Twenty-four hr later, cells were either mock-infected or infected with WNV Eg101 (MOI of 5) and at 24 hr after infection cells were fixed, permeabilized, incubated with the indicated antibodies and analyzed by confocal microscopy. Anti-GST antibody (green) detected GST-tagged Oas1b, anti-calnexin antibody (red) detected ER, anti-CoxIV antibody (red) detected mitochondria and Hoechst (blue) stained nuclei.

A C-terminally truncated Oas1b mutant consisting of amino acids 1-353 of full length Oas1b and referred to as Oas1bΔTM (Figure 2.1A) was next cloned into the yeast two-hybrid bait vector pGBKT7. When the Oas1bΔTM protein was used as the bait in a two-hybrid assay with the Mouse Brain cDNA library, 23 unique candidate partner peptides were identified. Interaction between each of these peptides and Oas1bΔTM was subsequently tested with yeast co-transformation assays as described in Materials and Methods. Growth of colonies on double selection media indicated that cells were co-transformed with both the bait and prey plasmids and growth of colonies on the quadruple selection media indicated that the two peptides interacted in yeast. Of the 23 putative peptide partners, an interaction with Oas1b was confirmed for only eight by yeast co-transformation assay on quadruple dropout selection media (Table 1). The protein origin of each of the putative peptide partners was predicted using a BLAST analysis.

Co-immunoprecipitation of putative binding partners and Oas1b

Since yeast two-hybrid analyses can produce false-positive results, *in vitro* co-immunoprecipitation assays were used to further confirm that the putative peptide partners interacted with Oas1bΔTM. Oas1bΔTM and each of the putative partners was *in vitro* transcribed and translated in the presence of ^{35}S-labeled methionine. Oas1bΔTM and one of the putative partners were then incubated together for 1 hr at RT and interaction was assessed by co-immunoprecipitation as described in Materials and Methods. The *in vitro* translated Oas1bΔTM had an N-terminal c-Myc tag and each of the putative partners had an N-terminal HA tag. Oas1bΔTM co-immunoprecipitated with the oxysterol binding protein related protein 1L (ORP1L) peptide as well as with the ATP binding cassette protein 3, subfamily F (ABCF3)

Table 1. Oas1bΔTM Yeast Two-Hybrid Analysis Results.

Clone No.	Putative Protein Partner
16-1 (169 aa)	OSBP-Related Protein 1L (Orp1L)
27-6-4 (214 aa)	Eukaryotic Elongation Factor 1a
42-3-5 (81 aa)	ATP-Binding Cassette subfamily f, member 3 (Abcf3)
49-2-2 (32 aa)	Heterogenous Nuclear Ribonucleoprotein
68a-2-3 (253 aa)	Microtubule-associated Protein 1A
84-1-2 (136 aa)	Nucleosome Assembly Protein 1-like 2
113-1 (223 aa)	Cytochrome C Oxidase Assembly Protein
163-1-2 (263 aa)	Euchromatic Histone Lysine N-Methyltransferase 2

*The length of the peptide in each clone is indicated in parentheses.

peptide (Figure 2.2A and B, respectively). None of the other putative peptide partners interacted with Oas1bΔTM *in vitro.* To determine whether these two peptides could also interact with Oas1bt, co-immunoprecipitation experiments were performed with *in vitro* synthesized, N-terminal c-Myc tagged Oas1bt and each of the two partners. The ORP1L peptide did not co-immunoprecipitate with Oas1bt (Figure 2.2C), suggesting that the interaction between this peptide and Oas1bΔTM occurs in a region located after the premature stop codon of Oas1bt and before the transmembrane domain of Oas1b. In contrast, the ABCF3 peptide did co-immunoprecipitate with Oas1bt (Figure 2.2D), indicating that this peptide interacts with both Oas1b and Oas1bt in a region upstream of the premature stop codon of Oas1bt. Also, a yeast two-hybrid screen using Oas1a as bait identified ABCF3 to interact, suggesting that ABCF3 interacts with multiple mouse OAS proteins and possibly human OAS proteins and isoforms.

Because the peptides used in the previous experiments represented only a portion of each of the putative interaction partners and the interactions were detected either *in vitro* or in yeast cells, the results could not predict whether the whole proteins would interact with full length Oas1b. The interaction of Oas1b and a full length partner was next tested in mammalian cells by co-immunoprecipitation. Oas1b is one of eight duplicated Oas1 genes in mouse cells (Perelygin et al., 2002). Due to the high degree of homology between the Oas1 proteins, it has not been possible to make an antibody that can specifically detect individual mouse Oas1 proteins. Therefore, a tagged Oas1b protein was transiently expressed. He MEFs were stably transfected with both 3xFLAG-tagged full length Oas1b and V5-tagged ORP1L (He-Oas1b/Orp1L), as described in the Materials and Methods. The *in vivo* interaction between Oas1b and either ORP1L or ABCF3 was assessed by co-immunoprecipitation as described in the Materials and Methods. Prior to lysis, cells were treated with DSP, a thiol-reversible chemical protein-

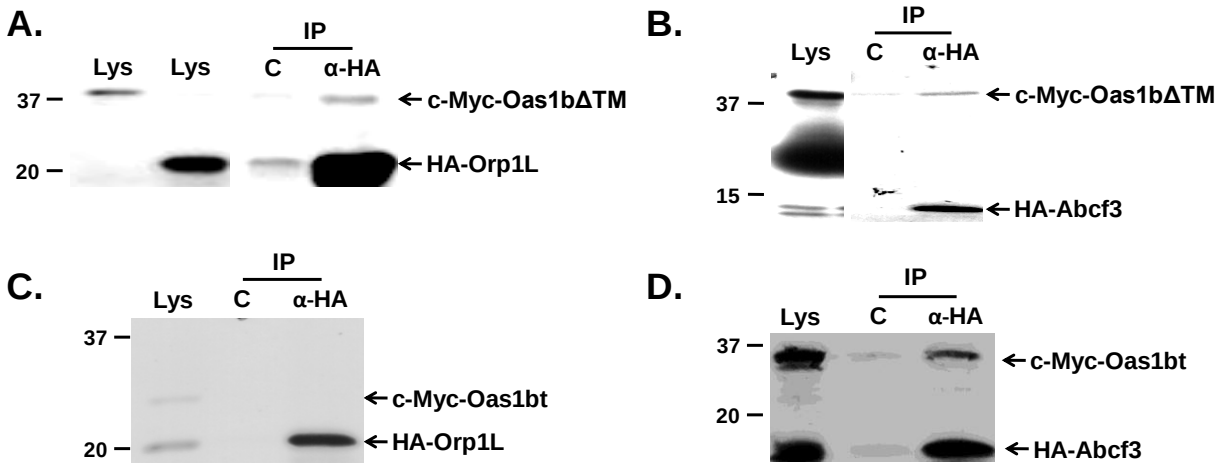

Figure 2.2. *In vitro* co-immunoprecipitation of Oas1bΔTM and putative partner peptides 16-1 (Orp1L) and 42-3-5 (Abcf3). Wheat germ extract was used to *in vitro* transcribe and translate Oas1bΔTM or Oas1bt and putative peptide clones in the presence of [^{35}S]-methionine. One of the Oas1b proteins and a candidate peptide were mixed and immunoprecipitated. Immunoprecipitated protein complexes were resolved by SDS-PAGE and detected by autoradiography. **(A)** ^{35}S-labeled c-Myc-tagged Oas1bΔTM and HA-16-1 (Orp1L) peptides were immunoprecipitated with anti-HA antibody. **(B)** ^{35}S-labeled c-Myc-tagged Oas1bΔTM and HA-42-3-5 (Abcf3) peptides were immunoprecipitated with anti-HA antibody. **(C)** ^{35}S-labeled c-Myc-tagged Oas1bt and HA-16-1 (Orp1L) peptides were immunoprecipitated with anti-HA antibody. **(D)** ^{35}S-labeled c-Myc-tagged Oas1bt and HA-42-3-5 (Abcf3) peptides were immunoprecipitated with anti-HA antibody. Lys-lysates; C-Control (agarose beads alone or anti-IgG antibody); α-HA-anti-HA antibody.

rosslinker, to stabilize transient or weak interactions. Antibody to the Oas1b FLAG tag immunoprecipitated both ORP1L and ABCF3 (Figure 2.3). The interaction of these proteins was also analyzed in WNV-infected cells. He-Oas1b/Orp1L cells were infected with WNV Eg101 at a MOI of 1 and harvested at 24 hr after infection. Both ORP1L and ABCF3 were immunoprecipitated by antibody to the Oas1b FLAG tag in infected cells (Figure 2.3). In contrast, anti-FLAG antibody did not immunoprecipitate WNV NS3 (Figure 2.3), suggesting that Oas1b does not interact directly with WNV replication complexes and that the co-immunoprecipitation results obtained were specific.

The effect of reducing ORP1L protein levels on virus infections

The previous experiments showed that ORP1L interacts with Oas1b *in vivo*. It was hypothesized that if ORP1L is an essential component of the Oas1b-mediated anti-flavivirus mechanism, then the WNV yield, as well as viral RNA (vRNA) and protein levels would increase when ORP1L is knocked down. ORP1L protein expression was reduced by stable expression of an ORP1L-specific shRNA in KI MEFs. Clonal cell lines were selected as described in the Materials and Methods. The KI shOrp1L-6 clonal cell line had the lowest ORP1L protein levels compared to the KI shCont-7 non-specific control cell line of the 19 lines tested (Figure 2.4A). KI shCont-7 and KI shOrp1L-6 cells were infected with WNV Eg101 at a MOI of 1 and clarified culture fluid, total cell RNA, and cell lysates were harvested at the indicated times after infection from duplicate wells. Virus yields were measured by plaque assay on BHK cells and the yields produced by KI shOrp1L-6 cells at 24 to 48 hr after infection were reduced compared to those from KI shCont-7 cells (Figure 2.4B). Intracellular viral RNA was detected by real time qRT-PCR using WNV NS1 region-specific primers and probe. Reduced

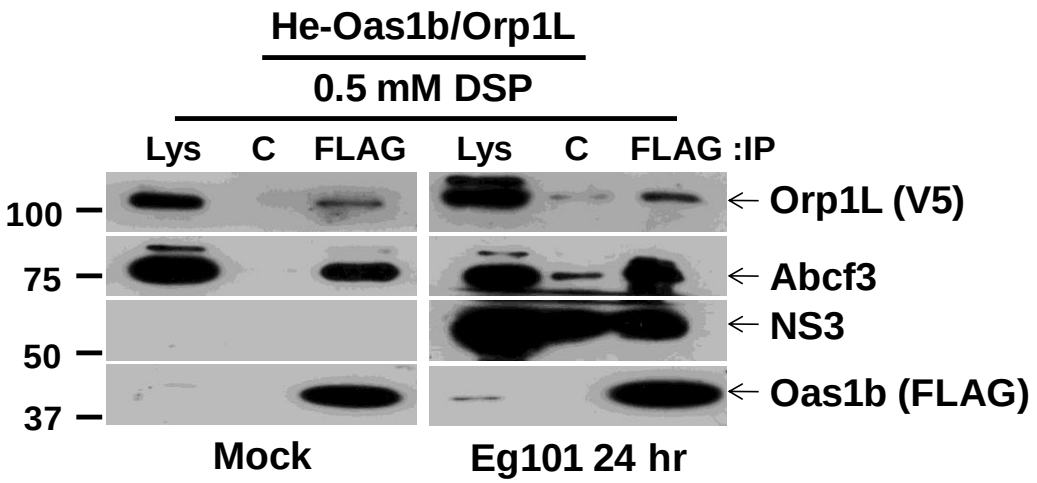

Figure 2.3. Mammalian cell co-immunoprecipitation of V5-tagged Orp1L and endogenous Abcf3 with FLAG-tagged Oas1b. He-Oas1b/Orp1L MEFs that express N-terminally FLAG-tagged Oas1b and C-terminally V5-tagged Orp1L were either mock-infected or infected with WNV Eg101 (MOI of 1), treated with 0.5 mM DSP for 30 min on ice to stabilize transient or weak interactions. The reaction was quenched with 50 mM Tris pH 7.5 for 15 min on ice, cells were harvested at 24 hr in lysis buffer. Lysates were immunoprecipitated with either control antibody or anti-FLAG antibody, as indicated. Western blotting was done to detect Orp1L (anti-V5 antibody), Abcf3 (anti-Abcf3 antibody), NS3(anti-NS3 antibody), and Oas1b protein (anti-FLAG antibody). Lys-lysates; C-Control (anti-IgG antibody-conjugated agarose); FLAG-anti-FLAG antibody-conjugated agarose.

viral RNA (vRNA) levels in KI shOrp1L-6 cells were observed from 24 to 48 hr after infection compared to those in KI shCont-7 cells (Figure 2.4C). Western blotting of the WNV NS3 protein showed that viral protein levels were also reduced in KI shOrp1L-6 cells compared to KI shCont-7 at 24 to 48 hr after infection (Figure 2.4D). To confirm that the results observed were due to the reduction of ORP1L protein and not to a decrease in cell viability, an MTT assay was performed. Approximately 15% cell death was observed at 48 hr after Eg101 infection in both cell lines compared to mock-infected cells (Figure 2.4E). It was noted that the efficiency of ORP1L knockdown by shRNA decreased with time after WNV infection suggesting that the RNAi pathway was antagonized in infected cells.

The antiviral activity of Oas1b is specific to flaviviruses. Therefore, if ORP1L is involved in the Oas1b-mediated resistance mechanism its reduction would be unlikely to affect an infection with a virus from another family. To test this hypothesis, wildtype B6 and KI MEFs were infected with a member of another positive strand RNA virus family, the alpha togavirus Sindbis virus (SinV), at an MOI of 20 and clarified culture fluid and infected cell lysates were harvested at the indicated times after infection from replicate wells. Virus yields and intracellular viral protein levels were similar from the two types of cells (Figure 2.5A and B). These results confirmed the flavivirus-specificity of Oas1b-mediated resistance. The affect of ORP1L knockdown on a SinV infection in Oas1b-expressing cells was next assessed. KI shCont-7 and KI shOrp1L-6 cell lines were infected with SinV at an MOI of 20. SinV yields from KI shOrp1L-6 MEFs were reduced by ~0.5-1 log compared to those from KI shCont-7 MEFs (Figure 2.5C). A reduction was also observed in SinV capsid protein levels in KI shOrp1L-6 MEFs compared to KI shCont-7 MEFs (Figure 2.5D). A negative effect on the yield of the negative strand RNA virus vesicular stomatitis virus (VSV) was also observed (Figure 2.5F).

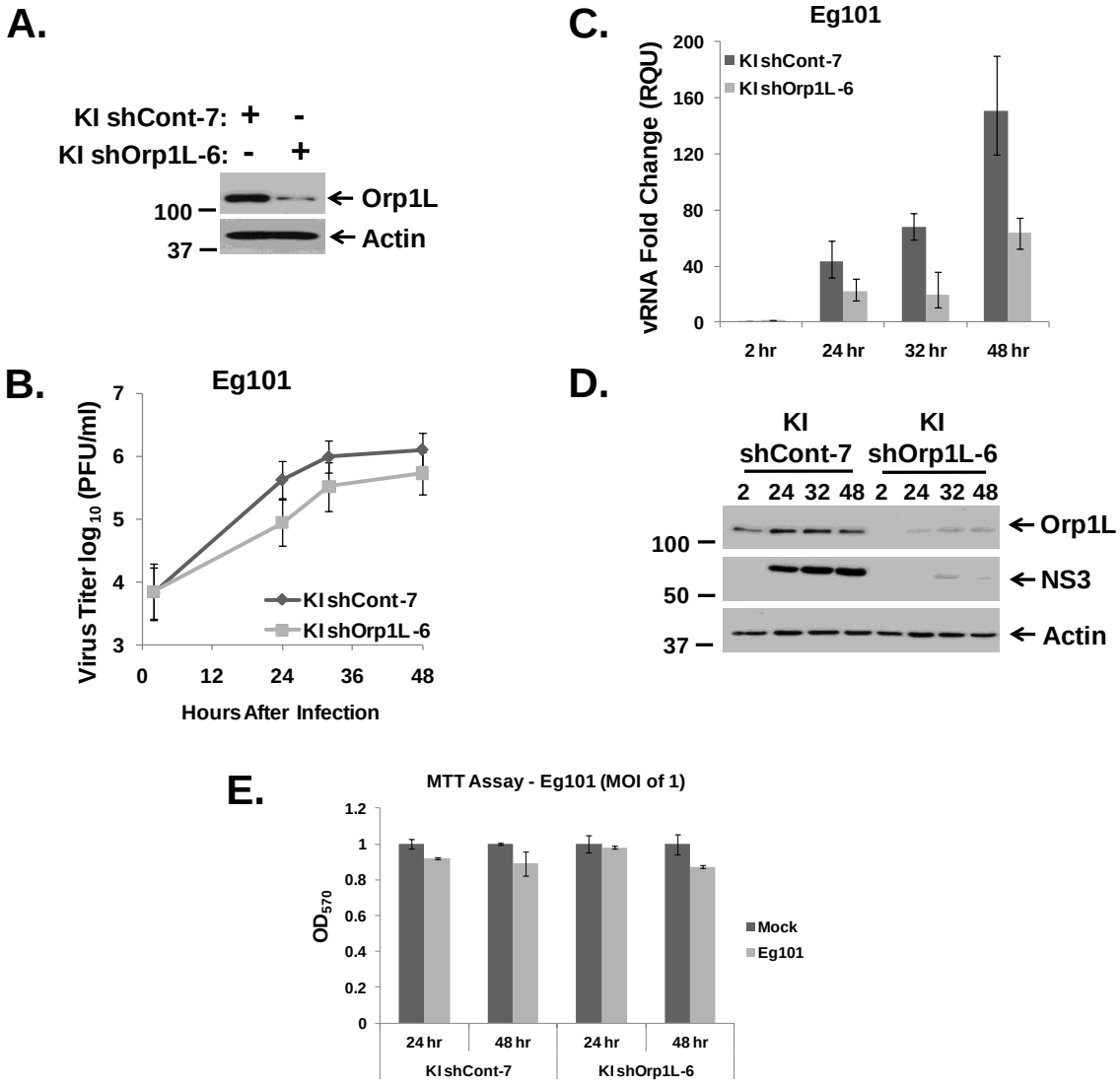

Figure 2.4. The effect of Orp1L knockdown on WNV infection in KI MEFs stably expressing shRNAs targeting Orp1L. (**A)** Western blot analysis of Orp1L protein levels in KI shCont-7 and KI shOrp1L-6 MEFs were detected using anti-Orp1L R247 antibody. KI shCont-7 and KI shOrp1L-6 MEFs were infected with WNV Eg101 at a MOI of 1. **(B)** Virus yields from infected KI shCont-7 and KI shOrp1L-6 MEFs were determined by plaque assay in BHK cells. **(C)** Viral RNA levels were assayed by real time qRT-PCR. **(D)** Viral protein (NS3) levels were measured by Western blotting. **(E)** KI shCont-7 and KI shOrp1L-6 MEFs were infected with WNV Eg101 at a MOI of 1 and analyzed for cell death using a Cell Titer 96® non-radioactive cell proliferation assay according to manufacturers protocol.

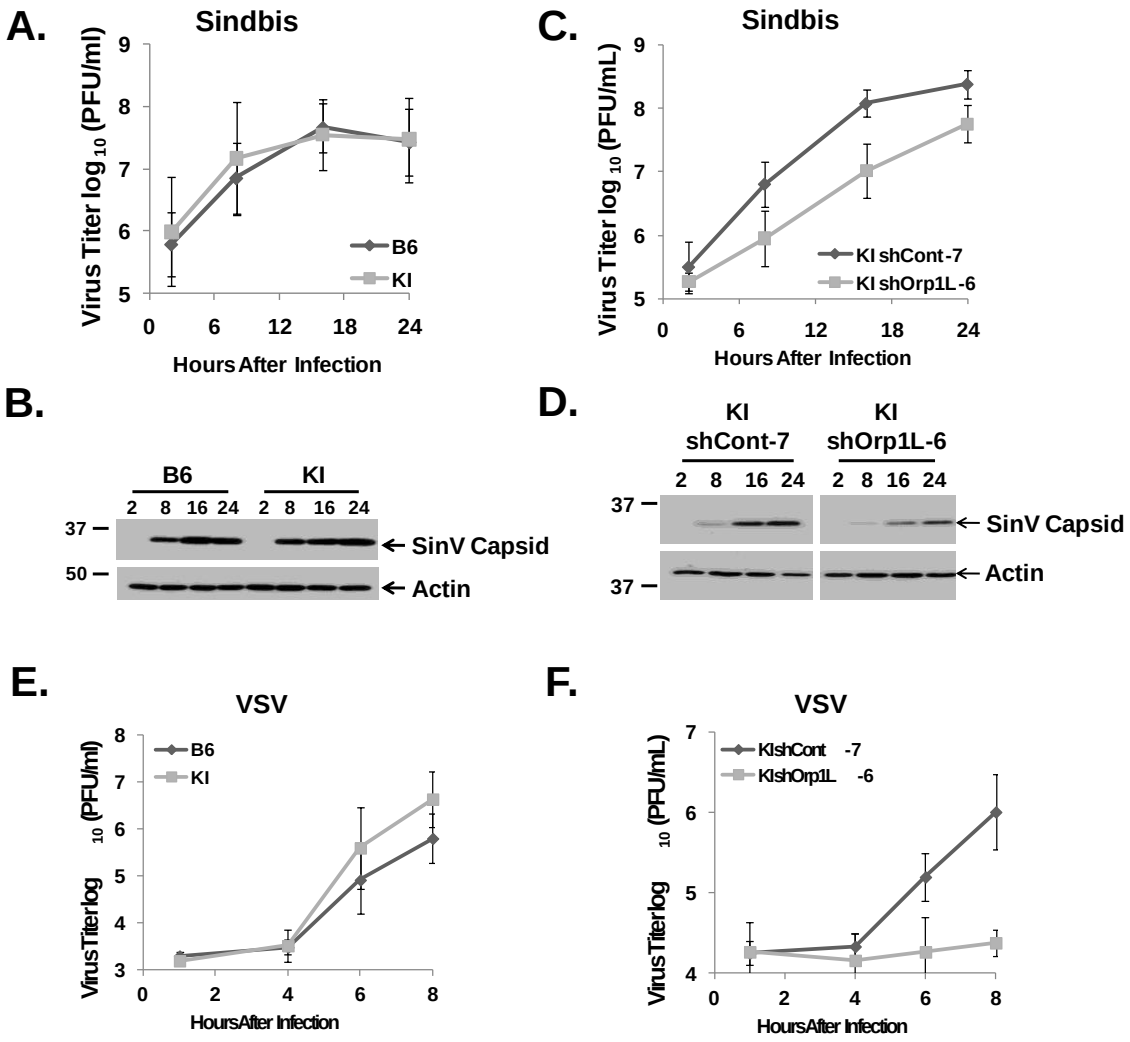

Figure 2.5. The effect of Orp1L knockdown on Sindbis virus and vesicular stomatitis virus infections. (A and B) Wildtype B6 (Oas1bt-expressing) and KI (Oas1b-expressing) cells were infected with Sindbis virus (SinV) at a MOI of 20. **(A)** SinV yields from B6 and KI MEFs were measured by plaque assay on BHK cells. **(B)** SinV capsid protein levels in B6 and KI-infected MEF lysates were determined by Western blotting. **(C and D)** KI shCont-7 and KI shOrp1L-6 cells were infected with SinV at a MOI of 20. **(C)** SinV yields from infected KI shCont-7 and KI shOrp1L-7 MEFs were measured by plaque assay in BHK cells. **(D)** SinV capsid protein levels from infected KI shCont-7 and KI shOrp1L-7 MEFs were determined by Western blotting. **(E)** Wildtype B6 (Oas1bt-expressing) and KI (Oas1b-expressing) cells were infected with Vesicular stomatitis virus (VSV) at a MOI of 5. VSV yields from B6 and KI MEFs were measured by plaque assay on BHK cells. **(F)** VSV yields from infected KI shCont-7 and KI shOrp1L-7 MEFs were measured by plaque assay in BHK cells.

The results suggest that ORP1L may be a proviral host cell protein that is utilized by different families of RNA viruses. However, knockdown of ORP1L was previously reported to enhance the movement of late endosomes (Vihervaara et al., 2011) and this could negatively affect the replication of viruses that enter cells by endocytosis by altering the fusion stage of viral genome release.

The effect of reducing ABCF3 protein levels on virus infections

Since ABCF3 was also shown to interact with Oas1b *in vivo*, the effect of reducing ABCF3 protein levels on WNV infection in KI cells was determined. shRNAs targeting ABCF3 or a non-specific shRNA control were transduced into KI cells and clonal cell lines were selected as described in Materials and Methods. The KI shAbcf3-8 clonal cell line had the greatest knockdown efficiency of ABCF3 protein as compared to the KI shCont-7 control cell lines of 21 lines tested (Figure 2.6A). KI shCont-7 and KI shAbcf3-8 MEFs were infected with WNV Eg101 at a MOI of 1 and samples were collected for analysis at the indicated times after infection. A slight increase in virus yields from the KI shAbcf3-8 cells were observed at 32 and 48 hr after infection compared to those from KI shCont-7 cells (Figure 2.6B). An increase in the levels of WNV vRNA and NS3 protein was also observed compared to those in KI shCont-7 cells (Figure 2.6C and D). An MTT assay done on KI shCont-7 and KI shAbcf3-8 cells at 24 and 48 hr after infection with WNV Eg101 at a MOI of 1 detected about 15% cell death at 48 hr after infection in both cell lines compared to mock-infected cells (Figure 2.6E). Similar to that which was seen with infection of KI shOrp1L-6 cells, a decrease in the efficiency of ABCF3 knockdown by shRNA was also observed with time after WNV infection.

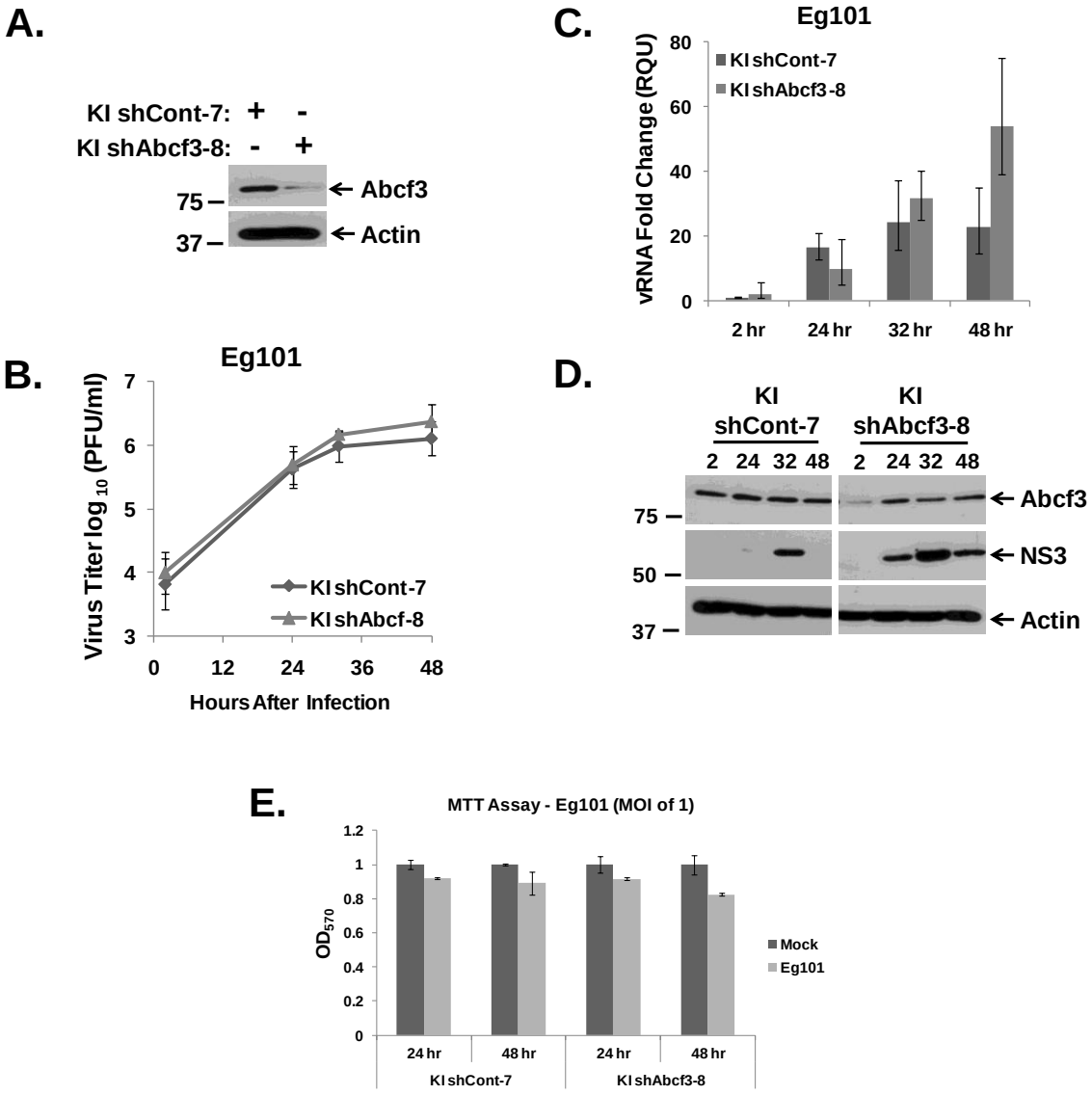

Figure 2.6. The effect of Abcf3 knockdown on WNV infection in KI MEFs stably expressing shRNAs targeting Abcf3. (**A)** Western blot analysis of Abcf3 protein levels in KI shCont-7 and KI shAbcf3-8 MEFs. KI shCont-7 and KI shAbcf3-8 MEFs were infected with WNV Eg101 at a MOI of 1. **(B)** Virus yields from infected KI shCont-7 and KI shAbcf3-8 MEFs were determined by plaque assay in BHK cells. **(C)** Viral RNA levels were assayed by real time qRT-PCR. **(D)** Viral protein (NS3) levels were measured by Western blotting. **(E)** KI shCont-7 and KI shAbcf3-8 MEFs were infected with WNV Eg101 at a MOI of 1 and analyzed for cell death using a Cell Titer 96® non-radioactive cell proliferation assay according to manufacturers protocol.

Since the antiviral activity of Oas1b is specific to flaviviruses, the affect on a SinV infection of knocking down ABCF3 was also tested. KI shCont-7 and KI shAbcf3-8 MEF cultures were infected with SinV at an MOI of 20 and samples were collected as described above at the indicated times after infection. SinV yields from KI shAbcf3-8 MEFs were the same as those from KI shCont-7 MEFs (Figure 2.7A). Similarly, SinV capsid protein levels did not change when ABCF3 proteins were knocked down (Figure 2.7B). VSV infections were also tested and virus yield was not shown to be affected by the knockdown of ABCF3 (Figure 2.7C). The data indicate that reduction of enhanced ABCF3 is involved in the Oas1b-mediated flavivirus-specific antiviral mechanism.

To test whether the antiviral activity of ABCF3 requires the presence of Oas1b, ABCF3 expression was knocked down in B6 cells that express Oas1bt. shRNAs targeting either ABCF3 or a nonspecific shRNA control were transduced into B6 cells and clonal cell lines were selected as described in the Materials and Methods. The B6 shAbcf3-8 clonal cell line had the greatest reduction of ABCF3 protein levels compared to the B6 shCont-3 control cells of 8 clones tested (Figure 2.8A). B6 shCont-3 and B6 shAbcf3-8 MEFs were infected with WNV Eg101 at an MOI of 1 and samples were collected as described above at the indicated times after infection. No effect on virus yield or vRNA or viral protein levels was detected in either type of cell (Figure 2.8B-D). These results indicate that the flavivirus-specific, antiviral activity of ABCF3 requires the presence of Oas1b.

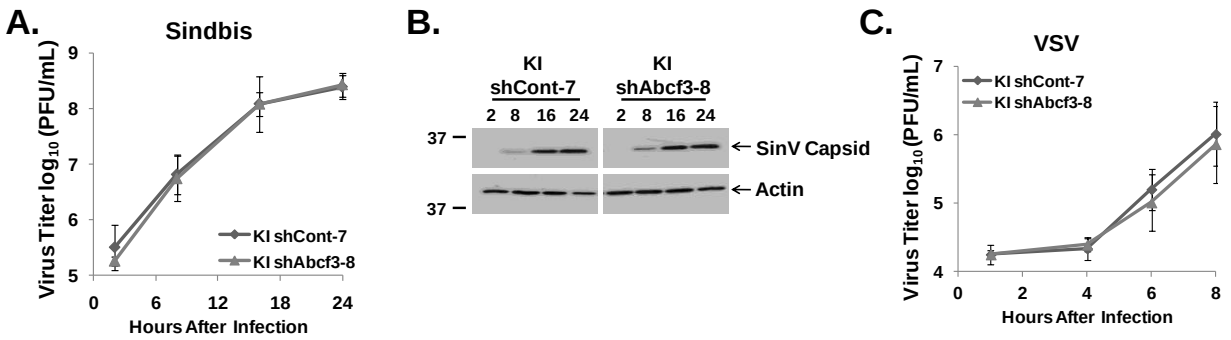

Figure 2.7. The effect of Abcf3 knockdown on SinVand VSV infections. KI shCont-7 and KI shAbcf3-8 MEFs were infected with SinV at a MOI of 20. **(A)** SinV yields from infected KI shCont-7 and KI shAbcf3-8 MEFs were measured by plaque assay in BHK cells. **(B)** SinV capsid protein levels from infected KI shCont-7 and KI shAbcf3-8 MEFs were determined by Western blotting. **(C)** KI shCont-7 and KI shAbcf3-8 MEFs were infected with VSV at a MOI of 5. VSV yields from infected KI shCont-7 and KI shAbcf3-8 MEFs were measured by plaque assay in BHK cells.

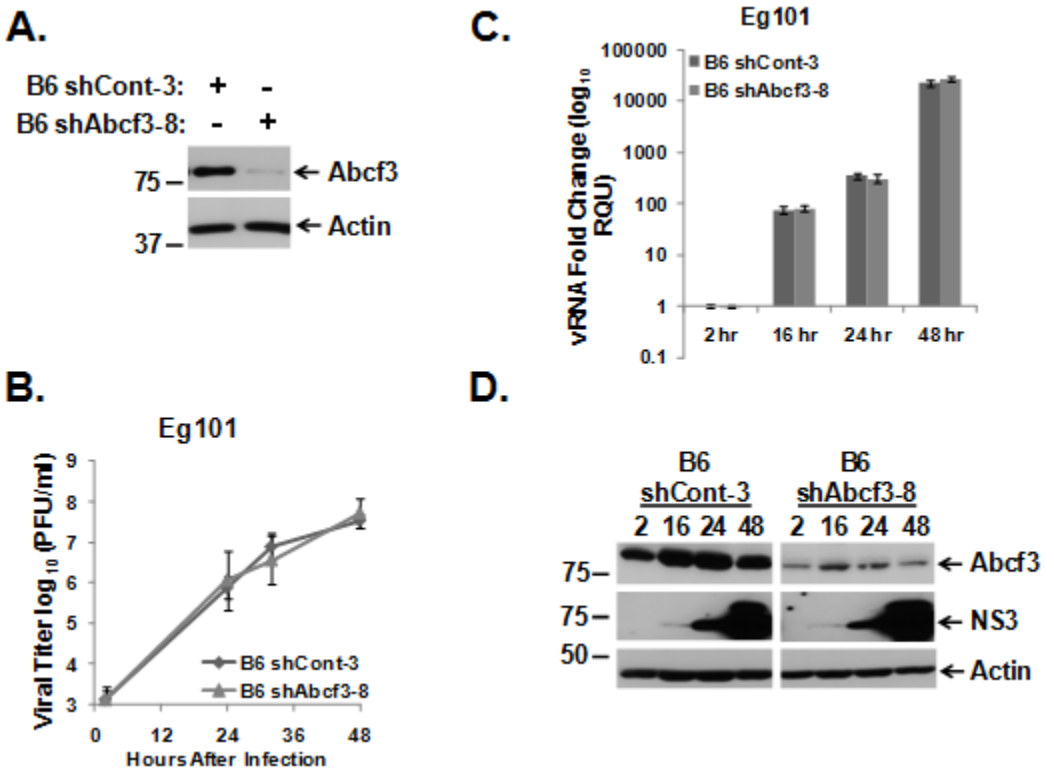

Figure 2.8. The effect of Abcf3 knockdown on WNV infection in B6 MEFs stably expressing shRNAs targeting Abcf3. (**A)** Western blot analysis of Abcf3 protein levels in B6 shCont-3 and B6 shAbcf3-8 MEFs. B6 shCont-3 and B6 shAbcf3-8 MEFs were infected with WNV Eg101 at a MOI of 1. **(B)** Virus yields from infected B6 shCont-3 and B6 shAbcf3-8 MEFs were determined by plaque assay in BHK cells. **(C)** Viral RNA levels were assayed by real time qRT-PCR. **(D)** Viral protein (NS3) levels were measured by Western blotting.

DISCUSSION

The enzymatically inactive Oas1b protein mediates its anti-flaviviral effect by an as yet unknown mechanism that is independent of the canonical RNase L pathway (Elbahesh et al., 2011a; Perelygin et al., 2002; Scherbik et al., 2007a). Twenty-three candidate binding partners of Oas1b were identified in a yeast two-hybrid screen of a mouse brain library and 8 of these were confirmed by co-transformation of yeast. However, only two of the candidate peptides, ORP1L and ABCF3, were identified as interaction partners of Oas1b *in vitro*. Full length proteins of these two partners were also shown to interact with Oas1b in mammalian cells. The lack of an *in vitro* Oas1b interaction for 6 of the 8 putative partners could be due to a false positive interaction in yeast or to misfolding or the lack of modification of the *in vitro* translated peptides. The interaction of each of these full length proteins with Oas1b still needs to be tested. The co-immunoprecipitation results suggest that Oas1b, ORP1L and ABCF3 form a complex in mammalian cells. Also, ORP1L and ABCF3 interact with different regions of the Oas1b protein, further supporting the idea that these proteins do not compete with each other for Oas1b binding.

ORP1L belongs to the oxysterol-binding protein (OSBP)-related protein family that is involved in processes such as cholesterol maintenance, sterol sensing, lipid transport, and cell signaling events (Lehto et al., 2001; Lehto and Olkkonen, 2003; Olkkonen et al., 2006; Xu et al., 2001; Yan et al., 2007b). ORP1L is one of two variants of ORP1, the other of which is ORP1S (Johansson et al., 2003). ORP1L contains an N-terminal extension of ankyrin repeats (a unique feature among the OSBP-related proteins) and a pleckstrin homology domain in addition to the OSBP domain, whereas ORP1S contains only the OSBP domain common to all OSBP-related proteins (Johansson et al., 2003). These two variants differ in their tissue expression, intracellular localization and function. ORP1S is predominantly expressed in skeletal muscle and heart, while

ORP1L is expressed in macrophages, brain and lungs (Johansson et al., 2003). ORP1S is a cytosolic protein while ORP1L localizes to late endosomes (LEs) and colocalizes with LE proteins such as Rab7, Rab9, Rab7-interacting lysosomal protein (RILP), and lysosomal associated membrane protein 1 (LAMP1) (Johansson et al., 2003; Johansson et al., 2005; Johansson et al., 2007). ORP1L was recently shown to be involved in LE movement along microtubules (Johansson et al., 2005; Johansson et al., 2007; Rocha et al., 2009; Vihervaara et al., 2011). Rab7 recruits RILP and ORP1L to form a complex. RILP, present in this complex, can interact with the $p150^{Glued}$ subunit of dynactin to recruit the dynein motor complex (Johansson et al., 2007). The dynein motor complex then facilitates minus-end-directed translocation of LEs towards the microtubule organizing center of the cell (Johansson et al., 2007; Rocha et al., 2009). The function of ORP1L in this complex is to sense the cholesterol content of LEs. In low cholesterol conditions, ORP1L is in an open conformation, exposing a motif containing two phenylalanines in an acidic tract (FFAT) that can interact with the vesicle-associated membrane protein (VAMP)-associated protein A (VAP-A) which removes the $p150^{Glued}$ subunit from the motor complex inhibiting the movement of LEs on microtubules. This results in a scattered distribution of LEs within the cell (Rocha et al., 2009). In contrast, when cholesterol levels are high the ORP1L is in a closed conformation in which the FFAT motif is not available for interaction with VAP-A. This facilitates minus-end directed transport of LEs (Rocha et al., 2009). A recent study on the effects of ORP1L on LE motility showed that knockdown of ORP1L expression results in an increase in LE motility, whereas ORP1L overexpression results in the clustering of LEs to the perinuclear region of the cell (Rocha et al., 2009; Vihervaara et al., 2011).

Flaviviruses attach to an unknown cell surface receptor(s) located in a cholesterol raft and then enter cells by endocytosis in clatherin-coated pits (Lindenbach, 2007; Medigeshi et al., 2008). Acidification of early endosomes leads to a conformational change in the viral envelope (E) protein but LE compartment-specific anionic lipids are required to trigger E fusion loop insertion into the membrane initiating fusion of the two membranes (Zaitseva et al., 2010). ORP1L sensing cholesterol in the lipid rafts of virion-containing LEs would remain in a closed conformation facilitating the movement of virion-containing LEs on microtubules (Olkkonen and Hynynen, 2009; Xu et al., 2001). For both WNV, SinV and VSV infections, late endosomes are the site of virion fusion during entry (Chu and Ng, 2004; Lu et al., 1999; Superti et al., 1987) and the negative effect of knocking down Orp1L each of these types of infection could be due to a non-specific effect of increased late endosome motility rather than to a specific effect on the flavivirus resistance mechanism. Alternative experimental strategies are therefore required to study the involvement of ORP1L in the Oas1b-mediated flavivirus resistance mechanism. The interaction of Oas1b with ORP1L may stop the movement of virus-containing LEs on microtubules and bring them close to the ER.

The ABC superfamily of ATP-binding proteins is one of the largest protein families known with highly conserved ABC proteins found in archaea, prokaryotes, and eukaryotes (Hollenstein et al., 2007; Linton and Higgins, 2007; Locher, 2009; Schriml and Dean, 2000; Sturm et al., 2009). ABC proteins are canonical transporters of numerous substrates and are typically exporters; however, prokaryotic ABC proteins can also function as importers (Hollenstein et al., 2007; Locher, 2009). Seven subfamilies of ABC proteins (a-g) have been identified in humans. Because the ABCE and ABCF subfamilies are non-canonical ABC transporters that lack transmembrane domains (Kerr, 2004; Sturm et al., 2009), it has been

suggested that they do not function as typical ABC transporters but instead are involved in other processes such as regulating translation initiation and/or elongation, ribosome assembly, and RNase L activity (Chen et al., 2006; Kerr, 2004; Martinand et al., 1999; Paytubi et al., 2008; Sturm et al., 2009; Tyzack et al., 2000). Although nothing is yet known about ABCF3 protein function in mammalian cells, recent reports have suggested that some proteins of both the ABCE and ABCF families may share host cell binding partners (Chen et al., 2006; Paytubi et al., 2008; Tyzack et al., 2000). Both ABCE and ABCF proteins have been shown to regulate protein synthesis by binding translation initiation factors. Data from the present study showed that reducing ABCF3 protein levels had the greatest effect on viral protein levels. The transmembrane tail of Oas1b specifically localizes it to the ER membrane, the site of flavivirus translation and replication and the recruitment of ABCF3 is required for its antiviral affect. The mechanism by which ABCF3 specifically decreases flavivirus replication is not yet known, but downregulation of WNV protein synthesis would lead to downregulation of viral RNA synthesis and progeny virus production. It is possible that the antiviral activity of ABCF3 depends on its specific localization to the ER membrane as mediated by binding to Oas1b, which is unique among OAS proteins in having a transmembrane domain.

The ABCE1 protein has also been reported to interact with partners that are not involved in translation. ABCE1 was initially reported to be a protein involved in inhibiting RNase L activation by binding 2-5As but it was subsequently shown to directly bind to RNase L (Bisbal et al., 1995). An equimolar ratio of ABCE1 and RNase L was shown to be required for inhibition (Bisbal et al., 1995). However, a previous studies in our lab showed that while RNase L activity partially reduces WNV yield, the effect was similar in cells expressing either full length or truncated Oas1b and the canonical RNase L pathway was shown not to be involved in the Oas1b-

mediated resistance to flavivirus-induced disease (Elbahesh et al., 2011a; Scherbik et al., 2006). ABCE1 was also reported to bind to TULA, a protein containing both ubiquitin binding domains and SH3 domains, leading to the inhibition of the production of HIV-1 viral particles (Agrawal et al., 2008; Carpino et al., 2004; Feshchenko et al., 2004; Kowanetz et al., 2004; Smirnova et al., 2008; Wattenhofer et al., 2001). ABCF3 was also found to interact with Oas1a and Oas1bt (Figure 2.2D). What functions it plays when interacting with these proteins are also not currently known. ABCF3 may interact with different partners and have different functions depending on the complex that it is in.

MATERIALS AND METHODS

Cell Lines

C3H/He (He), C3H/RV, C57BL/6 (B6) and C57BL/6-Oas1bKI (KI) SV40-transformed mouse embryofibroblast (MEF) lines, as well as BHK-21 W12 cells, were maintained in minimal essential medium (MEM) supplemented with 5% heat-inactivated fetal bovine serum (FBS), glutamine, and 10 µg/mL gentamicin at 37ºC in 5% CO_2.

He MEFs were transiently transfected with a p3xFLAG-Oas1b plasmid using Lipofectamine 2000, according to the manufacturer's protocol (Invitrogen). Transfected cells were selected using 250 µg/mL G418 (Sigma) to create a heterogeneous population of cells stably expressing FLAG-Oas1b, referred to here as He-Oas1b cells. Stable integrants from individual foci were selected from cloning rings and subsequently expanded. Homogeneous clonal cell lines were generated by plating cells at a limiting dilution, harvesting colonies with cloning rings and expanding the individual colony cell populations. Multiple clones were

selected and analyzed for FLAG-Oas1b protein expression. Clone #12 (He-Oas1b-12) had the highest Oas1b expression level and was used for experiments.

He-Oas1b-12 cells were transfected with pEF6-V5/HIS-TOPO-Orp1L using Lipofectamine 2000, according to manufacturer's protocol (Invitrogen). These cells were then selected using 5 µg/mL Blasticidin S hydrochloride (Sigma), as well as G418, to obtain a cell population that stably expressed both FLAG-Oas1b and V5-Orp1L, called He-Oas1b/Orp1L.

The KI (Oas1b-expressing) and B6 (Oas1bt-expressing) MEF lines were previously described (Scherbik et al., 2007a) and used for RNAi studies. KI cells were transduced with lentiviral-packaged shRNA targeting either mouse Orp1L (sc-62716-V), mouse Abcf3 (sc-140761-V), or a non-specific shRNA control (sc-108060-V) (Santa Cruz Biotechnology) according to the manufacturer's protocol. Heterogeneous cell populations stably expressing the targeted shRNAs were selected using 5 µg/mL puromycin dihydrocholoride (Santa Cruz Biotechnology). Clonal lines were selected by plating cells at a limiting dilution, harvesting colonies with cloning rings and expanding the individual colony cell populations. The knockdown efficiency of each clone was determined using Western blotting to detect protein and real time qRT-PCR to detect mRNA. The KI shControl clone #7 (KI shCont-7) cells had comparable levels of Orp1L and Abcf3 to the wildtype KI cells and were used in the experiments. The same protocol was used to generate B6 shControl clone #3 (B6 shCont-3) cells.

cDNA Constructs

The full length Oas1b cDNA was amplified from C3H/RV RNA by RT-PCR, cloned into a pScreen vector (Invitrogen) and then subcloned into the pGBKT7 vector (Clontech) using Nco1 and BamH1 restriction enzyme sites. Similarly, full length Oas1b was amplified from

C3H/RV RNA, cloned into a TOPO vector (Invitrogen) and then subcloned into the pEBG vector (a gift from Dr. Hobman, University of Alberta) that fuses an N-terminal GST tag onto the expressed protein (GST-Oas1b). Also, truncated Oas1b (Oas1bt) was amplified from C3H/He RNA, cloned into a TOPO vector and then subcloned into the pEBG vector (GST-Oas1bt). A construct expressing an Oas1b protein without the predicted C-terminal transmembrane domain (Oas1bΔTM) was generated by PCR amplification of the cDNA sequence corresponding to amino acids 1-353 of the Oas1b protein using the forward primer 5′-CATATGATGGAGCAGGATCTG-3′ and the reverse primer 5′-GAATTCCTAATACTTCATTGG-3′ followed by cloning into a TOPO vector and then subcloning into pGBKT7 (Clontech) using Nde1 and EcoR1 restriction enzyme sites. For mammalian cell expression, Oas1b cDNA was subcloned from a pNTAP-Oas1b plasmid into the p3xFLAG-CMV-10 vector (Sigma) using EcoR1 and Xba1 restriction sites (p3xFLAG-Oas1b). Full length Orp1L cDNA was reverse transcribed from He cell RNA using a Thermoscript RT-PCR kit (Invitrogen) with the Orp1LF forward primer 5′-GCCATGAACACAGAAGCAGAACAGCAGCTTCTC-3′ and the Orp1LR reverse primer 5′-ATAAATATCAGGCAAATTGAAGTAGTTTCTGTC-3′ then PCR amplified using the Platinum Taq DNA Polymerase High Fidelity kit (Invitrogen) using the Orp1LF and Orp1LR primers and subsequently cloned into the pEF6-V5/HIS-TOPO vector (Invitrogen), creating the pEF6-V5/HIS-TOPO-Orp1L (pEF6-Orp1L) construct for mammalian cell expression. All constructs were sequenced to verify that they contained the correct sequence.

Transient Transfection

BHK cells were seeded to approximately 80% confluency and transiently transfected with cDNA expressing GST-Oas1b, GST-Oas1bt, or GST tag alone using Lipofectamine 2000 (Invitrogen) according to manufacturer's protocol.

Viruses

A stock of lineage 1 WNV strain Eg101 was prepared by infecting a monolayer of BHK cells at a multiplicity of infection (MOI) of 0.1 and harvesting culture fluid at 32 hr after infection. Clarified culture fluid ($5x10^7$ PFU/ml) was aliquoted and stored at -80ºC. A stock of Sindbis virus strain SAAR339 ($7x10^9$ PFU/ml) was prepared as a 10% (wt/vol) newborn mouse brain homogenate.

Plaque Assay

Infectivity titers were determined by infecting monolayers of BHK cells in duplicate well of a six-well plate with serial 10-fold dilutions of clarified culture fluid. After adsorption for 1 hr at RT, the virus inoculum was removed and the wells were overlaid with 1% SeaKem ME agarose (Bio-Whittaker Molecular Applications, Rockland, Maine), mixed 1:1 with 2x MEM containing 5% FBS, and incubated for 72 hr at 37ºC in 5% CO_2. Plaque assays were performed in BHK cells with the same protocol for SinV but the plates were incubated for 48 hr. After removal of the agarose plugs, cells were stained with 0.05% crystal violet in 10% ethanol.

Yeast Two-Hybrid Analysis

Yeast two-hybrid analyses were performed according to manufacturer's protocol (Clontech). Oas1bΔTM was cloned into the pGBKT7 vector (Clontech) which was transformed into AH109 yeast cells (bait). The Oas1bΔTM-transformed AH109 cells were mated with pre-transformed Y187 yeast cells (Mouse Brain cDNA library (prey)) (Clontech). Yeast two-hybrid analysis yielded a mating efficiency of ~1.58% and approximately $2.1x10^6$ clones were screened. Diploid yeast cells were plated onto triple drop-out (TDO; SD/-His/-Leu/-Trp) agarose selection plates and incubated at 30ºC. Colonies were selected from TDO plates and re-streaked onto quadruple drop-out (QDO; SD/-Ade/-His/-Leu/-Trp) agarose plates for a more stringent secondary selection. Colonies growing on QDO selection plates were then further tested for Gal4-mediated MEL1 activation, one of the Gal4-responsive reporter genes of the yeast two-hybrid system. Alpha-glactosidase production from MEL1 turns X-α-Gal into a blue product and therefore suggests a positive interaction.

Yeast Co-transformation

A yeast co-transformation analysis was performed according to the manufacturer's protocol (Clontech). Oas1bΔTM-transformed AH109 yeast cells were mated with individual putative partner positive clones transformed into Y187 yeast cells and diploid cells were plated onto double drop-out (DDO; SD/-Leu/-Trp) selection plates to confirm co-transformation, as well as onto QDO plates to confirm a positive interaction identified in the yeast two-hybrid screen.

In Vitro Transcription and Translation

Putative positive clones and bait constructs were *in vitro* transcribed and translated in the presence of 20 µCi ^{35}S-labeled methionine (EasyTag^{TM} Met L-[^{35}S] Perkin Elmer), according to manufacturer's protocol (Promega).

In Vitro Co-immunoprecipitation

Two ^{35}S-methionine-labeled, *in vitro* translated peptides were incubated together for 1 hr at RT. The reaction was then divided into two and incubated with either a control (agarose alone or anti-IgG antibody) or with anti-HA antibody (Roche) for 1 hr with rotation at 4ºC, after which Protein G agarose (Roche) was added and rotation was continued at 4ºC overnight. The beads were then washed 3 times in lysis buffer (1% Triton X-100, 0.1% SDS, 150 mM NaCl, 50 mM Tris HCl pH 7.4, and fresh protease inhibitor). The beads were centrifuged and 30 µl of 2x sample buffer (20% SDS, 25% glycerol, 0.5 M Tris HCl pH 6.8, and 0.5% bromophenol blue) was added and the samples were boiled at 95ºC to denature the protein complexes. Immunoprecipated proteins were separated by SDS-PAGE in 10% polyacrylamide gels. Gels were washed 3 times in fixing solution (10% acetic acid and 30% methanol) to remove free radiolabeled methionine and then incubated for 30 min at RT in Autofluor (National Diagnostics), incubated for 5 min at RT in an anti-cracking buffer (7% acetic acid, 7% methanol, and 1% glycerol), and then dried onto 3 mm chromatography paper (Whatman) using a Model 543 Gel Dryer (BIO-RAD). Dried gels were exposed to HyBlot CL® autoradiography film (Denville) at -80ºC and bands were detected by autoradiography.

Mammalian Cell Co-immunoprecipitation

Approximately $2x10^7$ cells were washed twice with 1xPBS and then treated with 0.5 mM dithiobis[succinimidyl propionate] (DSP) for 30 min at RT to crosslink cellular proteins. The reaction was quenched with 50 mM Tris pH 7.5 for 15 min on ice. The cells were rinsed in 1xPBS, incubated on ice for 30 min after the addition of 1.5 ml lysis buffer and then passed through a 21 gauge syringe. Cell lysates were clarified by centrifugation at 2,000 x g at 4ºC for 5 min. The supernatant was divided in two and incubated with either anti-IgG antibody-conjugated Protein G agarose beads (Sigma) or with anti-FLAG antibody-conjugated Protein G agarose beads (Sigma) at 4ºC overnight. The beads were washed 3 times in lysis buffer to remove unbound proteins, centrifuged and 30 µl of 2x sample buffer was added. Sample buffer contains β-mercaptoethanol which reverses the chemically crosslinked proteins from the DSP treatment. The beads were boiled at 95ºC for 5 min to denature the protein complexes and the samples were sonicated. Immunoprecipitated proteins were separated by SDS-PAGE and transferred to a nitrocellulose membrane for 1 hr at 100V. After transfer, membranes were blocked for 1 hr at RT in 5% non-fat dry milk (NFDM), incubated with a primary antibody diluted in 5% NFDM overnight at 4ºC, washed 3 times for 10 min in 1xTBS+Tween 20 and then incubated with a secondary antibody diluted in 5% NFDM for 1 hr at RT. Membranes were washed twice in 1xTBS+Tween 20, once in 1xTBS for 10 min at RT and then incubated in SuperSignal West Pico Chemiluminescent Substrate (Thermo Scientific) for 5 min at RT and bands were detected by autoradiography.

Antibodies

The primary antibodies used in immunoblotting experiments were: mouse anti-c-Myc and mouse anti-HA (Roche), mouse anti-FLAG, rabbit anti-FLAG, and rabbit Abcf3 (Sigma), goat anti-V5 (Bethyl Laboratories), goat anti-NS3 (R&D Systems), and rabbit anti-Orp1L R247 (a kind gift from Dr. Olkkonen, Helsinki, Finland). The primary antibodies used in confocal microscopy studies were: mouse anti-GST, rabbit anti-GST (Cell Signaling), rabbit anti-Calnexin (Sigma), mouse anti-CoxIV (Invitrogen), and mouse anti-dsRNA (Hungary). Secondary antibodies used for immunoblotting experiments included anti-Rabbit-HRP, anti-Mouse-HRP (Cell Signaling), and anti-Goat-HRP (SCBT). Secondary antibodies used for confocal microscopy studies included donkey anti-Mouse Alexa Fluor 594, donkey anti-Mouse Alexa Fluor 488, donkey anti-Rabbit Alexa Fluor 488, and donkey anti-Rabbit Alexa Fluor 594 (Invitrogen).

Confocal Microscopy

BHK cells were seeded onto 3 mm coverslips (Fisher Scientific) in 24-well plates and 20 hr later infected with WNV Eg101 at an MOI of 1, fixed with 4% paraformaldehyde in phosphate buffered saline (PBS) for 10 min at RT, permeablized with 0.1% Triton X-100 in PBS for 10 min, and rinsed three times with PBS, and incubated overnight at 4ºC in blocking buffer (5% horse serum in PBS). Primary antibodies were diluted in blocking buffer and incubated with cells for 1 hr at RT. The cells were washed three times for 10 min in PBS and then incubated with the secondary antibodies and 0.5 µg/ml Hoechst 33258 dye (Invitrogen) for 1 hr at RT. Coverslips were mounted using ProLong Gold Antifade reagent (Invitrogen) and images were

taken with a LSM 510 confocal microscope (Zeiss, Oberkochen, Germany) using a 63x water-immersion objective. Images were analyzed using Zeiss LSM Image Browser software.

Real time qRT-PCR

Total cellular RNA was isolated from B6 and KI cells with TriReagent (Molecular Research Center). Cellular and viral RNA were quantified using a TaqMan One-Step RT-PCR Master Mix Reagents Kit (Applied Biosystems) according to manufacturer's protocol. Mouse Orp1L (Mm_00498552_m1) and mouse Abcf3 (Mm_00658695_m1) cellular RNA levels were measured using predesigned primer and probe sets (Applied Biosystems). WNV Eg101 NS1 RNA was measured using a previously described primer and probe set (Scherbik et al., 2006). Mouse GAPDH was used as an internal loading control.

MTT Assay

Cells were plated to ~100% confluency in 96-well plates and infected with WNV Eg101 at a MOI of 1. Cell viability was determined at 24 hr and 48 hr after infection using a CellTiter 96® non-radioactive cell proliferation assay done according to manufacturer's protocol (Promega).

CHAPTER 3

Specific Aim 2: To analyze the formation of virus-induced stress granules during infection of BHK cells with a WNV lineage 1/2-based infectious clone.

INTRODUCTION

West Nile virus is maintained in nature in a mosquito-bird transmission cycle and has recently become endemic in the United States. Humans and horses are occasionally infected but are dead end hosts (Brinton, 2002; Lindenbach, 2007). Infections in humans are usually asymptomatic but some individuals develop fever and/or flu-like symptoms and a few of these progress to central nervous system disease (Brinton, 2002; Lindenbach, 2007). WNV belongs to the family *Flaviviridae*, genus *Flavivirus,* which includes other mosquito-borne human pathogens such as dengue virus, yellow fever virus (YFV) and Japanese encephalitis virus. The WNV genome is a positive-sense, single-stranded RNA that contains a 5′ cap but no 3′ poly(A) tail (Lindenbach, 2007). It is approximately 11,000 nts in length and encodes a single polyprotein that is co- and post-translationally processed by both host and viral proteases into three structural [capsid (C), membrane (M) and envelope (E)] and seven non-structural (NS1, NS2a, NS2b, NS3, NS4a, NS4b and NS5) proteins (Lindenbach, 2007). Most of the more than 70 strains of WNV are classified in either lineage 1 or 2 (Bakonyi et al., 2006; Lanciotti et al., 2002; Prilipov et al., 2002). Lineage 1 WNV strains are endemic in northern Africa, Europe, the Middle East, parts of Asia and the Americas, while lineage 2 WNV strains are typically found in sub-Saharan Africa (Bakonyi et al., 2006; Lanciotti et al., 2002; Prilipov et al., 2002).

In response to several types of cellular stress, eukaryotic translation initiation factor 2 alpha (eIF2α) Ser51 is phosphorylated by one of four kinases: protein kinase R (PKR), activated by dsRNA (viral infection); heme-regulated initiation factor 2α (HRI), activated by oxidative stress; PKR-like endoplasmic reticulum kinase (PERK), activated by unfolded proteins in the endoplasmic reticulum (ER); and general control nondepressible 2 (GCN2), activated by amino acid starvation (Anderson and Kedersha, 2008). Phosphorylation of eIF2α reduces the amount of available eIF2-GTP-tRNA complexes and thus inhibits translation initiation resulting in polysome disassembly through ribosome runoff. RNA-binding proteins such as TIA-1, TIAR, and G3BP can then bind to the 5′ end of the mRNA with a stalled initiation complex and aggregate with other mRNA-bound proteins forming microscopically visible stress granules (SGs) (Anderson and Kedersha, 2002a, 2008). SGs recruit many additional proteins including RNA-stabilizing proteins (Anderson and Kedersha, 2008; Brennan and Steitz, 2001). Although cap-dependent translation is suppressed in stressed cells, translation from internal ribosome entry site (IRES) elements and alternative ORFs, such as those in the mRNAs of heat shock proteins, chaperones, and some transcription factors (i.e. ATF4), still occurs (Vattem and Wek, 2004). If a cell survives the stress, SGs dissociate and the mRNAs resume translation (Brennan and Steitz, 2001). However, if a cell is unable to recover and enters apoptosis, stalled mRNAs in SGs are transported to and degraded by processing bodies (PBs) (Sheth and Parker, 2003; Teixeira et al., 2005). Some virus infections have been shown to suppress SG formation (Dougherty et al., 2011; McInerney et al., 2005; White et al., 2007). Lineage 1 WNV Eg101 infections in BHK cells were previously reported not to induce SGs but to inhibit SG induction by arsenite treatment (Emara and Brinton, 2007). A subsequent study showed that infections with the lineage 2/1 infectious

chimeric W956IC virus activated PKR while WNV Eg101 infections did not (Elbahesh et al., 2011b).

In the present study, SG induction in BHK cells by infections with additional natural lineage 1 or lineage 2 WNV strains and W956IC was compared. None of the natural lineage 1 or lineage 2 WNV strains tested induced SGs by 24 hr after infection while W956IC virus infections efficiently induced SGs starting at 12 hr after infection. All SG-positive, WNV-infected cells had elevated levels of phosphorylated eIF2α. PKR was identified as the kinase phosphorylating eIF2α in WNV-infected cells. Mapping experiments done with a set of WNV chimeric viruses suggested that interactions between viral nonstructural proteins and/or between viral nonstructural proteins and cell proteins are altered in W956IC-infected cells. Increased levels of SG-positive, chimeric virus-infected cells correlated with higher levels of early viral RNA synthesis and the presence of viral dsRNA that was not protected by intracellular membranes.

RESULTS

Efficiency of SG formation induced by different strains of WNV

It was previously reported that lineage 2-based W956IC virus infections induced PKR phosphorylation while lineage 1 WNV Eg101 infections did not (Elbahesh et al., 2011b). WNV Eg101 infections were previously reported not to induce SGs (Emara and Brinton, 2007). To determine whether different strains of WNV varied in the efficiency with which they induced SGs, BHK cells were infected with WNV lineage 1 strains, Eg101, NY99 or Tx113; with WNV lineage 2 strains, B956, Mg78, or SPU; or with a lineage 1/2-based chimeric WNV infectious clone, W956IC virus. Cells were fixed at 36 hr after infection and analyzed by confocal

microscopy. Less than 3% of the infected cells were SG-positive by 36 hr after infection with each of the lineage 1 and 2 WNV strains tested (Figure 3.1A), confirming our previous results (Emara and Brinton, 2007). In contrast, W956IC infections induced SGs in ~30% of the infected BHK cells by 36 hr after infection (Figure 3.1A and C).

The time course of SG formation in Eg101- and W956IC-infected cells was next analyzed. BHK cells were infected with either WNV Eg101 or W956IC (MOI of 1) and then fixed and analyzed for SGs at various times after infection. Less than 0.5% of the mock-infected cells contained SGs at either 24 hr or 36 hr after infection (Figure 3.1B and C). No SG-positive WNV Eg101-infected cells were detected at either 6 hr or 12 hr after infection, whereas SG-positive W956IC-infected cells were observed by 12 hr. By 24 hr (less than 1%) and by 36 hr (less than 3%) of Eg101-infected cells contained SGs (Figure 3.1B and C). In contrast, ~20% of the W956IC-infected cells were SG-positive at 24 hr after infection and ~30% were SG-positive by 36 hr (Figure 3.1B and C). Differential efficiency of SG induction by Eg101 and W956IC virus infections was also observed in C3H/He MEFs, C57BL/6 MEFs, and HEK 293T cells (data not shown). Although the number of SG-positive infected cells and the time at which they initially appeared differed among the cell lines tested, W956IC infections consistently induced SGs at earlier times after infection as well as higher levels of SG-positive, infected cells compared to Eg101 infections.

During stress, stalled pre-mRNA complexes are held in SGs and when the fate of the cell is decided, either mRNA translation is reinitiated or the mRNAs are transferred to PBs for degradation (Anderson and Kedersha, 2008; Beckham and Parker, 2008; Sheth and Parker, 2003). Alterations of PB number occurs in response to various stress stimuli and our lab previously reported that the number of PBs in WNV Eg101 and dengue 2 virus infected BHK

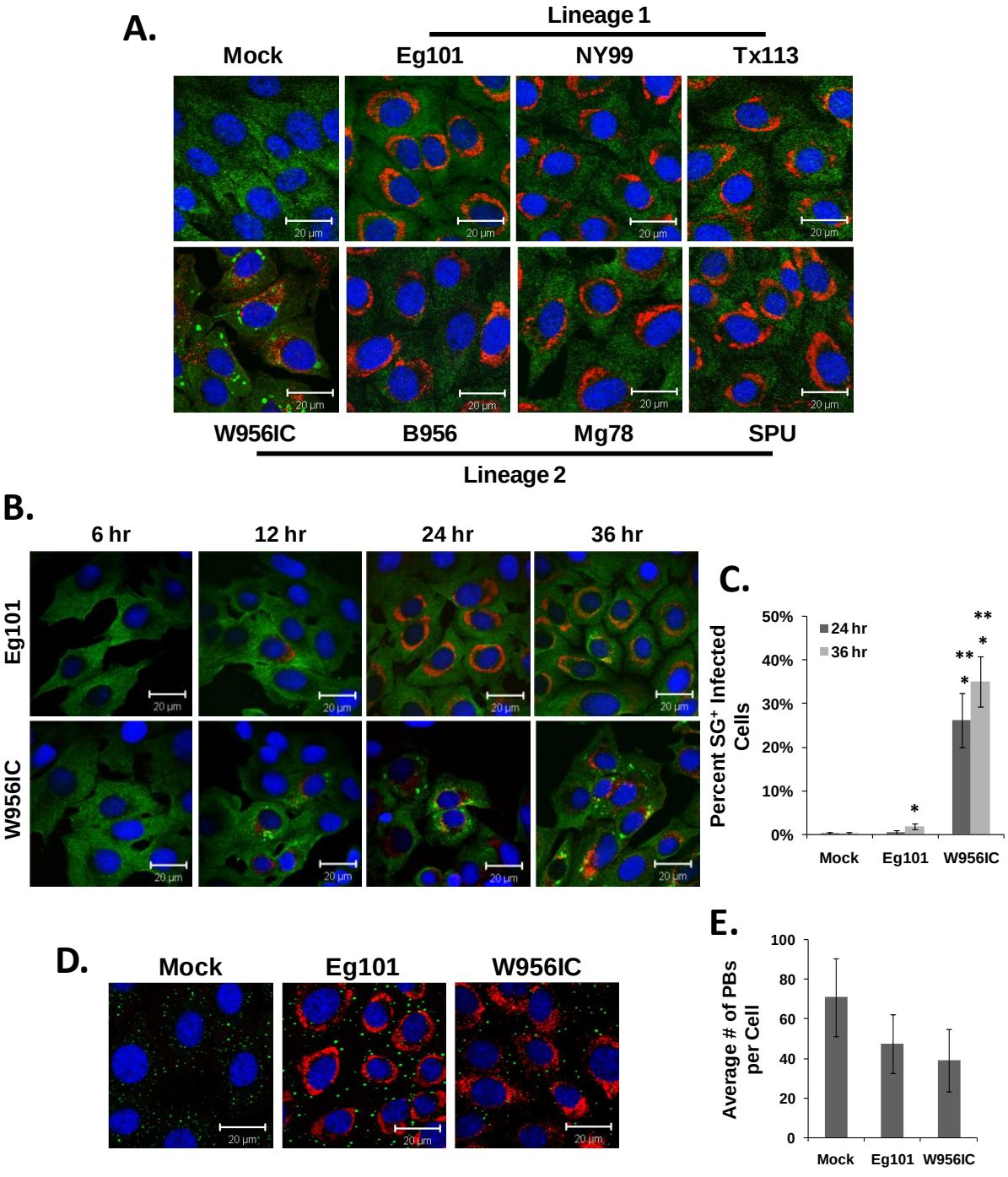
A.
Lineage 1
Mock
Eg101
NY99
Tx113
W956IC
B956
Mg78
SPU
Lineage 2
B.
6 hr
12 hr
24 hr
36 hr
Eg101
W956IC
C.
Percent SG+ Infected Cells
24 hr
36 hr
Mock
Eg101
W956IC
D.
Mock
Eg101
W956IC
E.
Average # of PBs per Cell
Mock
Eg101
W956IC

Figure 3.1. Stress granule formation induced by different strains of WNV. (A) BHK cells were infected with the indicated lineage 1 or lineage 2 WNV strain at a MOI of 1, fixed at 36 hr after infection and analyzed by confocal microscopy. Anti-G3BP antibody (green) was used to detect SGs, anti-dsRNA antibody (red) to detect WNV-infected cells and Hoechst dye (blue) to detect nuclei. Merged images are shown. **(B)** BHK cells were infected with either Eg101 (lineage 1) or W956IC (lineage 2-based infectious clone) at a MOI of 1 and analyzed for SG formation at the indicated times after infection. Antibody staining was the same as in panel A. Cells were collected at the indicated times after infection. Merged images are shown. **(C)** SG-positive infected cells were counted to determine the percentage of Eg101- and W956IC-infected cells containing SGs. * - represents significance compared to mock-infected cells at a 95% confidence interval ($p < 0.05$). ** - represents significance compared to Eg101-infected cells at a 95% confidence interval ($p < 0.05$). **(D)** BHK cells were infected with either Eg101 or W956IC at a MOI of 1 and analyzed for PB formation in infected cells. Anti-Dcp1a antibody (green) was used as a marker for PBs, anti-dsRNA antibody (red) was used to detect virus-infected cells, and Hoechst dye (blue) was used to detect nuclei. Merged images are shown. **(E)** PBs were counted to determine the average number per infected cell. * - represents significance compared to mock-infected cells at a 95% confidence interval ($p < 0.05$). Error bars indicate standard deviation of the mean.

cells was reduced by 24 hr after infection (Emara and Brinton, 2007; Teixeira et al., 2005). To determine the effect of a W956IC virus infection on PBs, W956IC-infected BHK cells were fixed at 36 hr after infection and analyzed by confocal microscopy. Mock-infected cells contained an average of ~70.93 PBs/cell, whereas Eg101-infected cells had ~47.5 PBs/cell and W956IC-infected cells had ~39.03 PBs/cell (Figure 3.1E). Both Eg101 and W956IC infections reduced PB numbers in infected cells with a slightly greater reduction seen in the W956IC-infected cells. PB numbers were also reduced in BHK cells infected with the NY99, Tx113, B956, Mg78, and SPU strains of WNV compared to mock infected cells (data not shown).

SG formation in WNV-infected cells is PKR-dependent

The phosphorylation of eIF2α which leads to SG formation in mammals is mediated by four kinases, PKR, PERK, GCN2 and HRI (Anderson and Kedersha, 2008). To determine which of these four eIF2α kinases mediates SG induction in WNV-infected cells, the eIF2α kinase knockout MEF cell lines $PKR^{-/-}$, $PERK^{-/-}$, $GCN2^{-/-}$, and $HRI^{-/-}$ (Han et al., 2001; Harding et al., 2000; Yang et al., 1995) were mock-infected or infected with WNV Eg101 or W956IC at a MOI of 1 and then fixed at 24 hr after infection and analyzed by confocal microscopy. C57BL/6 (B6) and $PERK^{+/+}$ (a second C57BL/6 cell line) MEFs that express all four of the eIF2α kinases were used as controls (Harding et al., 2001). SGs were detected in both Eg101- and W956IC-infected control, $PERK^{-/-}$, $GCN2^{-/-}$ and $HRI^{-/-}$ MEFs (Figure 3.2A). Quantification of the number of SG-positive, infected cells indicated that the control, $PERK^{-/-}$, $GCN2^{-/-}$, and $HRI^{-/-}$ MEF cultures each contained 8-12% SG-positive Eg101-infected cells or 15-20% SG-positive W956IC-infected cells at 24 hr (Figure 3.2B). However, no SGs were observed in $PKR^{-/-}$ cells infected with either virus (Figure 3.2A and B), indicating that SG induction in WNV-infected cells is PKR-

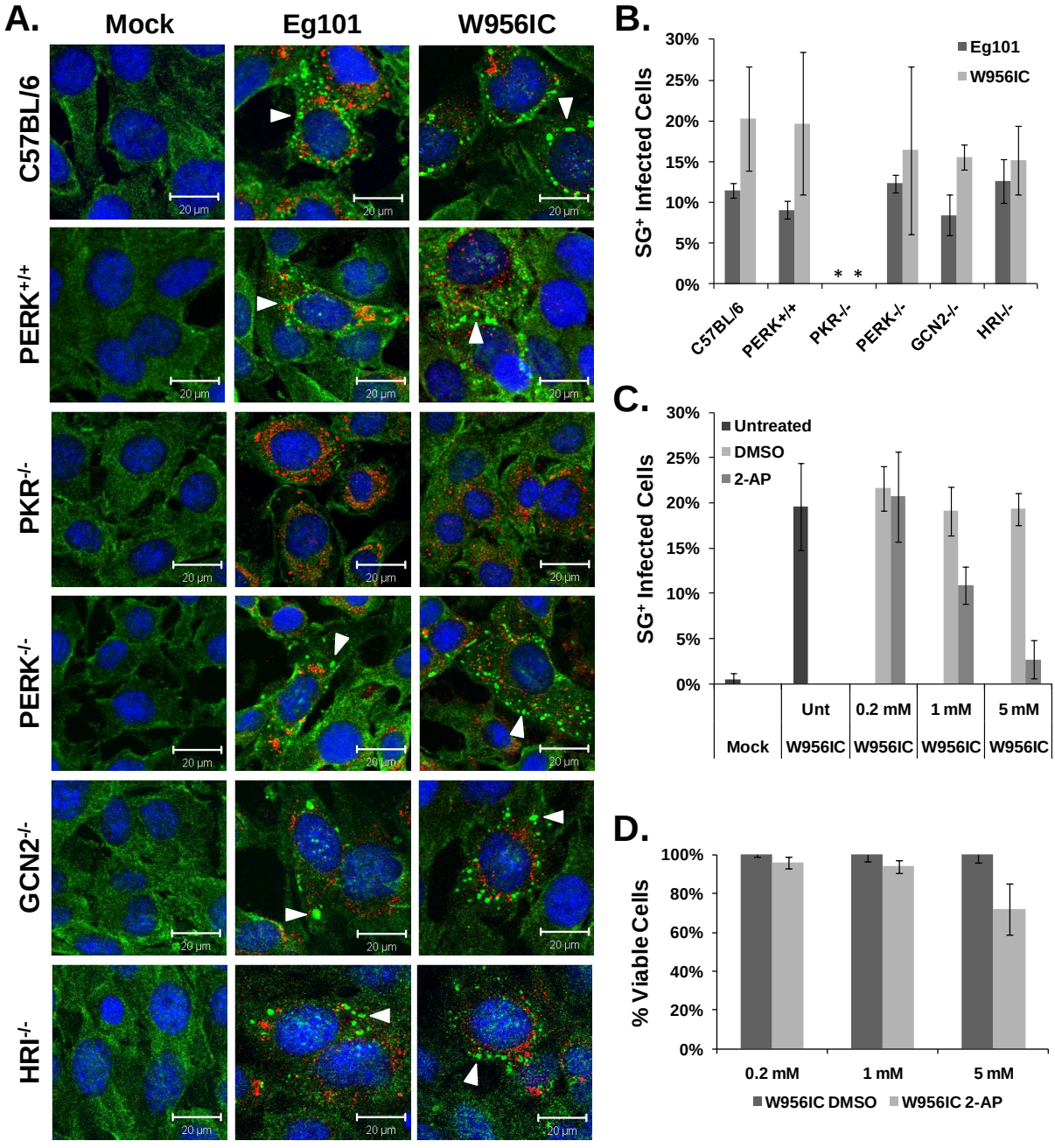
A.
Mock
Eg101
W956IC
C57BL/6
PERK+/+
PKR-/-
PERK-/-
GCN2-/-
HRI-/-
20 µm
B.
SG+ Infected Cells
30%
25%
20%
15%
10%
5%
0%
Eg101
W956IC
* *
C57BL/6
PERK+/+
PKR-/-
PERK-/-
GCN2-/-
HRI-/-
C.
SG+ Infected Cells
Untreated
DMSO
2-AP
Unt
0.2 mM
1 mM
5 mM
Mock
W956IC
W956IC
W956IC
W956IC
D.
% Viable Cells
100%
80%
60%
40%
20%
0%
0.2 mM
1 mM
5 mM
W956IC DMSO
W956IC 2-AP

Figure 3.2. Stress granule formation induced by WNV infection is PKR-dependent. (A) Control MEFs (C57Bl/6 and $PERK^{+/+}$) and eIF2α kinase knockout MEFs ($PKR^{-/-}$, $PERK^{-/-}$, $GCN2^{-/-}$, and $HRI^{-/-}$) were infected with WNV Eg101 or W956IC at a MOI of 1, fixed at 24 hr after infection and analyzed by confocal microscopy. SGs were detected with anti-G3BP antibody (green), WNV-infected cells with anti-dsRNA antibody (red), and nuclei with Hoechst dye (blue). Arrows denote SG-positive cells. Merged images are shown. **(B)** The total number of cells and the number of SG-positive, infected cells were counted and the percentage of infected cells containing SGs was determined as described in the Materials and Methods. * - represents significance compared to $PERK^{+/+}$ control cells for the indicated infection at a 95% confidence interval ($p < 0.05$). **(C)** During the course of infection, BHK cells were treated with different concentrations of 2-AP or DMSO (vehicle control), infected with W956IC at a MOI of 1, fixed at 24 hr after infection and analyzed by confocal microscopy to observe SG formation in infected cells. The percent of SG-positive, infected cells was calculated. **(D)** An MTT assay measuring cell viability during treatment of BHK cells infected with W956IC and treated with different concentrations of 2-AP or DMSO was performed as described in the Materials and Methods. Error bars indicate standard deviation of the mean.

dependent. Unlike BHK cells, these MEF cell lines are interferon (IFN)-competent and it was previously reported that IFN production during WNV Eg101 infections leads to elevated levels of PKR and phosphorylated PKR in IFN-competent cells as compared to $IFN^{-/-}$ cells (Elbahesh et al., 2011b), possibly leading to the slight induction of SGs in Eg101-infected MEF cell cultures; however, W956IC-infected MEFs still induced higher levels of SG-positive, infected cells compared to Eg101-infected cells.

As an alternative means of showing that PKR is the kinase responsible for the formation of SGs in WNV-infected cells, BHK cells were incubated with 2-aminopurine (2-AP), a purine analog that is a potent PKR inhibitor (Hu and Conway, 1993; Lindquist et al., 2011b). BHK cells were infected with W956IC virus (MOI of 1) for an hr and then incubated in media containing 2-AP or DMSO (solvent control) for 24 hr. Approximately 20% of the W956IC-infected cells were SG-positive in untreated, DMSO-treated and 0.2 mM 2-AP-treated cultures (Figure 3.2C). Only 10% of W956IC-infected cells were SG-positive in the 1 mM 2-AP-treated cultures and 3% were SG-positive in 5 mM 2-AP-treated cultures (Figure 3.2C). An MTT assay showed a <4% decrease in cell viability after of 0.2 mM 2-AP treatment, <6% decrease after 1 mM 2-AP treatment, and ~25% decrease after 5 mM 2-AP treatment of W956IC-infected cells (Figure 3.2D). The results suggest that the dose-dependent decrease in SG formation observed with 2-AP treatment was not due to a decrease in cell viability and further confirm that PKR is the kinase responsible for SG formation during infection.

To determine whether PKR plays an antiviral role during WNV infections, wildtype C57BL/6 and $PKR^{-/-}$ MEFs were infected with Eg101 or W956IC at a MOI of 1. Clarified culture fluids and cell lysates were collected for growth curve and Western blot analyses. These results showed that Eg101 infections, which slightly induce SGs in MEFs, were only slightly

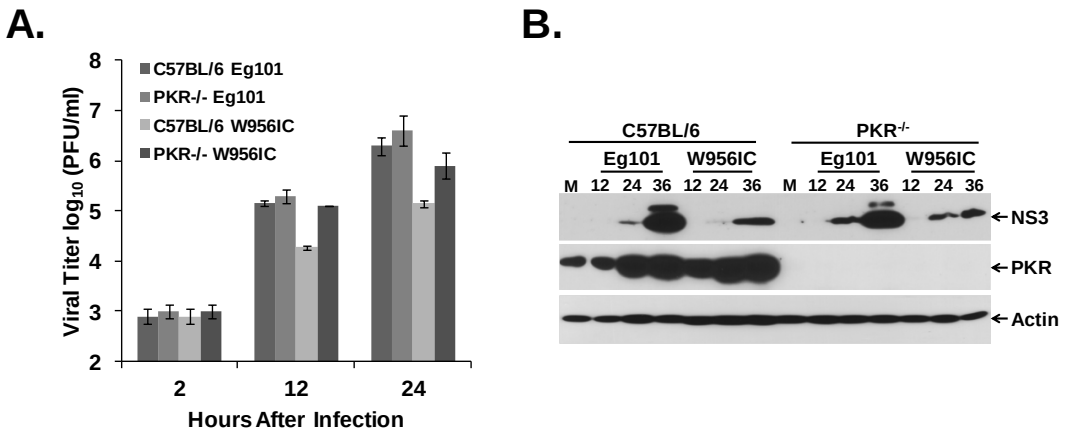

Figure 3.3. WNV Eg101 and W956IC infections replicate to higher levels in PKR$^{-/-}$ MEFs. (A) Wildtype C57BL/6 and PKR$^{-/-}$ MEFs were infected with WNV Eg101 and W956IC at a MOI of 1. Virus yields were measured by plaque assay at the indicated times after infection. **(B)** Western blot analysis of C57BL/6 and PKR$^{-/-}$ MEFs infected with WNV Eg101 or W956IC at a MOI of 1. Lysates were collected in RIPA buffer at the indicated times after infection and analyzed using antibodies to viral NS3, PKR, and actin.

increased in both the viral titers and viral NS3 protein in $PKR^{-/-}$ MEFs as compared to control cells, whereas W956IC infections that significantly induce SGs in MEFs showed dramatic increases in both viral titers and viral NS3 protein in $PKR^{-/-}$ MEFs (Figure 3.3A and B). These results suggest that PKR activation leading to SG formation during WNV infections is antiviral and suggests that avoiding PKR activation during WNV infection is advantageous to viral synthesis.

W956IC infections induce higher levels of phosphorylated PKR and phosphorylated eIF2α in BHK cells at early times after infection

Since activation of the Type I interferon signaling pathway has been reported to result in PKR activation (Su et al., 2006), BHK cells that are not responsive to Type I interferon were used for all subsequent experiments to insure that the PKR activation observed was due to the infection. Consistent with the higher number of SG-positive cells in W956IC-infected BHK cultures, higher levels of activated PKR (phosphorylated at Thr451) and phosphorylated eIF2α would also be expected in these cultures compared to WNV Eg101-infected cultures. Cell lysates collected at various times after infection with WNV Eg101 or W956IC were analyzed by Western blotting for total and phosphorylated PKR and eIF2α. PKR phosphorylation was not detected in any of the WNV Eg101-infected lysates; however, phosphorylated PKR was detected in the W956IC samples from 16 through 28 hr after infection (Figure 3.4A). eIF2α phosphorylation in W956IC-infected cells was detected starting at 16 hr after infection (Figure 3.4A). Because a more sensitive Western blot detection system was used in this study than in our previous study (Emara and Brinton, 2007), some phosphorylated eIF2α was detected at 24 and 28 hr after infection with WNV Eg101. In contrast, similar levels of total eIF2α were detected by

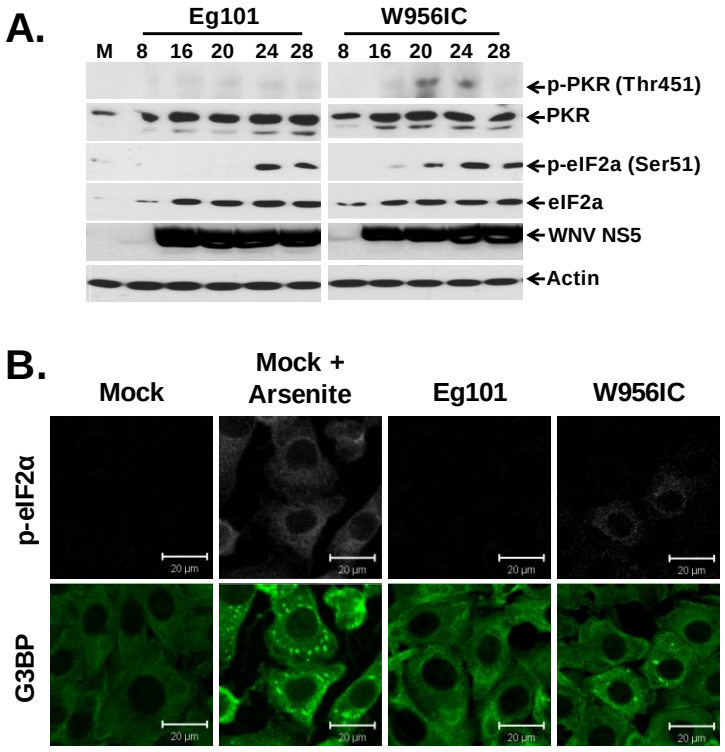

Figure 3.4. W956IC-infected cells have elevated levels of phosphorylated PKR and eIF2α. (A) Western blot analysis of BHK cells infected with WNV Eg101 or W956IC at a MOI of 1. Lysates were collected in RIPA buffer at the indicated times after infection and analyzed using antibodies specific for the detection of phosphorylated PKR (Thr541), PKR, phosphorylated eIF2α (Ser51), eIF2α, and actin. **(B)** BHK cells were infected with WNV Eg101 or W956IC at a MOI of 1, fixed at 24 hr after infection and analyzed by confocal microscopy. Anti-G3BP antibody (green) was used to detect SGs and anti-p-eIF2α antibody (white) to detect p-eIF2α. More than 95% of the cells were infected.

16 hr after infection with either virus. The increase in eIF2α phosphorylation in the Eg101-infected cells in the absence of PKR phosphorylation suggested that it was due to the activation of another eIF2α kinase. The increase in phosphorylated eIF2α at later times of infection correlated with the increase in SG-positive, WNV Eg101-infected BHK cells from <1% at 24 hr to <3% at 36 hr after infection.

To determine whether SG-positive, infected cells contained elevated levels of phosphorylated eIF2α, BHK cells were infected with WNV Eg101 or W956IC, fixed at 24 hr after infection and analyzed by confocal microscopy. The level of p-eIF2α was high in all cells that were SG-positive (Figure 3.4B). However, not all p-eIF2α-positive cells contained SGs (data not shown) suggesting that there may be a threshold level of p-eIF2α needed for SG induction or that additional cell factors/conditions may also be involved in SG formation.

Mapping the viral determinants involved in enhanced SG induction by W956IC virus infection

The W956IC cDNA plasmid is very stable in bacteria and has been a useful tool for recovering WNV genomes with engineered mutations (Basu and Brinton, 2011). The W956IC cDNA was constructed from a highly passaged WNV B956 virus stock designated 956D117B3 (Yamshchikov et al., 2001). The 956D117B3 sequence differs from that of B956 by 32 single nt substitutions within the coding region (Yamshchikov et al., 2004; Yamshchikov et al., 2001). Although 956D117B3 cDNA was used to construct the majority of the W956IC infectious clone, the C-terminus of the NS5 gene through the 3′ UTR region was amplified from WNV Eg101 genomic RNA (Yamshchikov et al., 2001). To identify viral components associated with less efficient SG induction, additional chimeric W956IC genomes were made by replacing one or

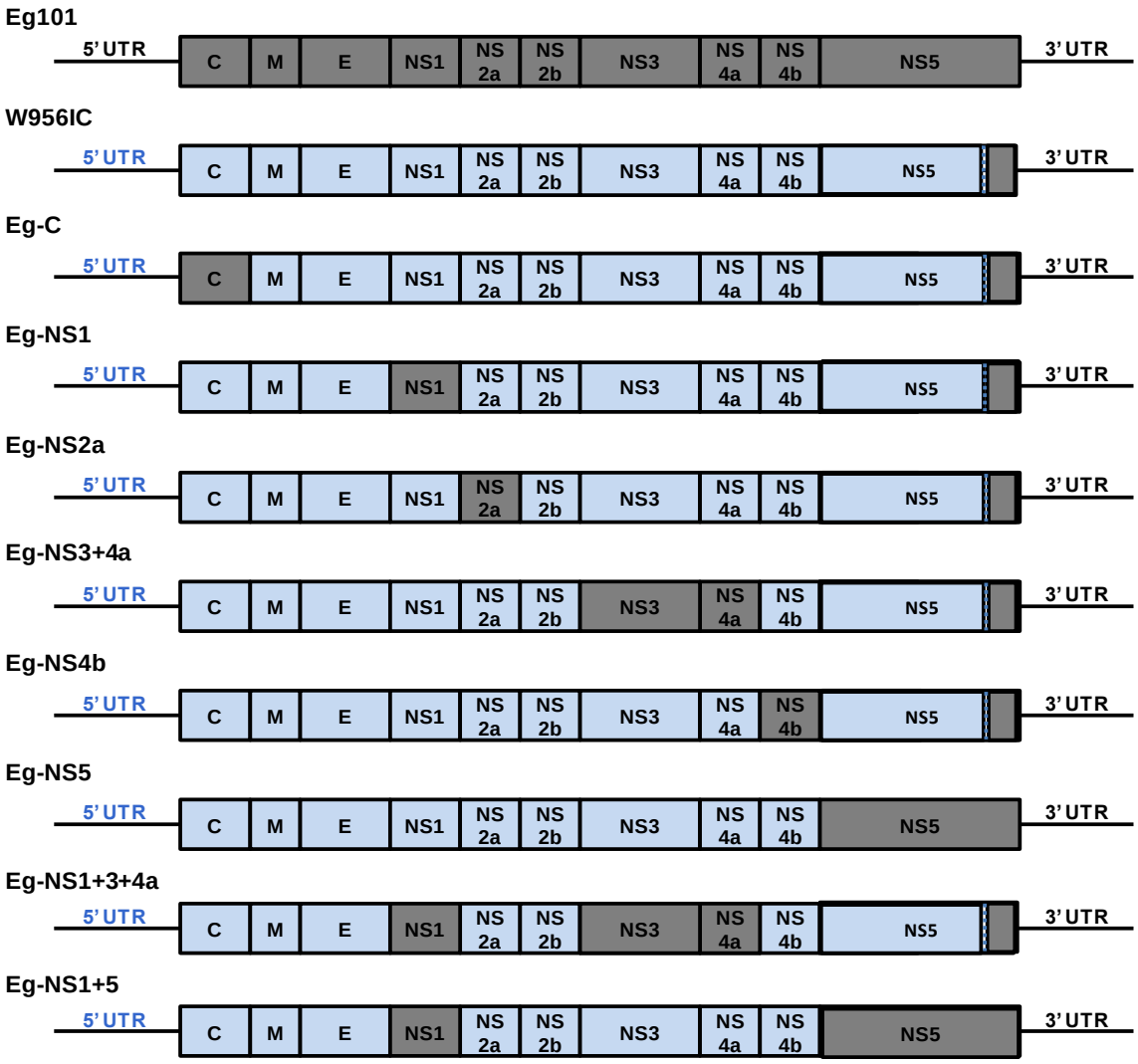

Figure 3.5. Schematic representation of the WNV W956IC-Eg101 chimera genomes. Eg101 sequences are shown in grey and W956IC sequences are shown in blue. The majority of the W956IC genome sequence is from D117B956 but the C-terminus of NS5 and the 3′ UTR are from Eg101. Additional chimeric viruses were created by replacing one or more W956IC genes with the Eg101 equivalent on the W956IC backbone.

more W956IC genes with the Eg101 equivalent as described in the Materials and Methods. Eg-C (capsid), Eg-NS1, Eg-NS2a, Eg-NS3+4a, Eg-NS4b, Eg-NS5, Eg-NS1+3+4a, and Eg-NS1+5 chimeric viruses were constructed (Figure 3.5). All of the chimeric WNV infectious clones constructed contained the 3′ UTR from Eg101 and all but the Eg-NS5 and Eg-NS1+5 clones contained the 956D117B3/Eg101 hybrid NS5 gene.

BHK cells were infected with one of the chimeric viruses, fixed at 36 hr after infection and analyzed for SGs by confocal microscopy. Consistent with the data shown in Figure 3.1, WNV Eg101 infections induced SGs in <3% of infected cells while W956IC infections induced SGs in ~30% of the infected cells at 36 hr after infection (Figure 3.6A and B). The Eg-NS1 (~7%), Eg-NS2a (~15%), Eg-NS3+4a (~8%), Eg-NS4b (~10%), and Eg-C (~20%) chimeric virus infections induced intermediate numbers of SG-positive, infected cells by 36 hr after infection, while the Eg-NS5 (<3%), Eg-NS1+3+4a (<3%), and Eg-NS1+5 (<3%) chimeric virus infections induced few SG-positive, infected cells similar to Eg101 infections (Figure 3.6A and B). The data indicate that either the replacement of the N-terminal region of NS5 or of the NS1, NS3 and NS4a genes with Eg101 sequence recreated the WNV Eg101 SG phenotype.

The growth kinetics of the various chimeric viruses was analyzed to determine whether the differential SG phenotypes were due to differences in the growth efficiencies of these viruses. BHK cells were infected with WNV Eg101, W956IC or one of the chimeric viruses at a MOI of 1 and culture fluid was collected at various times after infection. Eg101 and W956IC infections produced similar virus yields at 24 and 36 hr after infection (Figure 3.6C). However, W956IC infections produced significantly more progeny virus than Eg101 infections at 12 hr after infection (Figure 3.6C). The yields produced by Eg-C, Eg-NS1, Eg-NS2a, Eg-NS3+4a, and Eg-NS4b chimeric virus infections at 12 hr were similar to that produced by a W956IC infection,

while the 12 hr yields from Eg-NS5, Eg-NS1+3+4a, and Eg-NS1+5 infections were comparable to that from an Eg101 infection (Figure 3.6C). Virus yields from the Eg-C, Eg-NS1, Eg-NS2a, Eg-NS3+4a, and Eg-NS4b chimeric virus infections at 24 and 36 hr were similar to those of both the Eg101 and W956IC infections (Figure 3.6C). However, the Eg-NS5 and Eg-NS1+3+4a chimeric virus infections produced slightly reduced virus yields at 24 and 36 hr after infection. Although the yield of Eg-NS1+5 virus was slightly decreased at 24 hr, levels comparable to Eg101 and W956IC virus infections were observed by 36 hr (Figure 3.6C). These data indicate that the replication efficiencies of none of the chimeric viruses were significantly compromised.

Since PKR is activated by double stranded regions of viral RNA (Garcia et al., 2007), the levels of intracellular viral plus strand RNA produced by Eg101, W956IC and the chimeric viruses early after infection was next assessed. BHK cells were infected with WNV Eg101, W956IC or a chimeric virus at a MOI of 1 and total cellular RNA was collected at 12 hr after infection. The number of viral genome copies per 1 µg of total RNA was quantified as described in the Materials and Methods. Consistent with the 12 hr viral yields, W956IC infections synthesized the highest levels of viral RNA by 12 hr after infection while Eg101 infections synthesized the least (Figure 3.6D). The Eg-C, Eg-NS1, Eg-NS2a, Eg-NS3+4a and Eg-NS4b chimeric virus infections produced higher levels of early intracellular viral RNA like a W956IC infection, while the Eg-NS5, Eg-NS1+3+4a, and Eg-NS1+5 infections produced lower levels of early viral RNA similar to an Eg101 infection (Figure 3.6D). The results indicate that more efficient SG induction in infected cells correlates with increased levels of viral RNA synthesis at early times after infection. The data further suggest that interaction between viral nonstructural proteins and possibly also between nonstructural proteins and viral RNA and/or cell proteins are

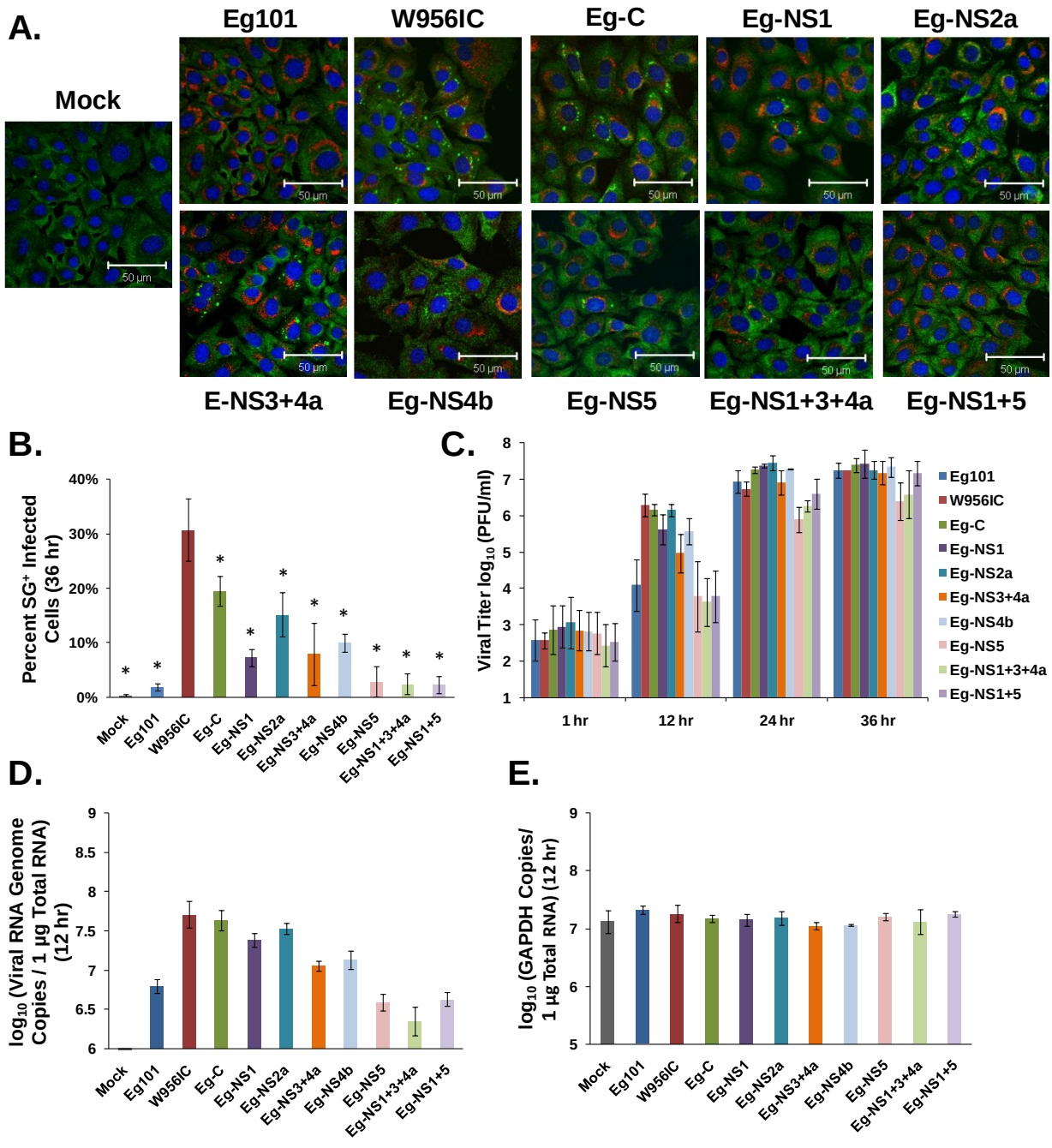
A.
Mock
Eg101
W956IC
Eg-C
Eg-NS1
Eg-NS2a
E-NS3+4a
Eg-NS4b
Eg-NS5
Eg-NS1+3+4a
Eg-NS1+5
50 µm
B.
Percent SG+ Infected Cells (36 hr)
40%
30%
20%
10%
0%
C.
Viral Titer log10 (PFU/ml)
1 hr
12 hr
24 hr
36 hr
D.
log10 (Viral RNA Genome Copies / 1 µg Total RNA) (12 hr)
E.
log10 (GAPDH Copies/ 1 µg Total RNA) (12 hr)

Figure 3.6. The levels of early viral RNA synthesis correlate with the level of SG-positive, infected cells and virus yield. (A) BHK cells were infected with the indicated WNV chimeric virus at a MOI of 1, fixed at 36 hr after infection and analyzed by confocal microscopy. SGs were detected with anti-G3BP antibody (green), WNV-infected cells with anti-dsRNA antibody (red), and nuclei with Hoechst dye (blue). Merged images are shown. **(B)** Total and SG-positive, infected cells were counted and the percentage of infected cells containing SGs was determined. * - Significance compared to W956IC was determined at a 95% confidence interval ($p < 0.05$). **(C)** BHK cells were infected with the indicated chimeric virus at a MOI of 1 and the virus yield was determined by plaque assay. **(D)** BHK cells were infected with the indicated chimeric virus at a MOI of 1 and total RNA was extracted and purified at 12 hr after infection. The number of viral genome copies in each sample was determined using probes targeting the viral NS1 gene as described in the Materials and Methods. **(E)** To determine the accuracy of loading, the amount of GAPDH RNA in each sample was measured to show that the same amount of total RNA was used throughout the experiment. Error bars indicate standard deviation of the mean.

involved in suppressing early viral RNA synthesis more effectively in cells infected with natural WNV strains.

Enhanced early viral RNA synthesis in W956IC-infected cells results in cytoplasmic exposure of viral dsRNA

Viral dsRNA in infected cells is sensed by the pathogen recognition receptors (PRRs), PKR, retinoic acid inducible gene I (RIG-I) and melanoma differentiation factor 5 (MDA5) (Garcia et al., 2007; Kato et al., 2008). Flavivirus dsRNAs are thought to evade detection by cell RNA sensors by localization within ER membrane vesicles (Overby et al., 2010). It was previously reported that treating cells with 0.01% Triton X-100 permeabilizes the plasma membrane but leaves the intracellular ER membranes intact while 0.1% Triton X-100 solubilizes both plasma and ER membranes (Mertens et al., 2010). Differential membrane permeabilization was used to assess viral dsRNA membrane association at early times after infection. BHK cells were infected with WNV Eg101 or W956IC at a MOI 5 and permeabilized with either 0.1% or 0.01% Triton X-100 at 12 hr after infection. After fixation and differential permeabilization, the cells were analyzed for the presence of viral dsRNA and SGs by confocal microscopy. Viral dsRNA was detected in the majority of Eg101- and W956IC-infected cells permeabilized with 0.1% Triton X-100 (Figure 3.7A). In contrast, after permeabilization with 0.01% Triton X-100, viral dsRNA was detected in ~25% of the W956IC-infected cells but in only ~4% of the Eg101-infected cells (Figure 3.7B). Similar to what was seen with the experiments quantifying SG-positive, infected cells, W956IC infections produced a higher number of cells with detectable dsRNA compared to Eg101 infections (Figure 3.7A). The higher percent of infected cells with detectable dsRNA with the 0.01% Triton X-100 treatment was likely due to the use of a MOI of

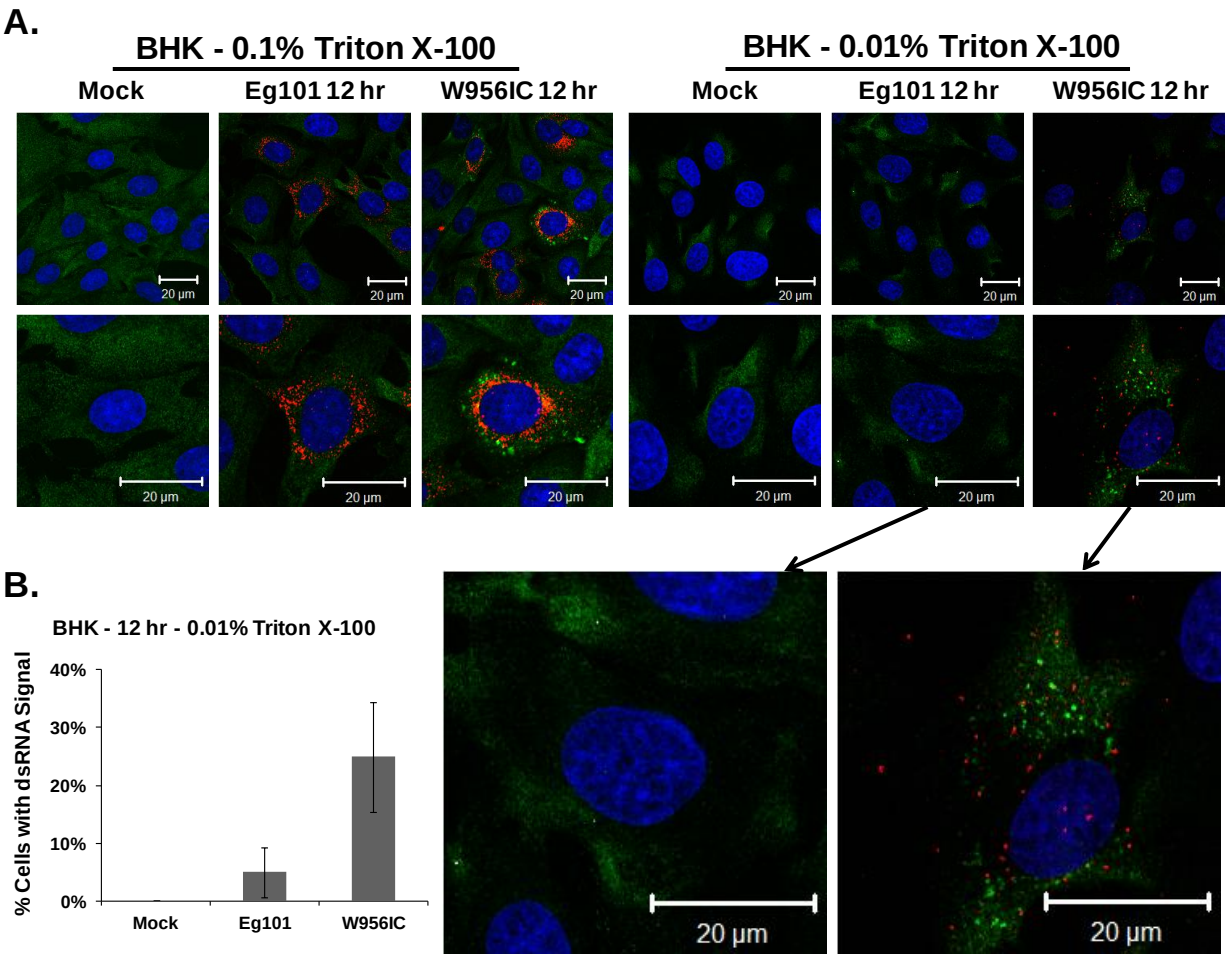

Figure 3.7. Exposed viral dsRNA was detected in 0.01% Triton X-100 permeabilized W956IC-infected but not Eg101-infected cells. (A) BHK cells were infected with WNV Eg101 or W956IC at a MOI of 5, fixed at 12 hr after infection, permeablized with either 0.1% or 0.01% Triton X-100 and analyzed by confocal microscopy. Anti-dsRNA antibody (red) was used to detect viral dsRNA, anti-G3BP (green) to detect SGs, and Hoechst dye (blue) to detect nuclei. Merged images are shown. (B) The total number of cells and the number of dsRNA signal-positive cells from 0.01% Triton X-100-treated cells were counted and the percentage of cells containing detectable dsRNA was determined.

5 instead of 1. Importantly, these data also showed that the W956IC-infected cells that contained elevated levels of exposed viral dsRNA also contained SGs (Figure 3.7A), suggesting that when viral dsRNA is not protected by cytoplamic membranes, it can activate PKR leading to eIF2α phosphorylation and SG formation. Why high levels of early viral RNA are produced in a few of the WNV Eg101-infected BHK cells and why a maximum of ~20-30% of W956IC-infected cells have high levels of early viral RNA is currently not known and suggest that additional cell factors may also be involved in the regulation early viral RNA synthesis levels.

DISCUSSION

The cytoplasmic PRR, PKR, is activated by viral dsRNA. Activated PKR phosphorylates Ser51 of eIF2α which attenuates cap-dependent translation and usually leads to the formation of SGs. Because the WNV genome is capped, its translation would be expected to be inhibited by eIF2α phosphorylation. In contrast, members of other flavivirus genera, such as pestiviruses and hepatitis C viruses, initiate translation from an IRES and their translation would not be expected to be affected by eIF2α phosphorylation (Robert et al., 2006). Another reason why flavivirus infections would benefit from not inducing the formation of SGs is our previous finding that the SG-nucleating proteins TIA-1 and TIAR facilitate plus-strand viral RNA synthesis (Emara and Brinton, 2008; Li et al., 2002). Infections with viruses have previously been reported to induce SGs through PKR activation but only in a subset of the infected cells (Hanley et al., 2010; Lindquist et al., 2011b; Venticinque and Meruelo, 2010). Infections with natural lineage 1 and lineage 2 strains of WNV did not activate PKR but infections with the chimeric W956IC virus did and SG induction by W956IC virus infections was shown to be dependent on PKR. Similar to our findings with WNV, infections with a respiratory syncytial virus (RSV) chimeric virus

(LeC) induced a higher number of SG-positive, infected cells than natural RSV strain infections through the activation of PKR (Groskreutz et al., 2010; Hanley et al., 2010; Lindquist et al., 2011a; Lindquist et al., 2011b). Although many types of viruses have evolved mechanisms to inhibit PKR activation (Garcia et al., 2007), a previous study from our lab showed that WNV Eg101 infections do not actively inhibit PKR activation but instead do not activate PKR (Elbahesh et al., 2011b). The slight increase in SG-positive, Eg101-infected cells observed at later times of infection (from ~1% at 24 hr to ~3% by 36 hr) could be caused by PERK activation due to induction of an unfolded protein response (UPR). Natural WNV infections were previously reported to induce the UPR at later times of infection (Ambrose and Mackenzie, 2011). The UPR can activate PERK, another of the eIF2α kinases. Activated PERK was previously detected in WNV-infected cells at later times of infection (Ambrose and Mackenzie, 2011).

The chimeric junction in the W956IC genome produces a 956D117B3/Eg101 hybrid NS5. This hybrid NS5 did not cause a reduction in the replication efficiency of the W956IC virus since the yields from Eg101 and W956IC infections were comparable at 24 to 36 hr. In fact, the chimeric W956IC virus synthesized RNA more efficiently at early times after infection than did Eg101. The increased levels of early viral RNA synthesis observed in W956IC-infected cells correlated with an increase in PKR activation and SG formation. The replication of flavivirus RNA in infected cells was previously reported to be biphasic (Chu and Westaway, 1985; Cleaves et al., 1981). Genomic and complementary minus strand RNAs are replicated symmetrically at low levels until about 10 to 12 hr after infection. Thereafter, RNA replication increases exponentially and is asymmetric with genome RNA synthesis predominating. The exponential increase in viral RNA replication occurs after sufficient virus-induced proliferation and

rearrangement of ER membranes has occurred (Lindenbach, 2007). Flavivirus infections as well as some other positive-sense RNA virus infections form vesicles in ER membranes that serve as the sites of exponential viral RNA synthesis and viral nonstructural proteins have been reported to be involved in cytoplasmic membrane remodeling (den Boon and Ahlquist, 2010; Gillespie et al., 2010; Welsch et al., 2009). These vesicles open to the cytoplasm through a small pore and data from several studies suggest that these vesicles protect viral dsRNA from detection by cytoplasmic sensors (den Boon and Ahlquist, 2010; Gillespie et al., 2010; Overby et al., 2010; van Hemert et al., 2008; Welsch et al., 2009).

How flavivirus RNA replication is differentially regulated during the early and late phases of viral RNA synthesis is not known. It was previously shown that cyclization of the genome through basepairing between 3′ and 5′ RNA sequences was required for RNA replication (Basu and Brinton, 2011; Hahn et al., 1987; Zhang et al., 2008). Even though in the chimeric W956IC genome, the 3′ cyclization, DAR and UAR sequences were from Eg101 and the 5′ cyclization, DAR and UAR sequences were from W956, the long distance 5′-3′ basepairing interactions were completely conserved (data not shown). It has also been reported that the WNV 5′ UTR interacts with the NS5 protein, which contains the methyltransferase and RNA-dependent RNA polymerase domains. Alteration of this RNA-protein interaction dramatically affected the replication efficiency of WNV (Dong et al., 2008). The WNV Eg101 and W956IC 5′ UTRs only differ by 1 nt located in a position that was not previously shown to be involved in the interaction with NS5, suggesting that this substitution would not affect viral RNA replication efficiency. It is possible that the viral nonstructural protein complexes assume different conformations during the early and late phases of viral RNA replication. Replication complex conformations could be mediated by interactions with different cell partners and/or different

cellular membrane microenvironments. The three WNV chimeras that displayed both low levels of early viral RNA synthesis and SG induction similar to Eg101 were Eg-NS5, Eg-NS1+3+4a and Eg-NS1+5. The polyprotein sequences of Eg101 and W956IC were aligned and revealed a number of amino acid changes in the nonstructural proteins as there are 32 aa changes in NS1, 30 aa changes in NS3+4a, and 33 aa changes in NS5. The majority of these mutations are within the same class and are unlikely to modify the function of these proteins. These analyses identified five mutations within NS1, NS3+4a and NS5 that are unique to W956IC and D117B956 compared to the various WNV strains tested and are currently being tested for their effect on early viral replication efficiency and SG induction. However, it is more likely that the difference in replication efficiencies between these viruses is due to a combination of mutations and not to a sole residue mutation as evidenced by the lack of a single viral protein causing the difference in SG induction. The finding that chimeras with either an NS5 with both its N- and C-terminal regions from Eg101 or a combination of the Eg101 NS1, NS3 and NS4a proteins produced low levels of early viral RNA synthesis support the hypothesis that viral nonstructural protein conformations and interactions within replication complexes play a role in down-regulating RNA synthesis early during natural WNV infections. Similarly, a previous study mapping flavivirus nonstructural proteins involved in inhibiting IFN signaling also did not identify a single protein as the cause for the difference and further supports the findings of the present study (Ambrose and Mackenzie, 2011).

It is currently not known how viral dsRNA is protected from cytoplasmic RNA sensors during early low level symmetric viral RNA synthesis. The results of the present study indicate that essentially all of the viral dsRNA present at 12 hr in the majority of Eg101-infected cells was associated with cytoplasmic membranes, while some of the dsRNA in ~25% of W956IC

virus-infected cells was not. This finding suggests that natural strains of WNV are able to carefully match the level of RNA replication with the degree of cytoplasmic membrane remodeling. When this coordination is dysregulated, such as in W956IC-infected cells, higher levels of early RNA replication exceeds the capacity of the available virus-induced membrane protection exposing some of the viral dsRNA and results in PKR activation, eIF2α phosphorylation and SG formation.

MATERIALS AND METHODS

Cells

All cell lines used were maintained at 37ºC in 5% CO_2. Baby hamster kidney 21 strain W12 (BHK) cells (Vaheri et al., 1965) and a C3H/He mouse embryo fibroblast (MEF) cell line (Scherbik et al., 2006) were maintained in minimal essential medium (MEM) supplemented with 5% heat-inactivated fetal bovine serum (FBS), glutamine, and 10 µg/ml gentamicin. C57BL/6, $PERK^{+/+}$, $PKR^{-/-}$, $PERK^{-/-}$, $GCN2^{-/-}$, and $HRI^{-/-}$ MEFs were maintained in Dulbecco's Modified Eagle Medium (DMEM) supplemented with 10% FBS, glutamine, and 10 µg/ml gentamicin. The $PERK^{-/-}$, $GCN2^{-/-}$, and $HRI^{-/-}$ cells are all allelic knockouts, whereas the $PKR^{-/-}$ cells express a nonfunctional PKR due to a deletion of the RNA-binding domain found in exons 2-4 (Yang et al., 1995). The $PERK^{+/+}$, $PERK^{-/-}$, $GCN2^{-/-}$ and $HRI^{-/-}$ MEFs were provided by David Ron (New York University School of Medicine, New York, NY) and the $PKR^{-/-}$ MEFs were provided by Robert Silverman (Lerner Research Institute, Cleveland Clinic, Cleveland, OH).

Viruses

WNV Eg101 and W956IC were prepared by infecting BHK cell monolayers at a multiplicity of infection (MOI) of 0.1 and harvesting culture fluid at 32 hr after infection. Clarified culture fluid was aliquoted and stored at -80ºC. Aliquots of WNV NY99, Tx113, B956, Mg78 and SPU were provided by Robert Tesh (University of Texas Medical Branch, Galveston) and stocks were grown in BHK cells as described for Eg101. Titers of the virus stocks were: Eg101 $1x10^8$; W956IC $5x10^7$; NY99 $1x10^8$; Tx113 $5x10^7$; B956 $1x10^7$; Mg78 $3x10^6$; and SPU $7x10^7$. Virus infectivity was assessed by plaque assay on BHK monolayers as previously described (Scherbik et al., 2007b).

Construction of chimeric viruses

The construction of the 956D117B3/Eg101 infectious clone SP6WNEg3′/Xba, here referred as W956IC, was described previously (Yamshchikov et al., 2001). The capsid, NS1, NS2A, NS3-NS4A, NS4B, NS5 lineage 2 genes or combinations of these genes were replaced in the W956IC backbone with the corresponding lineage 1 genes from Eg101. RNA was purified from WNV Eg101 and specific cDNA fragments were obtained by RT-PCR amplification using specific primers and the SuperScript® One-Step RT-PCR System with Platinum® Taq DNA Polymerase (Invitrogen). The primers were designed based on the Eg101 sequence (GenBank# AF260968). Nt changes, that did not alter the amino acid sequence, were included in some primers to introduce unique restriction sites present in the W956IC sequence. The nt coordinates indicated below are from the 956D117B3 sequence (GenBank# M12294). To create a W956IC chimera with a capsid gene from Eg101 (Eg-Cap), a fragment containing two unique BglII sites (89-465 nts) was amplified from Eg101 RNA and a fragment containing two MfeI sites (465-918

nts) was amplified from W965IC, a BglII-MfeI fragment was obtained by overlapping PCR and cloned into W956IC. Additional chimeras were created by amplifying the following fragments from Eg101 RNA and cloning them into W956IC: Eg-NS1, a MunI (nt 2393) - NsiI (nt 3513) fragment; Eg-NS2a, a NsiI (nt 3513) - BstB1 (nt 5135) fragment; Eg-NS3+4a, a BstB1 (nt 5135) - SphI (nt 6777) fragment; Eg-NS4b, a SphI (nt 6777) - FseI (nt 7021) fragment; and Eg-NS5, a FseI (nt 7021) - AvrII (nt 8901) fragment. For the Eg-NS1+3+4a chimera, a MunI (nt 2393) - NsiI (nt 3513) fragment was amplified from Eg101 and cloned to the Eg-NS3+4a chimera and for the Eg-NS1+5 chimera, a MunI (nt 2393) - NsiI (nt 3513) fragment was amplified from Eg101 and cloned into the Eg-NS5 chimera. All of the chimeric clones were validated by sequencing. The sequences of the primers used in this study are available upon request.

Confocal Microscopy

Confocal microscopy was performed as previously described (Emara and Brinton, 2007). Virus-infected cells were detected with anti-dsRNA antibody (English & Scientific Consulting; Szirak, Hungary). SGs were detected with anti-G3BP (Ras-GAP-SH3-binding protein) (Abcam and Sigma Aldrich). Anti-Dcp1a antibody (a gift from J. Lykke-Anderson; University of Colorado, Boulder, CO) was used to detect PBs. AlexaFluor 350-, AlexaFluor 488-, or AlexaFluor 594-labeled secondary antibodies (Invitrogen) were diluted in blocking buffer containing 0.5 µg/ml Hoechst 33258 dye (Molecular Probes, Bedford, MA) to detect nuclei. Images were taken using a LSM 510 confocal microscope (Zeiss, Oberkochen, Germany) with either a 63x water-immersion or 100x oil-immersion objective. Images were analyzed with Zeiss LSM Image Browser software.

SG-Postive Infected Cell Quantification

A wide-field immunofluorescence microscope with a 40x objective was used to acquire images of large fields of WNV-infected cells stained with anti-dsRNA antibody to detect infected cells and anti-G3BP to detect SG-positive, infected cells at the indicated times after infection and/or treatment. The percentage of SG-positive, infected cells was calculated. 100 cells per field, from four or more fields of view per treatment, were counted. Quantification was done on cells from three separate experiments and statistical significance was determined at a 95% confidence interval.

Quantification of viral RNA

In vitro transcribed viral genome RNA of a known concentration was serially diluted and used to generate a standard curve ($y = -0.2472x + 10.751$, where "x" represents the cycle threshold (CT)) by real time RT-PCR. This standard curve was then used to determine the absolute amount of viral RNA in each cell extract sample. BHK cells were infected with a strain of WNV at a MOI of 1 and lysed 12 hr after infection. Total cell RNA was purified using TriReagent (Molecular Research Center) according to the manufacturer's protocol and quantified by spectophotometry at OD_{260}. The mean CT value for each RNA sample was determined by real time RT-PCR using a probe targeting the WNV NS1 gene. The mean CT value was plotted on the standard curve to estimate the number of viral genome copies per 1 µg of total RNA in each cellular extract.

Western blotting

Western blot analyses were performed as previously described (Scherbik et al., 2006). Primary antibodies include: anti-p-PKR (T451) (Millipore), anti-PKR (SCBT), anti-p-eIF2α (Ser51), anti-eIF2α (Cell Signaling), anti-NS3 (R&D Systems), and anti-actin (Abcam). The secondary antibodies included anti-rabbit-HRP, anti-mouse-HRP (Cell Signaling), and anti-goat-HRP (SCBT). All antibodies were diluted in 5% NFDM except for p-PKR and p-eIF2α, which were in 5% BSA.

Plaque Assay

Virus yields were determined as previously described (Scherbik et al., 2007b).

MTT Assay

Confluent monolayers in 96-well plates were infected with W956IC at a MOI of 1. Virus was adsorbed for 1 hr at room temperature and the cells were then incubated in fresh media containing different concentrations of 2-aminopurine (2-AP) or DMSO (solvent control) for 24 hr at 37ºC in 5% CO_2. A CellTiter 96® non-radioactive cell proliferation assay was the done according to the manufacturer's protocol (Promega).

ADDITIONAL DATA

Previous work in the lab showed that WNV Eg101 and dengue 2 virus infections did not induce the formation of SGs but inhibited the formation of SGs by oxidative stress (i.e. arsenite treatment) (Emara and Brinton, 2007). None of the natural lineage 1 or lineage 2 WNV strains tested induced SG formation in infected cells, but that W956IC infections did (Figure 3.1). The ability of these additional natural WNV strains and W956IC infections to inhibit the formation of arsenite-induced (HRI-mediated) SGs was also tested. BHK cells were infected with WNV Eg101, NY99, Tx113, W956IC, B956, Mg78 or SPU at a MOI of 1, treated with 0.5 mM arsenite for 30 min prior to fixation at 17 or 24 hr, and analyzed by immunofluorescence. SGs were detected in each of the WNV strains at 17 hr after infection (Figure 3.8A) and was consistent with previously published data suggesting that the ability of SG inhibition was less efficient at earlier times of a WNV infection (Emara and Brinton, 2007). Similar to Eg101, infections with each natural WNV strain tested were able to inhibit the formation of SGs by arsenite treatment at 24 hr after infection (Figure 3.8B and C). This was also the case for W956IC infections that normally induce higher numbers of SG-positive cells. For each virus strain tested, the inhibition of SGs at 17 hr after infection was less efficient (Figure 3.8A). These results suggest that the ability of WNV strains to inhibit arsenite-induced SG formation increases with time after infection.

PERK has been reported to be activated by the treatment of cells with dithiothreitol (DTT) which causes unfolded proteins to accumulate in the ER and leads to the unfolded protein response (Liang et al., 2006). To confirm that DTT treatment induces the formation of SGs, BHK cells were treated with 1 mM, 2 mM or 10 mM DTT for 30 min or 60 min prior to fixation and analyzed for SGs by immunofluorescence. The 2 mM and 10 Mm DTT concentrations

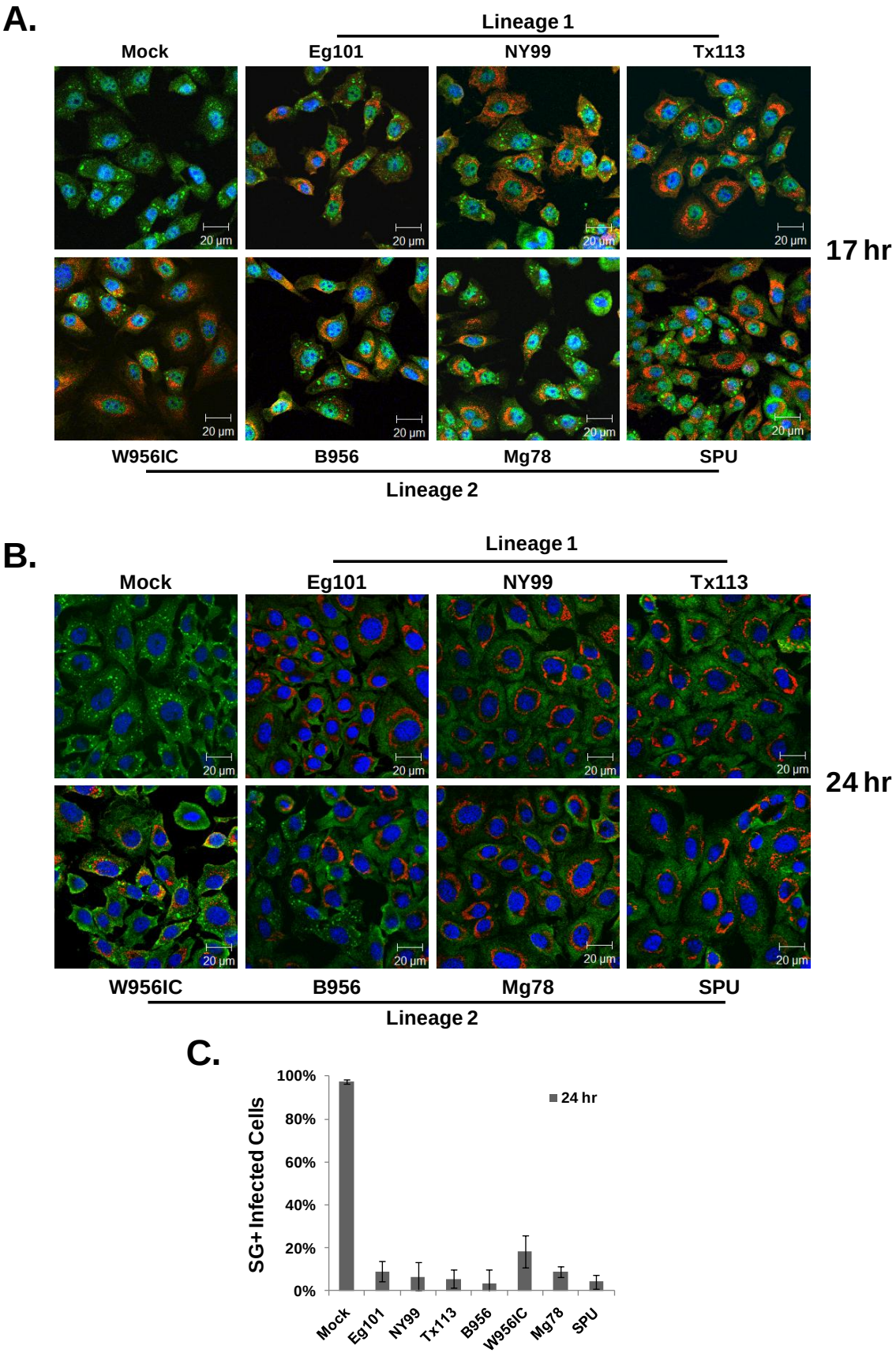
A.
Lineage 1
Mock
Eg101
NY99
Tx113
20 µm
17 hr
W956IC
B956
Mg78
SPU
Lineage 2
B.
Lineage 1
Mock
Eg101
NY99
Tx113
20 µm
24 hr
W956IC
B956
Mg78
SPU
Lineage 2
C.
SG+ Infected Cells
100%
80%
60%
40%
20%
0%
24 hr
Mock
Eg101
NY99
Tx113
B956
W956IC
Mg78
SPU

Figure 3.8. The effect of infections with various WNV strains on arsenite-induced, HRI-mediated SG formation. BHK cells were infected with individual strains of WNV at a MOI of 1, treated with 0.5 mM arsenite for 30 min starting at 16.5 hr **(A)** or at 23.5 hr after infection **(B)**, then fixed and analyzed by confocal microscopy. SGs were visualized using either anti-TIAR antibody (green) **(A)** or anti-G3BP antibody (green) **(B)**, WNV-infected cells were visualized using anti-dsRNA antibody (red), and cell nuclei were visualized with Hoechst dye (blue). **(C)** SG-positive, infected cells treated with arsenite were quantified.

induced higher levels of SGs in BHK cells than 1 mM DTT (Figure 3.9A); however, the 10 mM DTT treatment for both 30 and 60 min caused increased cytopathic effects. The 30 min 2 mM DTT treatment induced higher levels of SGs than the 60 min treatment and treatment with this concentration for 30 min was used for additional experiments. To determine whether WNV infections could also inhibit the formation of PERK-induced SGs, BHK cells were infected with individual strains of WNV at a MOI of 1, treated with 2 mM DTT at 23.5 hr for 30 min, then fixed and analyzed by immunofluorescence. Only B956 infections were found to be able to inhibit the formation of DTT-induced, PERK-mediated SG formation; SGs were observed in ~15% of B956-infected cells and in ~70% of cells infected with the other WNV strains tested (Figure 3.9B and C).

Studies were next done to analyze whether natural WNV infections could inhibit PKR-induced SG formation. As presented above, W956IC infections induce the formation of SGs through the activation of PKR (Figure 3.2). Therefore, BHK cells were infected with W956IC to induce the activation of PKR during infection and a natural WNV strain to determine whether the natural strain infections could inhibit PKR-induced SG formation. BHK cells were first infected with an individual natural WNV strain and then subsequently co-infected with W956IC 30 min later. Both infections were done at an MOI of 5 to increase the likelihood that most cells would be coinfected with both viruses. Cells were fixed at 24 hr after co-infection and analyzed by immunofluorescence. SGs were observed in ~20±5% of the infected cells for each WNV strain co-infected with W956IC, similar to W956IC infections alone, indicating that none of the WNV strains tested could inhibit the formation of W956IC-induced, PKR-mediated SGs (Figure 3.10).

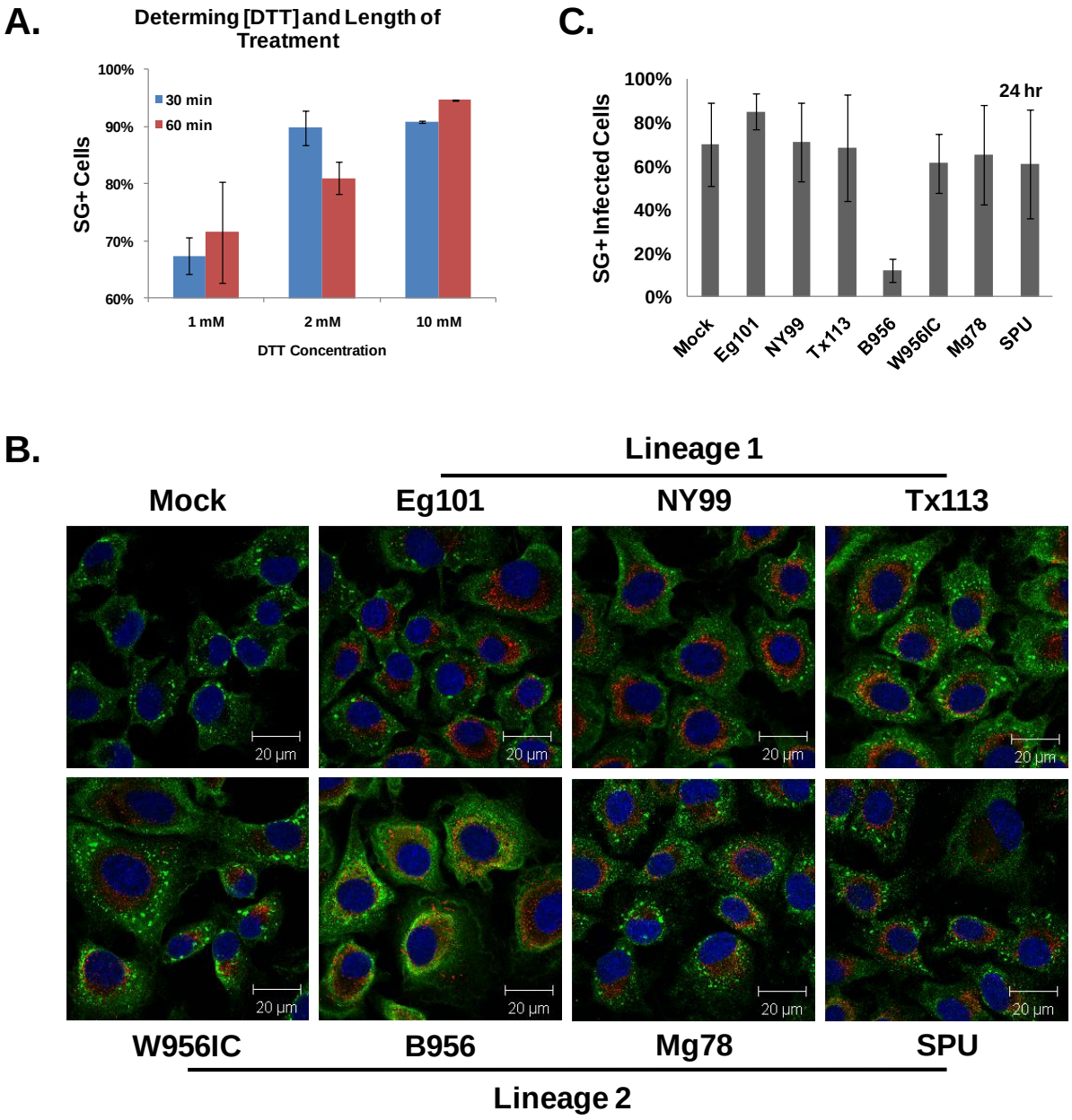

Figure 3.9. The effect of various WNV strain infections on DTT-induced, PERK-mediated SG formation. (A) BHK cells were treated for 30 or 60 min with 1 mM, 2 mM or 10 mM concentrations of DTT to activate PERK and induce SGs. SG-positive cells were quantified. **(B)** BHK cells were infected with individual WNV strains at a MOI of 1, treated with 2 mM DTT for 30 min prior to fixation at 24 hr after infection, and analyzed by immunofluorescence. SGs were visualized with anti-G3BP antibody (green), WNV-infected cells were visualized with anti-dsRNA antibody (red), and nuclei were visualized with Hoechst dye (blue). **(C)** SG-positive, infected cells were quantified.

It has been reported that inhibiting the ubiquitin proteasome system with 10 μM MG132 leads to GCN2 activation and SG formation (Mazroui et al., 2007). However, no SGs were observed in preliminary experiments with this treatment in BHK cells; therefore, it could not be determined whether WNV infections could inhibit the formation of GCN2-induced SGs. It has been suggested that UV treatment of cells can also induce the formation of SGs through GCN2 activation; however, experiments testing this treatment have not yet been done. More work is required to determine whether infections with natural WNV strains are capable of inhibiting GCN2-mediated SG formation.

Heat shock is another stress known to induce the formation of SGs (Grousl et al., 2009; Piotrowska et al., 2010); however, the mechanism of heat shock-induced SG formation in mammalian cells is unknown. In yeast cells, heat shock also induces the formation of SGs. GCN2 is the only known eIF2α kinase in yeast but gcn2Δ yeast cells treated with heat shock still induced the formation of SGs suggesting that SG formation by heat shock treatment is independent of eIF2α phosphorylation (Grousl et al., 2009). To determine whether WNV infections can inhibit the formation of SGs by heat shock, BHK cells were infected with different WNV strains at a MOI of 1 for 24 hr, incubated at 45°C for 20 min, then fixed and analyzed for SGs by immunofluorescence. None of the WNV strain infections tested inhibited heat shock-induced SGs (Figure 3.11). Overall, the data from these experiments suggest that the ability of WNV infections to inhibit SG formation is specific to the oxidative stress response pathway.

A preliminary study done by a former member of the lab suggested that the WNV NS5 protein immunoprecipitated with HRI (data not shown). It is possible that WNV infections specifically inhibit HRI-induced SG formation through the inhibition of either HRI activation or

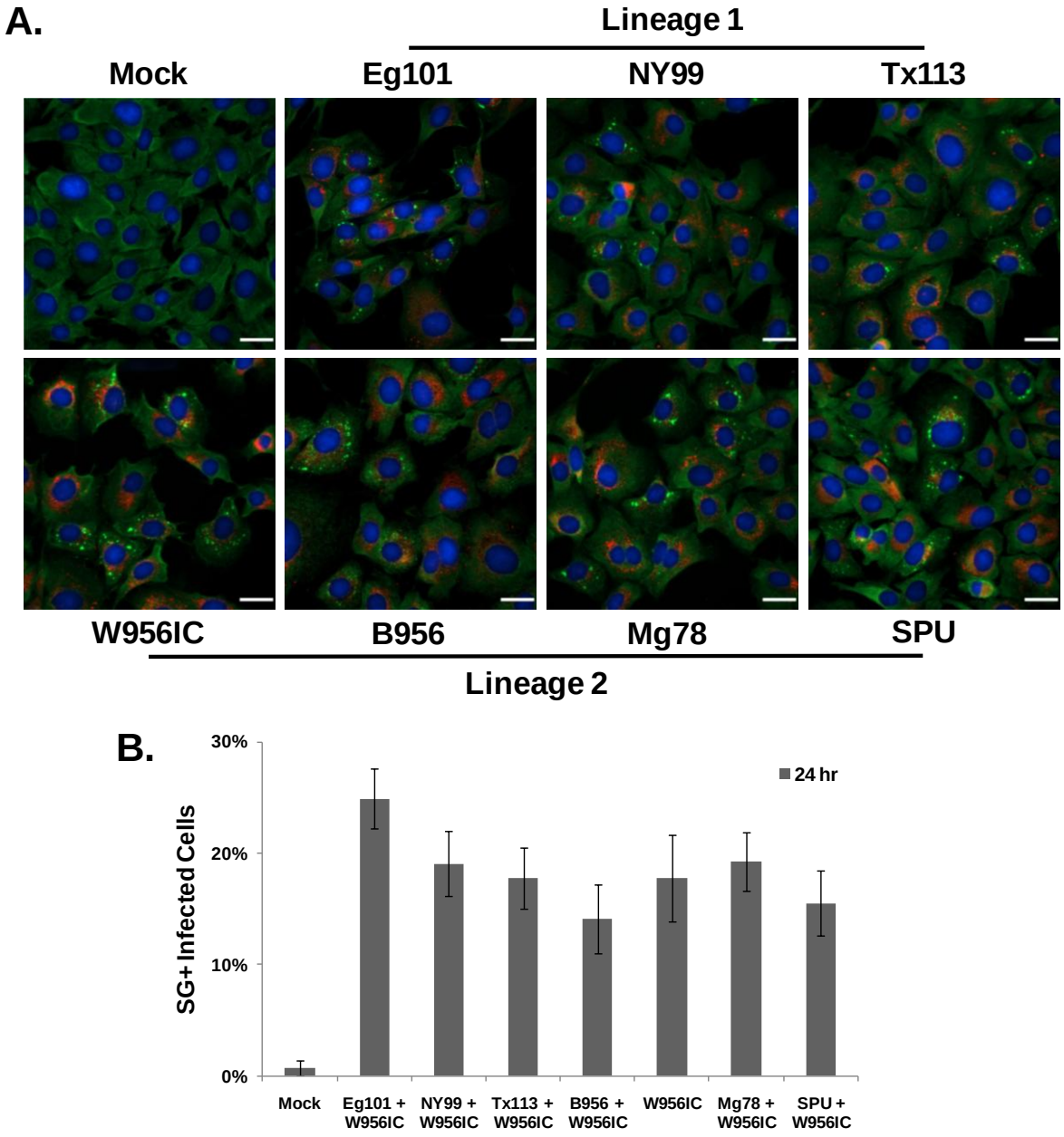

Figure 3.10. The effect of various WNV strain infections on W956IC-induced, PKR-mediated SG formation. (A) BHK cells infected with an individual natural WNV strain and then co-infected with W956IC, known to induce PKR-dependent SGs, 30 min later. Each virus was used at a MOI of 5 to increase the likelihood of co-infection. Co-infected cells were fixed at 24 hr and analyzed by immunofluorescence. SGs were visualized using anti-G3BP antibody (green), WNV-infected cells were visualized using anti-dsRNA antibody, and nuclei were visualized using Hoechst dye (blue). Scale bar represents 20 µm. **(B)** SG-positive, infected cells were quantified.

its ability to function as a kinase through an NS5-HRI interaction. To determine whether the WNV NS5 protein is able to specifically inhibit HRI-induced SG formation, BHK cells stably expressing WNV NS5 were created. These cells were treated with 0.5 mM arsenite for 30 min, fixed and analyzed for SG formation by immunofluorescence. The results showed that NS5 protein expression does not inhibit the formation of HRI-induced SGs (Figure 3.12). However, it has recently been suggested that a functional interaction of the NS5 protein with another cell protein required in situ protease cleavage from a polyprotein (Ashour et al., 2009). Whether this may also be the case for NS5-mediated inhibition of HRI-induced SG formation was not tested. Overall, these data show that the inhibition of SG formation by WNV infection is specific to the HRI kinase pathway; however, the mechanism of this inhibition is currently under further investigation. It is interesting that WNV strains do not induce SG formation during infection but that they actively suppress the formation of SGs specific to oxidative stress. Furthermore, the efficiency of this suppression increases through the course of infection. It has been reported that numerous virus infections induce oxidative stress through the formation of reactive oxygen species or nitric oxide (Akaike and Maeda, 2000; Chen et al., 2009; Hosakote et al., 2009; Schweizer and Peterhans, 1999; Tardif et al., 2005). It is possible that the inhibition of HRI-mediated SG formation by WNV infections is a non-specific byproduct of an active inhibition of the antiviral oxidative stress response pathways by viral components in infected cells.

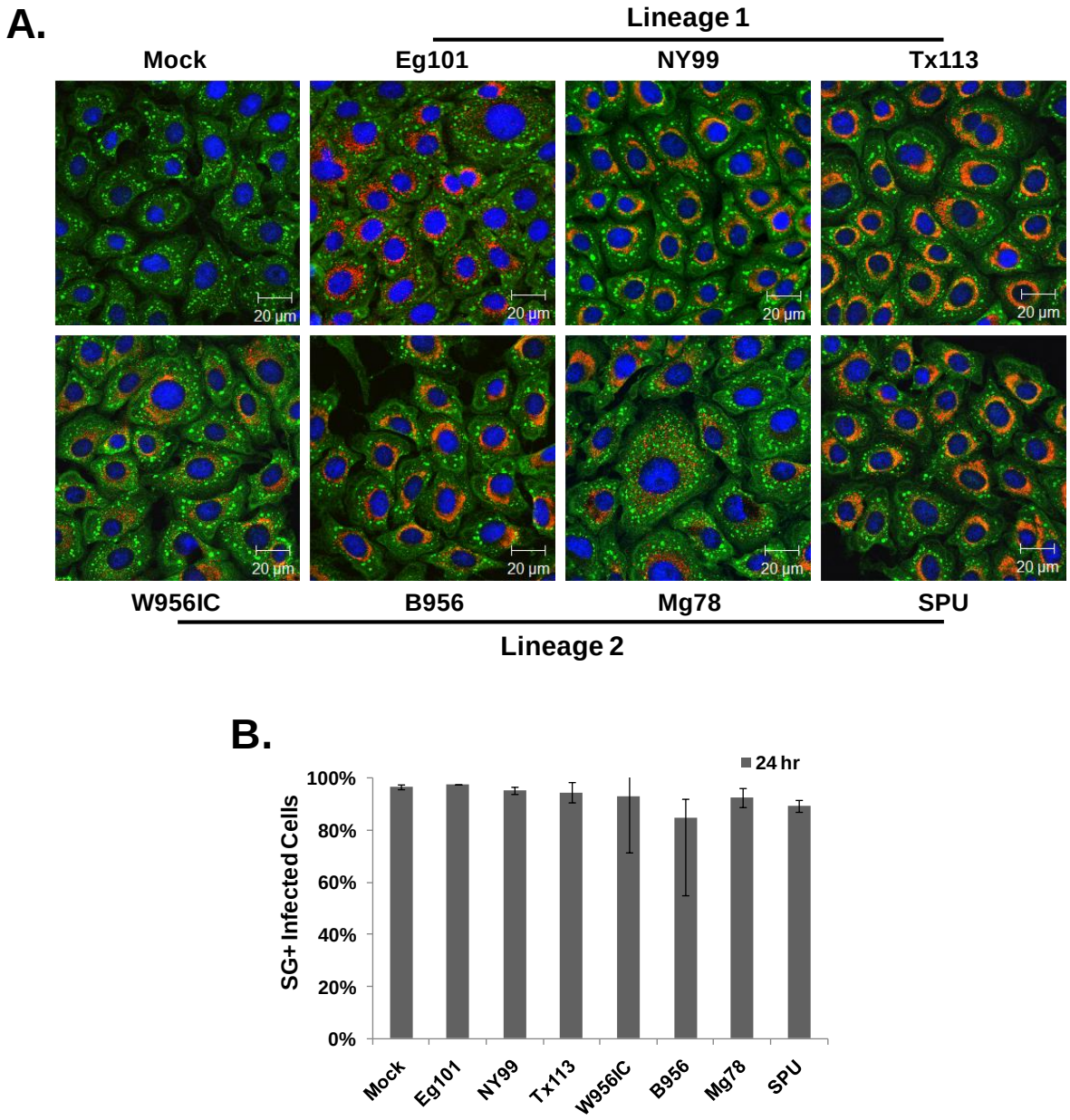

Figure 3.11. The effect of various WNV strain infections on heat shock-induced SG formation. (A) BHK cells were infected with individual WNV strains at a MOI of 1, incubated at 45°C for 20 min prior to fixation at 24 hr after infection, and analyzed for SGs by immunofluorescence. SGs were visualized using anti-G3BP antibody (green), WNV-infected cells were visualized using anti-dsRNA antibody (red), and nuclei were visualized using Hoechst dye (blue). **(B)** SG-positive, infected cells were quantified.

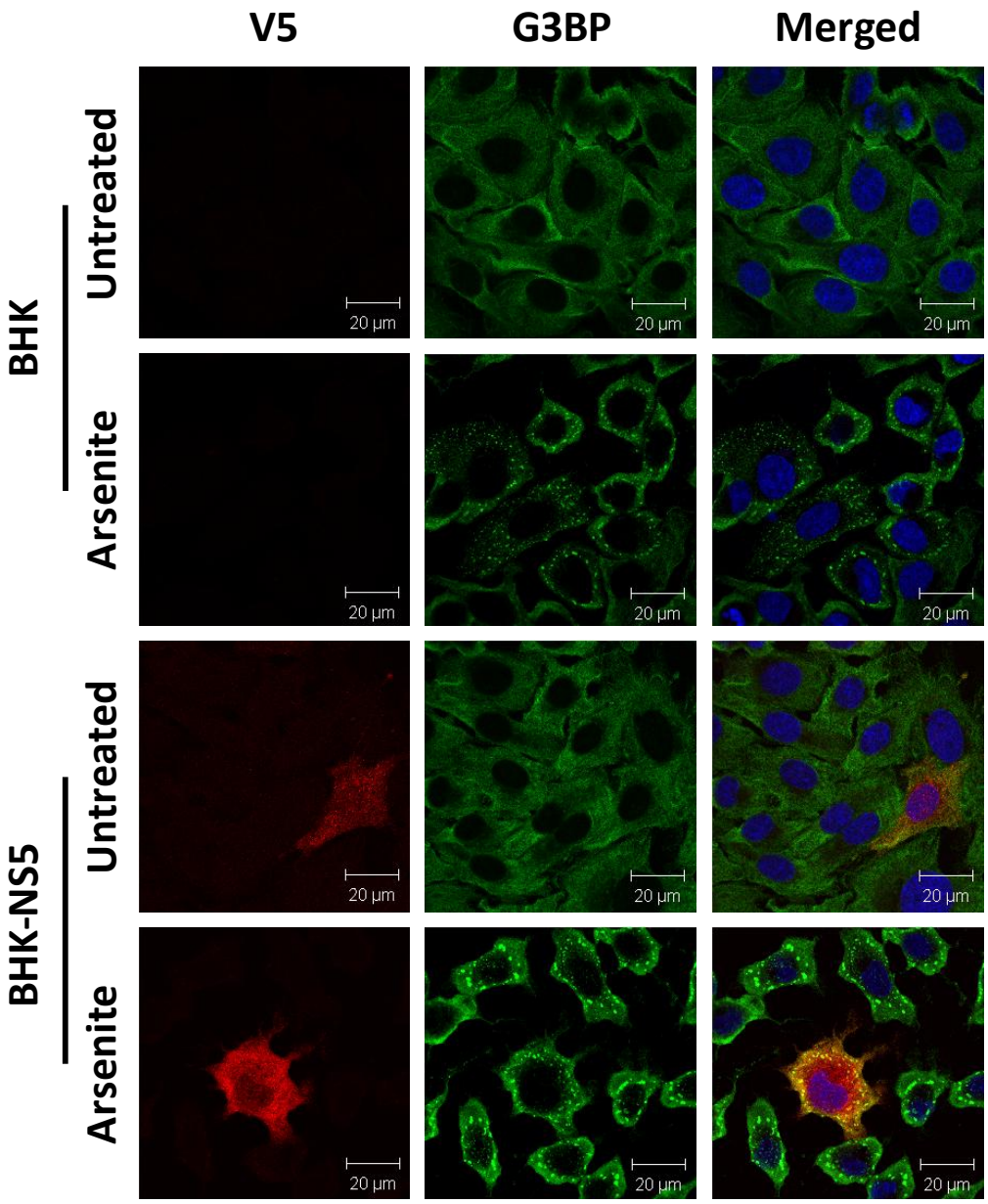

Figure 3.12. The effect of WNV NS5 protein expression on arsenite-induced SG formation. Control BHK cells or BHK cells stably expressing WNV NS5 (BHK-NS5) were left untreated or treated with 0.5 mM arsenite for 30 min, then fixed and analyzed for SGs by immunofluorescence. SGs were visualized using anti-G3BP antibody (green) and NS5-expressing cells were visualized using anti-V5 antibody (red).

CHAPTER 4

SIGNIFICANCE/FUTURE DIRECTIONS

Oas1b-Mediated Resistance to Flavivirus-Induced Disease

The majority of the viruses known today were discovered because of a disease they caused in an infected host. Advances in technology and therapeutics have substantially improved the ability to control viral infections. However, natural genetically-mediated host resistance or susceptibility to infectious viruses has been described in both mice and humans (Lee et al., 2003). One example of the alleles of a single gene conferring resistance or susceptibility to disease is *Flv*^{r}, which was shown to confer resistance to flavivirus-induced disease (Webster and Clow, 1936; Webster and Johnson, 1941). The product of *Flv*^{r} was identified as Oas1b, a member of the antiviral oligoadenylate synthetase gene family (Mashimo et al., 2002; Perelygin et al., 2002). However, additional studies showed that the products of both the resistance and susceptibility alleles were inactive synthetases and therefore the specific anti-flaviviral activity of Oas1b was not mediated by OAS synthetase activation of RNase L (Elbahesh et al., 2011a; Scherbik et al., 2006). The work of the current study was aimed at identifying interaction partners of Oas1b as a means of gaining insights about the mechanism of the Oas1b-mediated anti-flavivirus activity. To our knowledge, this study is the first to identify host cell binding partners of Oas1b.

One of the binding partners identified was ORP1L, a member of an oxysterol binding protein family. It was expected that if ORP1L acted as an antiviral protein, then knocking down the levels of this protein would result in an increase in extracellular WNV yield and intracellular viral RNA and protein levels; however, a decrease was observed in WNV yield and viral RNA

and protein levels. Also, decreases were observed in both SinV and VSV yields, suggesting that this proviral effect was not specific to flaviviruses. However, it was previously reported that the reduction of ORP1L protein levels increased LE motility (Rocha et al., 2009; Vihervaara et al., 2011). Each of the viruses showing reduced replication when ORP1L was knocked down utilize the host endocytic pathway to enter cells (Chu and Ng, 2004; Lu et al., 1999; Superti et al., 1987) and increased LE mobility could negatively affect the efficiency of virion entry and fusion by endocytosis. As an additional means of showing that the effect of ORP1L knockdown is not specific to the flavivirus resistance mechanism, the effect of ORP1L knockdown on the replication of viruses that do not use the endocytic pathway for entry (i.e. vaccinia virus) could be tested.

It was previously reported that overexpression of ORP1L causes clustering of LEs near microtubule organizing centers (Rocha et al., 2009; Vihervaara et al., 2011). ORP1L could be overexpressed in future experiments to compare the effect on WNV replication in cells expressing Oas1b or Oas1bt. If overexpression of ORP1L leads to a decrease in the efficiency of WNV infection in both susceptible Oas1bt-expressing and resistant Oas1b-expressing cells, this would indicate a non-specific effect of LE clustering which could be analyzed further by confocal microscopy using anti-Rab7 antibody to detect LEs. Rab7 was previously shown to extensively colocalize with LEs and to interact with ORP1L (Johansson et al., 2005; Rocha et al., 2009). Alternatively, overexpression of ORP1L could enhance the specific flavivirus resistance mechanism since the slowed movement and clustering of LEs in the perinuclear region of cells (the preferred site of WNV replication processes) might enhance the ORP1L-Oas1b interaction. If this is the case, cells overexpressing ORP1L and Oas1b would provide a good model for further studies of the involvement of ORP1L in the flavivirus resistance mechanism. To further

determine the flavivirus resistance specificity of the effect of ORP1L overexpression, these cells could also be infected with SinV or VSV. The replication of neither of these viruses would be expected to be affected if the effect is specific to the flavivirus resistance mechanism. If both reducing and increasing ORP1L protein levels causes non-specific effects on LE function, then other techniques will be needed to analyze the involvement of ORP1L in the flavivirus resistance mechanism.

The other Oas1b interaction partner identified was ABCF3. ABCF3 was shown to mediate WNV-specific antiviral activity. Even though Oas1b was present, WNV replicated to higher levels when ABCF3 protein levels were reduced, suggesting that the specific anti-flaviviral activity of Oas1b depends on the presence of ABCF3. Also, the antiviral activity of ABCF3 required the presence of Oas1b, further confirming that the Oas1b-mediated flavivirus resistance mechanism involves ABCF3. Currently, nothing is known about the cellular functions of the ABCF3 protein except that it belongs to the F subfamily of the superfamily of ATP-binding cassette-containing proteins. Canonically, these proteins are involved in the transport of substrate across membranes but the subfamily E and F members lack the typical transmembrane domains required for translocation of substrates across membranes (Hollenstein et al., 2007; Locher, 2009). Members of the E and F subfamilies have also been shown to bind translation initiation factors and have been suggested that to be involved in regulating protein synthesis (Chen et al., 2006; Kerr, 2004; Paytubi et al., 2008; Tyzack et al., 2000). Interestingly, results from the current study showed an increase in WNV protein levels, viral RNA and virus yields when ABCF3 protein levels were reduced, suggesting that the ABCF3 protein may negatively regulate WNV genome translation. Decreased viral translation would negatively affect both viral RNA synthesis and virus production. Cellular binding partners of ABCF3 could be identified in

future experiments as another means of elucidating its normal cell functions and the mechanism of its anti-flaviviral activity.

Although ABCF3 is normally expressed in cells, its anti-flaviviral function was only observed when Oas1b was also present. ABCF3 was also shown to interact with Oas1bt and Oas1a in both yeast two-hybrid and *in vitro* interaction assays. The main difference between these Oas1 proteins is their localization within the cell. Oas1b was shown in the present study to localize to the ER membrane and is the only member of the OAS family of proteins in any species tested so far found to localize to this compartment of the cell. These data imply that the interaction between Oas1b and ABCF3 specifically localizes ABCF3 in close proximity to WNV RNA translation/replication sites. Future studies could investigate whether ER membrane localization of ABCF3 is required for its antiviral affect. ABCF3 cDNA could be cloned into an expression vector that fuses a transmembrane ER localization signal to the ABCF3 protein (pER-ABCF3). The overexpression of this construct in C3H/He (He; Oas1bt-expressing) cells would be expected to directly localize ABCF3 to the ER membrane. Control He, He-ABCF3 and He-ER-ABCF3 cell lines could be created and then infected with WNV and the effect on WNV yield, viral RNA and viral protein levels determined. It would be expected that He-ABCF3 cells will produce WNV yields similar to the control cells since Oas1b is not expressed in these cells and therefore cannot localize ABCF3 to the sites of WNV replication. In contrast, He-ER-ABCF3 cells might produce reduced viral yields since the ABCF3 protein is localized to the ER membrane.

Knockdown of ORP1L and of ABCF3 was performed using cells stably expressing specific shRNAs. However, the levels of these proteins partially recovered during the course of infection even though no increase in the levels of these proteins is observed with time after

infection in control cells. These data suggest that WNV infections can inhibit the RNAi pathway. Other arbovirus infections have been reported to counteract the RNAi pathway in insect cells (Li and Ding, 2005; Sanchez-Vargas et al., 2009). However, this ability has not been previously reported for flaviviruses. It is expected that Oas1b-expressing mammalian cells and mice with ORP1L or ABCF3 gene knockouts would provide better model systems for studying the involvement of these proteins in flavivirus genetic resistance. However, it should be noted that ORP1L knockout mice may show disease due to the disregulation of endosomes (Vihervaara et al., 2011; Yan et al., 2007a).

The results obtained in this study were used to develop a model for the involvement of the Oas1b-ABCF3-ORP1L complex in flavivirus resistance (Figure 4.1). After attachment of virion E protein to receptors on susceptible cells (Figure 4.1A), flaviviruses are endocytosed through clatherin-coated pits (Chu and Ng, 2004). Previous studies reported that cholesterol-rich membrane microdomains in the plasma membrane are required for WNV entry into cells since cholesterol-depleted cells failed to internalize WNV particles (Medigeshi et al., 2008). Acidification of the endosome leads to conformational changes in E and then LE-specific anionic lipids facilitate E-mediated fusion of the viral envelope and host endosomal membranes and release of the viral genome (Zaitseva et al., 2010). Movement of LEs along microtubule networks requires the recruitment of RILP and ORP1L by Rab7 which is located on the outer surface of LEs. RILP in this complex can interact with the $p150^{Glued}$ subunit of the dynein-dynactin motor complex and mediate LE movement towards the center of the cell (Johansson et al., 2005; Johansson et al., 2007). After the release of the viral genome, endosomes either continue onto lysosomes for degradation or recycle back to the plasma membrane. Truncated Oas1b (Oas1bt) binds to ABCF3 but Oas1bt does not properly localize ABCF3 within the cell

for it to exert its anti-flaviviral activity. The tripartite protein complex of Oas1b, ORP1L and ABCF3 may be critical to the flavivirus-resistance mechanism. During infection of resistant cells (Figure 4.1B), LEs move along the microtubule as described above. In resistant cells, full length Oas1b is inserted in the ER membrane and is bound to ABCF3, providing a specific location for this antiviral complex within the cell. When LEs move along microtubules and encounter the ER-bound Oas1b protein, ORP1L interacts with Oas1b, forming a tripartite protein complex with ABCF3. This complex docks the LE. When fusion of the virion with the LE occurs, the genome is released near the Oas1b-ABCF3-ORP1L complex, allowing ABCF3 to exert its as yet defined anti-flaviviral activity. It is proposed that the LE-associated tripartite protein complex would only affect the initial stages of infection. If Oas1b-ABCF3 protein complexes were always bound with ORP1L then it would lead to the dysregulation of LEs and thus affect the entry of numerous viruses that use the endocytic pathway and would not be specific to flaviviruses. However, the fact that ORP1L and ABCF3 bind different regions of Oas1b suggests that each is involved in the resistance mechanism. Oas1b-ABCF3 complexes are likely to exist throughout the ER membrane where they continually act antiviral towards flaviviruses during the course of an infection. The studies presented here showed that DSP treatment was required for consistent immunoprecipitation of ORP1L with Oas1b, thus suggesting that this interaction is transient. WNV infections induce ER membrane proliferation and ORP1L senses membrane cholesterol and it is possible that the transient interaction of Oas1b with ORP1L provides lipid sensing that moves these anti-flaviviral protein complexes to regions of virus replication.

It was previously reported that the ORP1L conformation changes depending on the cellular cholesterol levels (Rocha et al., 2009). Future experiments could be done to determine the conformation of ORP1L in WNV-infected cells. When cholesterol levels in LEs are high, the

ORP1L conformation is closed. This is the conformation expected for virion-containing LEs in infected cells since these LEs are expected to contain elevated levels of cholesterol from endocytosed cholesterol-rich lipid rafts. Results from the current study showed that Oas1b interacts with ORP1L under both mock- and WNV-infected conditions; however, ORP1L was overexpressed in these cells and ORP1L as well as LEs were likely clustered in the perinuclear area facilitating an interaction with Oas1b on ER membranes. Future studies analyzing the ORP1L conformation could be done in resistant or susceptible cells to determine whether the presence of Oas1b affects ORP1L conformation. Also, ORP1L conformation studies could also be done in mock- and WNV-infected cells to determine whether WNV infections alter the conformation of ORP1L.

It was hypothesized that the interaction between Oas1b and ORP1L leads to the docking of LEs but whether this docking is transient or permanent is unknown. Studies have shown that VAP-A, an ER integral membrane protein, interacts with ORP1L during low cholesterol conditions. Under these conditions, the ORP1L conformation is open, exposing the FFAT motif that can interact with VAP-A. This interaction allows VAP-A to remove the $p150^{Glued}$ subunit of the dynactin-dynein motor complex inhibiting the movement of the LEs (Rocha et al., 2009). Future experiments could be done to determine whether VAP-A removes $p150^{Glued}$ from motor complexes in WNV infected resistant cells. Preliminary data indicate that the VAP-A protein colocalizes with WNV markers in infected cells at the ER membrane, suggesting that VAP-A may be in the same area as the Oas1b-ABCF3-ORP1L protein complex. The dissociation of the motor complex by VAP-A could be an additional means by which LE mobility is inhibited in WNV-infected resistant cells, thus aiding in the manipulation of the host endocytic pathway so

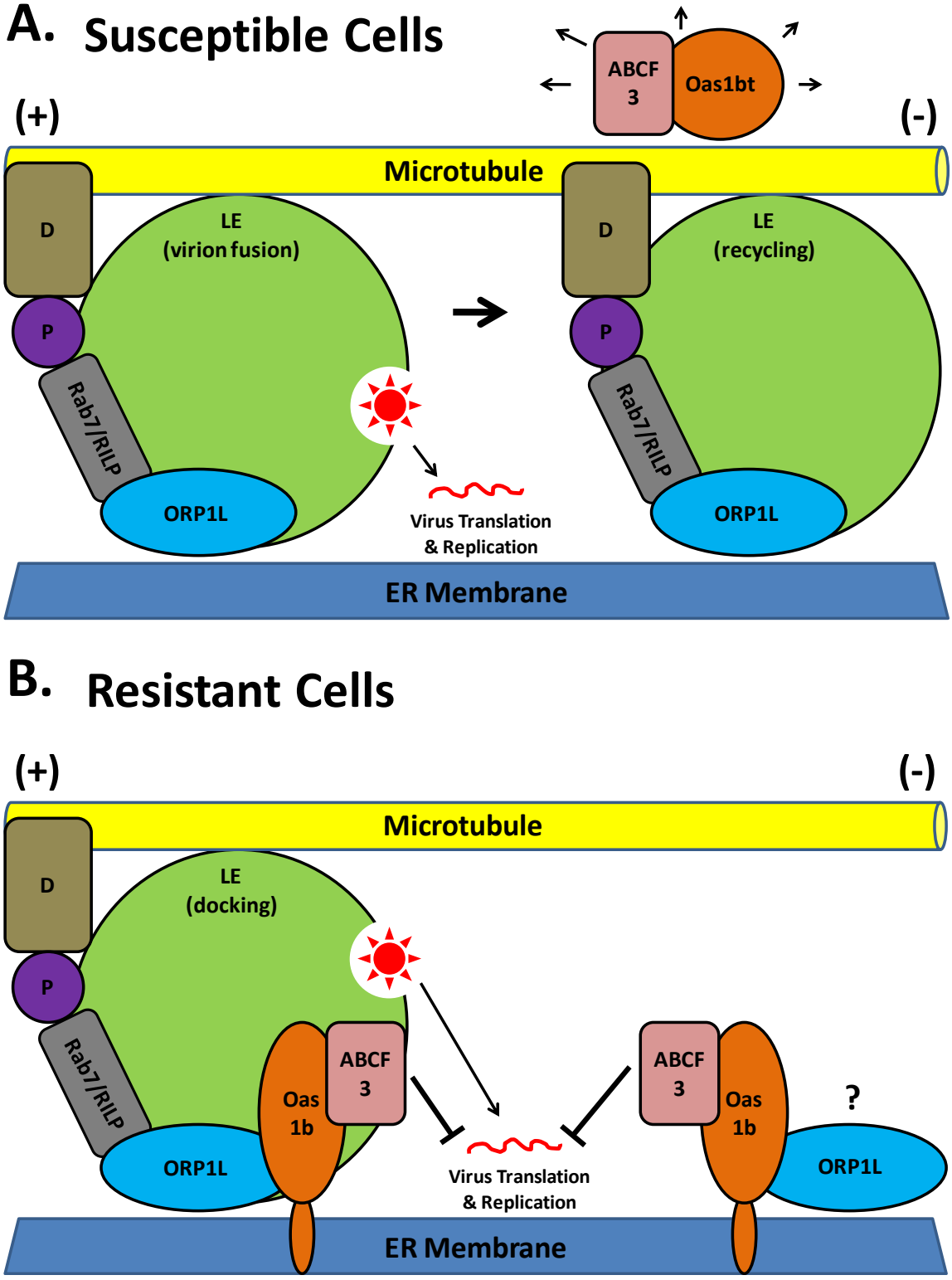
A. Susceptible Cells
ABCF 3
Oas1bt
(+)
(-)
Microtubule
D
P
Rab7/RILP
ORP1L
LE
(virion fusion)
LE
(recycling)
Virus Translation
& Replication
ER Membrane
B. Resistant Cells
(+)
(-)
Microtubule
D
P
Rab7/RILP
ORP1L
LE
(docking)
ABCF 3
Oas 1b
Virus Translation
& Replication
?
ER Membrane

Figure 4.1. Proposed model of Oas1b-ABCF3-ORP1L protein complex. (**A)** Susceptible cells express truncated Oas1b (Oas1bt) that also interacts with ABCF3; however, this complex is not localized to the correct compartment of the cell to exert a flavivirus-specific antiviral affect. LEs carrying WNV virions release the viral genome at the ER where translation/replication occurs. **(B)** Resistant cells express full length Oas1b that localizes to the ER membrane and forms a tripartite complex with ABCF3 and ORP1L. Oas1b binding to ORP1L results in virion fusion occurring within close proximity of the Oas1b-ABCF3-ORP1L complex. Translation/replication of the viral genome is then exposed to the anti-flaviviral activity of ABCF3**.** Oas1b-ABCF3 complexes that may transiently interact with ORP1L likely exist throughout the ER where they continue to provide flavivirus specific antiviral activity during the course of an infection. LE-late endosome. D-dynein-dynactin motor complex. P-p150^{Glued} subunit of dynactin.

that the release of the viral genome occurs in close proximity to the anti-flavivirus protein complexes.

SG Formation During WNV Infections

The current study confirmed that natural WNV infections do not induce the formation of SGs. However, infections with the W956IC infectious clone virus induce SGs through the activation of PKR. A previous study showed that natural WNV infections do not activate PKR (Elbahesh et al., 2011b) and the data presented here suggest that natural WNV infections do not induce the formation of SGs. It is not known how WNV infections evade detection by host cell cytoplasmic RNA sensors but data from the current study suggest that infections with natural WNV strains suppress the level of their early viral RNA synthesis. In contrast, W956IC infections produce higher early levels of viral RNA. During WNV infection, intracellular, perinuclear ER membrane vesicles form and are the sites of late exponential viral genome RNA synthesis (Gillespie et al., 2010; Welsch et al., 2009). However, it is currently not known what type of membrane microenvironment is induced by flavivirus infections to protect viral RNA made at early times after infection from cytoplasmic RNA sensors. Previous studies showed that a low level of symmetric genome and minus strand viral RNA synthesis is maintained prior to the formation of the vesicle structures that support exponential genome RNA synthesis (Cleaves et al., 1981). However, W956IC infections do not regulate early RNA synthesis as efficiently and so produce increased amounts of viral RNA at early times after infection. The data also suggest that an insufficient number of early membrane microenvironments are present to protect the increased level of early viral RNA in W956IC-infected cells. Some viral RNA is therefore exposed in the cytoplasm which leads to PKR activation, eIF2α phosphorylation and SG

formation. It is likely that the membrane microenvironment protecting viral RNA early in infection during symmetric viral RNA synthesis differs dramatically from the membrane microenvironment that protects viral RNA later in the infection cycle when asymmetric synthesis of the viral plus strand occurs. This study is the first to show a correlation between the extent of suppression of early RNA replication and induction of the SG response.

The mapping data obtained with chimeric virus genomes showed that either NS5, or a combination of NS1, NS3 and NS4a, were critical for regulating early viral RNA synthesis and controlling the induction of SGs. Each of these nonstructural proteins is a critical component of the WNV replication complex and the specific contacts between them, as well as with the viral RNA, and possibly other cell proteins, are thought to be important for modulating the efficiency of viral RNA synthesis (Brooks et al., 2002; Dong et al., 2008; Johansson et al., 2001; Kapoor et al., 1995). There are 24 aa substitutions in NS1, 22 aa substitutions in NS3+4a, and 29 aa substitutions in NS5 between the WNV Eg101 and W956IC protein sequences. Future studies could be done to identify the critical mutation(s) contributing to the suppression of viral RNA synthesis at early times after infection. Data from these studies would provide insights about how WNV polymerase function is differentially regulated during the infection cycle.

REFERENCES:

Adams, E.J., Juo, Z.S., Venook, R.T., Boulanger, M.J., Arase, H., Lanier, L.L., Garcia, K.C., 2007. Structural elucidation of the m157 mouse cytomegalovirus ligand for Ly49 natural killer cell receptors. Proc Natl Acad Sci U S A 104, 10128-10133.

Agrawal, R., Carpino, N., Tsygankov, A., 2008. TULA proteins regulate activity of the protein tyrosine kinase Syk. J Cell Biochem 104, 953-964.

Akaike, T., Maeda, H., 2000. Nitric oxide and virus infection. Immunology 101, 300-308.

Ambrose, R.L., Mackenzie, J.M., 2011. West Nile virus differentially modulates the unfolded protein response to facilitate replication and immune evasion. J Virol 85, 2723-2732.

Anderson, P., Kedersha, N., 2002a. Stressful initiations. J Cell Sci 115, 3227-3234.

Anderson, P., Kedersha, N., 2002b. Visibly stressed: the role of eIF2, TIA-1, and stress granules in protein translation. Cell Stress Chaperones 7, 213-221.

Anderson, P., Kedersha, N., 2006. RNA granules. J Cell Biol 172, 803-808.

Anderson, P., Kedersha, N., 2007. On again, off again: the SRC-3 transcriptional coactivator moonlights as a translational corepressor. Mol Cell 25, 796-797.

Anderson, P., Kedersha, N., 2008. Stress granules: the Tao of RNA triage. Trends Biochem Sci 33, 141-150.

Arase, H., Mocarski, E.S., Campbell, A.E., Hill, A.B., Lanier, L.L., 2002. Direct recognition of cytomegalovirus by activating and inhibitory NK cell receptors. Science 296, 1323-1326.

Ariumi, Y., Kuroki, M., Kushima, Y., Osugi, K., Hijikata, M., Maki, M., Ikeda, M., Kato, N., 2011. Hepatitis C Virus Hijacks P-Body and Stress Granule Components around Lipid Droplets. J Virol 85, 6882-6892.

Ashour, J., Laurent-Rolle, M., Shi, P.Y., Garcia-Sastre, A., 2009. NS5 of dengue virus mediates STAT2 binding and degradation. J Virol 83, 5408-5418.

Assenberg, R., Mastrangelo, E., Walter, T.S., Verma, A., Milani, M., Owens, R.J., Stuart, D.I., Grimes, J.M., Mancini, E.J., 2009. Crystal structure of a novel conformational state of the flavivirus NS3 protein: implications for polyprotein processing and viral replication. J Virol 83, 12895-12906.

Avirutnan, P., Hauhart, R.E., Somnuke, P., Blom, A.M., Diamond, M.S., Atkinson, J.P., 2011. Binding of flavivirus nonstructural protein NS1 to C4b binding protein modulates complement activation. J Immunol 187, 424-433.

Bakonyi, T., Ivanics, E., Erdelyi, K., Ursu, K., Ferenczi, E., Weissenbock, H., Nowotny, N., 2006. Lineage 1 and 2 strains of encephalitic West Nile virus, central Europe. Emerg Infect Dis 12, 618-623.

Basu, M., Brinton, M.A., 2011. West Nile virus (WNV) genome RNAs with up to three adjacent mutations that disrupt long distance 5'-3' cyclization sequence basepairs are viable. Virology 412, 220-232.

Beckham, C.J., Light, H.R., Nissan, T.A., Ahlquist, P., Parker, R., Noueiry, A., 2007. Interactions between brome mosaic virus RNAs and cytoplasmic processing bodies. J Virol 81, 9759-9768.

Beckham, C.J., Parker, R., 2008. P bodies, stress granules, and viral life cycles. Cell Host Microbe 3, 206-212.

Berger, E.A., Murphy, P.M., Farber, J.M., 1999. Chemokine receptors as HIV-1 coreceptors: roles in viral entry, tropism, and disease. Annu Rev Immunol 17, 657-700.

Bessaud, M., Pastorino, B.A., Peyrefitte, C.N., Rolland, D., Grandadam, M., Tolou, H.J., 2006. Functional characterization of the NS2B/NS3 protease complex from seven viruses belonging to different groups inside the genus Flavivirus. Virus Res 120, 79-90.

Best, S.M., Morris, K.L., Shannon, J.G., Robertson, S.J., Mitzel, D.N., Park, G.S., Boer, E., Wolfinbarger, J.B., Bloom, M.E., 2005. Inhibition of interferon-stimulated JAK-STAT signaling by a tick-borne flavivirus and identification of NS5 as an interferon antagonist. J Virol 79, 12828-12839.

Bisbal, C., Martinand, C., Silhol, M., Lebleu, B., Salehzada, T., 1995. Cloning and characterization of a RNAse L inhibitor. A new component of the interferon-regulated 2-5A pathway. J Biol Chem 270, 13308-13317.

Boyle, J.F., Weismiller, D.G., Holmes, K.V., 1987. Genetic resistance to mouse hepatitis virus correlates with absence of virus-binding activity on target tissues. J Virol 61, 185-189.

Brennan, C.M., Steitz, J.A., 2001. HuR and mRNA stability. Cell Mol Life Sci 58, 266-277.

Brinton, M.A., 1986. Replication of flaviviruses. Plenum Publishing Corp., New York.

Brinton, M.A., 2002. The molecular biology of West Nile Virus: a new invader of the western hemisphere. Annual review of microbiology 56, 371-402.

Brinton, M.A., 2008. Molecular Biology of West Nile virus, in: Diamond, M.S. (Ed.), West Nile Encephalitis Virus Infection: Viral Pathogenesis and the Host Immune Response. Springer, N.Y., N.Y., pp. pp97-136.

Britt, W.J., Chesebro, B., 1980. H-2D (Rfv-1) gene influence on recovery from Friend virus leukemia is mediated by nonleukemic cells of the spleen and bone marrow. J Exp Med 152, 1795-1804.

Brooks, A.J., Johansson, M., John, A.V., Xu, Y., Jans, D.A., Vasudevan, S.G., 2002. The interdomain region of dengue NS5 protein that binds to the viral helicase NS3 contains independently functional importin beta 1 and importin alpha/beta-recognized nuclear localization signals. J Biol Chem 277, 36399-36407.

Brown, M.G., Dokun, A.O., Heusel, J.W., Smith, H.R., Beckman, D.L., Blattenberger, E.A., Dubbelde, C.E., Stone, L.R., Scalzo, A.A., Yokoyama, W.M., 2001. Vital involvement of a natural killer cell activation receptor in resistance to viral infection. Science 292, 934-937.

Carpino, N., Turner, S., Mekala, D., Takahashi, Y., Zang, H., Geiger, T.L., Doherty, P., Ihle, J.N., 2004. Regulation of ZAP-70 activation and TCR signaling by two related proteins, Sts-1 and Sts-2. Immunity 20, 37-46.

Chambers, T.J., McCourt, D.W., Rice, C.M., 1990a. Production of yellow fever virus proteins in infected cells: identification of discrete polyprotein species and analysis of cleavage kinetics using region-specific polyclonal antisera. Virology 177, 159-174.

Chambers, T.J., Weir, R.C., Grakoui, A., McCourt, D.W., Bazan, J.F., Fletterick, R.J., Rice, C.M., 1990b. Evidence that the N-terminal domain of nonstructural protein NS3 from yellow fever virus is a serine protease responsible for site-specific cleavages in the viral polyprotein. Proc Natl Acad Sci U S A 87, 8898-8902.

Chen, S.O., Fang, S.H., Shih, D.Y., Chang, T.J., Liu, J.J., 2009. Recombinant core proteins of Japanese encephalitis virus as activators of the innate immune response. Virus Genes 38, 10-18.

Chen, Z.Q., Dong, J., Ishimura, A., Daar, I., Hinnebusch, A.G., Dean, M., 2006. The essential vertebrate ABCE1 protein interacts with eukaryotic initiation factors. J Biol Chem 281, 7452-7457.

Chu, J.J., Leong, P.W., Ng, M.L., 2006. Analysis of the endocytic pathway mediating the infectious entry of mosquito-borne flavivirus West Nile into Aedes albopictus mosquito (C6/36) cells. Virology 349, 463-475.

Chu, J.J., Ng, M.L., 2004. Infectious entry of West Nile virus occurs through a clathrin-mediated endocytic pathway. J Virol 78, 10543-10555.

Chu, P.W., Westaway, E.G., 1985. Replication strategy of Kunjin virus: evidence for recycling role of replicative form RNA as template in semiconservative and asymmetric replication. Virology 140, 68-79.

Chung, K.M., Liszewski, M.K., Nybakken, G., Davis, A.E., Townsend, R.R., Fremont, D.H., Atkinson, J.P., Diamond, M.S., 2006. West Nile virus nonstructural protein NS1 inhibits complement activation by binding the regulatory protein factor H. Proc Natl Acad Sci U S A 103, 19111-19116.

Cleaves, G.R., Ryan, T.E., Schlesinger, R.W., 1981. Identification and characterization of type 2 dengue virus replicative intermediate and replicative form RNAs. Virology 111, 73-83.

Collier, N.C., Schlesinger, M.J., 1986. The dynamic state of heat shock proteins in chicken embryo fibroblasts. J Cell Biol 103, 1495-1507.

Daniels, K.A., Devora, G., Lai, W.C., O'Donnell, C.L., Bennett, M., Welsh, R.M., 2001. Murine cytomegalovirus is regulated by a discrete subset of natural killer cells reactive with monoclonal antibody to Ly49H. J Exp Med 194, 29-44.

Dauber, B., Pelletier, J., Smiley, J.R., 2011. The herpes simplex virus 1 vhs protein enhances translation of viral true late mRNAs and virus production in a cell type-dependent manner. J Virol 85, 5363-5373.

Dean, M., Carrington, M., Winkler, C., Huttley, G.A., Smith, M.W., Allikmets, R., Goedert, J.J., Buchbinder, S.P., Vittinghoff, E., Gomperts, E., Donfield, S., Vlahov, D., Kaslow, R., Saah, A., Rinaldo, C., Detels, R., O'Brien, S.J., 1996. Genetic restriction of HIV-1 infection and progression to AIDS by a deletion allele of the CKR5 structural gene. Hemophilia Growth and Development Study, Multicenter AIDS Cohort Study, Multicenter Hemophilia Cohort Study, San Francisco City Cohort, ALIVE Study. Science 273, 1856-1862.

den Boon, J.A., Ahlquist, P., 2010. Organelle-like membrane compartmentalization of positive-strand RNA virus replication factories. Annu Rev Microbiol 64, 241-256.

Dong, H., Zhang, B., Shi, P.Y., 2008. Terminal structures of West Nile virus genomic RNA and their interactions with viral NS5 protein. Virology 381, 123-135.

Dougherty, J.D., White, J.P., Lloyd, R.E., 2011. Poliovirus-mediated disruption of cytoplasmic processing bodies. J Virol 85, 64-75.

Dveksler, G.S., Pensiero, M.N., Cardellichio, C.B., Williams, R.K., Jiang, G.S., Holmes, K.V., Dieffenbach, C.W., 1991. Cloning of the mouse hepatitis virus (MHV) receptor: expression in human and hamster cell lines confers susceptibility to MHV. J Virol 65, 6881-6891.

Egloff, M.P., Benarroch, D., Selisko, B., Romette, J.L., Canard, B., 2002. An RNA cap (nucleoside-2'-O-)-methyltransferase in the flavivirus RNA polymerase NS5: crystal structure and functional characterization. EMBO J 21, 2757-2768.

Elbahesh, H., Jha, B.K., Silverman, R.H., Scherbik, S.V., Brinton, M.A., 2011a. The Flvr-encoded murine oligoadenylate synthetase 1b (Oas1b) suppresses 2-5A synthesis in intact cells. Virology 409, 262-270.

Elbahesh, H., Scherbik, S.V., Brinton, M.A., 2011b. West Nile virus infection does not induce PKR activation in rodent cells. Virology.

Emara, M., Brinton, M.A., 2008. Mutation of mapped TIA-1/TIAR binding sites in the 3' terminal stem loop of the West Nile virus minus-strand RNA in an infectious clone negatively affects genomic RNA synthesis. J Virol.

Emara, M.M., Brinton, M.A., 2007. Interaction of TIA-1/TIAR with West Nile and dengue virus products in infected cells interferes with stress granule formation and processing body assembly. Proc Natl Acad Sci U S A 104, 9041-9046.

Falgout, B., Markoff, L., 1995. Evidence that flavivirus NS1-NS2A cleavage is mediated by a membrane-bound host protease in the endoplasmic reticulum. J Virol 69, 7232-7243.

Farrell, H.E., Vally, H., Lynch, D.M., Fleming, P., Shellam, G.R., Scalzo, A.A., Davis-Poynter, N.J., 1997. Inhibition of natural killer cells by a cytomegalovirus MHC class I homologue in vivo. Nature 386, 510-514.

Ferlenghi, I., Clarke, M., Ruttan, T., Allison, S.L., Schalich, J., Heinz, F.X., Harrison, S.C., Rey, F.A., Fuller, S.D., 2001. Molecular organization of a recombinant subviral particle from tick-borne encephalitis virus. Mol Cell 7, 593-602.

Feshchenko, E.A., Smirnova, E.V., Swaminathan, G., Teckchandani, A.M., Agrawal, R., Band, H., Zhang, X., Annan, R.S., Carr, S.A., Tsygankov, A.Y., 2004. TULA: an SH3- and UBA-containing protein that binds to c-Cbl and ubiquitin. Oncogene 23, 4690-4706.

Garcia, M.A., Meurs, E.F., Esteban, M., 2007. The dsRNA protein kinase PKR: virus and cell control. Biochimie 89, 799-811.

Gatza, M.L., Marriott, S.J., 2006. Genotoxic stress and cellular stress alter the subcellular distribution of human T-cell leukemia virus type 1 tax through a CRM1-dependent mechanism. J Virol 80, 6657-6668.

Geoffroy, M.C., Chelbi-Alix, M.K., 2011. Role of promyelocytic leukemia protein in host antiviral defense. J Interferon Cytokine Res 31, 145-158.

Gilks, N., Kedersha, N., Ayodele, M., Shen, L., Stoecklin, G., Dember, L.M., Anderson, P., 2004. Stress granule assembly is mediated by prion-like aggregation of TIA-1. Mol Biol Cell 15, 5383-5398.

Gillespie, L.K., Hoenen, A., Morgan, G., Mackenzie, J.M., 2010. The endoplasmic reticulum provides the membrane platform for biogenesis of the flavivirus replication complex. J Virol 84, 10438-10447.

Gorbalenya, A.E., Donchenko, A.P., Koonin, E.V., Blinov, V.M., 1989. N-terminal domains of putative helicases of flavi- and pestiviruses may be serine proteases. Nucleic Acids Res 17, 3889-3897.

Groschel, D., Koprowski, H., 1965. Development of a virus-resistant inbred mouse strain for the study of innate resistance to Arbo B viruses. Arch Gesamte Virusforsch 17, 379-391.

Groskreutz, D.J., Babor, E.C., Monick, M.M., Varga, S.M., Hunninghake, G.W., 2010. Respiratory syncytial virus limits alpha subunit of eukaryotic translation initiation factor 2 (eIF2alpha) phosphorylation to maintain translation and viral replication. J Biol Chem 285, 24023-24031.

Grousl, T., Ivanov, P., Frydlova, I., Vasicova, P., Janda, F., Vojtova, J., Malinska, K., Malcova, I., Novakova, L., Janoskova, D., Valasek, L., Hasek, J., 2009. Robust heat shock induces eIF2alpha-phosphorylation-independent assembly of stress granules containing eIF3 and 40S ribosomal subunits in budding yeast, Saccharomyces cerevisiae. J Cell Sci 122, 2078-2088.

Hahn, C.S., Hahn, Y.S., Rice, C.M., Lee, E., Dalgarno, L., Strauss, E.G., Strauss, J.H., 1987. Conserved elements in the 3' untranslated region of flavivirus RNAs and potential cyclization sequences. Journal of molecular biology 198, 33-41.

Haller, O., Kochs, G., 2002. Interferon-induced mx proteins: dynamin-like GTPases with antiviral activity. Traffic 3, 710-717.

Han, A.P., Yu, C., Lu, L., Fujiwara, Y., Browne, C., Chin, G., Fleming, M., Leboulch, P., Orkin, S.H., Chen, J.J., 2001. Heme-regulated eIF2alpha kinase (HRI) is required for translational regulation and survival of erythroid precursors in iron deficiency. EMBO J 20, 6909-6918.

Hanley, K.A., Lee, J.J., Blaney, J.E., Jr., Murphy, B.R., Whitehead, S.S., 2002. Paired charge-to-alanine mutagenesis of dengue virus type 4 NS5 generates mutants with temperature-sensitive, host range, and mouse attenuation phenotypes. J Virol 76, 525-531.

Hanley, L.L., McGivern, D.R., Teng, M.N., Djang, R., Collins, P.L., Fearns, R., 2010. Roles of the respiratory syncytial virus trailer region: effects of mutations on genome production and stress granule formation. Virology 406, 241-252.

Harding, H.P., Novoa, I., Zhang, Y., Zeng, H., Wek, R., Schapira, M., Ron, D., 2000. Regulated translation initiation controls stress-induced gene expression in mammalian cells. Mol Cell 6, 1099-1108.

Harding, H.P., Zeng, H., Zhang, Y., Jungries, R., Chung, P., Plesken, H., Sabatini, D.D., Ron, D., 2001. Diabetes mellitus and exocrine pancreatic dysfunction in perk-/- mice reveals a role for translational control in secretory cell survival. Mol Cell 7, 1153-1163.

Hayes, E.B., Komar, N., Nasci, R.S., Montgomery, S.P., O'Leary, D.R., Campbell, G.L., 2005. Epidemiology and transmission dynamics of West Nile virus disease. Emerg Infect Dis 11, 1167-1173.

Heinz, F.X., Allison, S.L., 2000. Structures and mechanisms in flavivirus fusion. Adv Virus Res 55, 231-269.

Heinz, F.X., Stiasny, K., Allison, S.L., 2004. The entry machinery of flaviviruses. Arch Virol Suppl, 133-137.

Hollenstein, K., Dawson, R.J., Locher, K.P., 2007. Structure and mechanism of ABC transporter proteins. Curr Opin Struct Biol 17, 412-418.

Hosakote, Y.M., Liu, T., Castro, S.M., Garofalo, R.P., Casola, A., 2009. Respiratory syncytial virus induces oxidative stress by modulating antioxidant enzymes. Am J Respir Cell Mol Biol 41, 348-357.

Hu, Y., Conway, T.W., 1993. 2-Aminopurine inhibits the double-stranded RNA-dependent protein kinase both in vitro and in vivo. J Interferon Res 13, 323-328.

Iyer, K., Burkle, L., Auerbach, D., Thaminy, S., Dinkel, M., Engels, K., Stagljar, I., 2005. Utilizing the split-ubiquitin membrane yeast two-hybrid system to identify protein-protein interactions of integral membrane proteins. Sci STKE 2005, pl3.

Johansson, M., Bocher, V., Lehto, M., Chinetti, G., Kuismanen, E., Ehnholm, C., Staels, B., Olkkonen, V.M., 2003. The two variants of oxysterol binding protein-related protein-1 display different tissue expression patterns, have different intracellular localization, and are functionally distinct. Mol Biol Cell 14, 903-915.

Johansson, M., Brooks, A.J., Jans, D.A., Vasudevan, S.G., 2001. A small region of the dengue virus-encoded RNA-dependent RNA polymerase, NS5, confers interaction with both the nuclear transport receptor importin-beta and the viral helicase, NS3. J Gen Virol 82, 735-745.

Johansson, M., Lehto, M., Tanhuanpaa, K., Cover, T.L., Olkkonen, V.M., 2005. The oxysterol-binding protein homologue ORP1L interacts with Rab7 and alters functional properties of late endocytic compartments. Mol Biol Cell 16, 5480-5492.

Johansson, M., Rocha, N., Zwart, W., Jordens, I., Janssen, L., Kuijl, C., Olkkonen, V.M., Neefjes, J., 2007. Activation of endosomal dynein motors by stepwise assembly of Rab7-RILP-p150Glued, ORP1L, and the receptor betalll spectrin. J Cell Biol 176, 459-471.

Justesen, J., Hartmann, R., Kjeldgaard, N.O., 2000. Gene structure and function of the 2'-5'-oligoadenylate synthetase family. Cell Mol Life Sci 57, 1593-1612.

Kakuta, S., Shibata, S., Iwakura, Y., 2002. Genomic structure of the mouse 2',5'-oligoadenylate synthetase gene family. J Interferon Cytokine Res 22, 981-993.

Kapoor, M., Zhang, L., Ramachandra, M., Kusukawa, J., Ebner, K.E., Padmanabhan, R., 1995. Association between NS3 and NS5 proteins of dengue virus type 2 in the putative RNA replicase is linked to differential phosphorylation of NS5. J Biol Chem 270, 19100-19106.

Kato, H., Takeuchi, O., Mikamo-Satoh, E., Hirai, R., Kawai, T., Matsushita, K., Hiiragi, A., Dermody, T.S., Fujita, T., Akira, S., 2008. Length-dependent recognition of double-stranded ribonucleic acids by retinoic acid-inducible gene-I and melanoma differentiation-associated gene 5. J Exp Med 205, 1601-1610.

Kedersha, N., Anderson, P., 2002. Stress granules: sites of mRNA triage that regulate mRNA stability and translatability. Biochem Soc Trans 30, 963-969.

Kedersha, N., Chen, S., Gilks, N., Li, W., Miller, I.J., Stahl, J., Anderson, P., 2002. Evidence that ternary complex (eIF2-GTP-tRNA(i)(Met))-deficient preinitiation complexes are core constituents of mammalian stress granules. Mol Biol Cell 13, 195-210.

Kedersha, N., Cho, M.R., Li, W., Yacono, P.W., Chen, S., Gilks, N., Golan, D.E., Anderson, P., 2000. Dynamic shuttling of TIA-1 accompanies the recruitment of mRNA to mammalian stress granules. J Cell Biol 151, 1257-1268.

Kedersha, N.L., Gupta, M., Li, W., Miller, I., Anderson, P., 1999. RNA-binding proteins TIA-1 and TIAR link the phosphorylation of eIF-2 alpha to the assembly of mammalian stress granules. J Cell Biol 147, 1431-1442.

Kerr, I.D., 2004. Sequence analysis of twin ATP binding cassette proteins involved in translational control, antibiotic resistance, and ribonuclease L inhibition. Biochem Biophys Res Commun 315, 166-173.

Khong, A., Jan, E., 2011. Modulation of stress granules and P bodies during dicistrovirus infection. J Virol 85, 1439-1451.

Kim, M., Mackenzie, J.M., Westaway, E.G., 2004. Comparisons of physical separation methods of Kunjin virus-induced membranes. J Virol Methods 120, 179-187.

Kim, Y.G., Yoo, J.S., Kim, J.H., Kim, C.M., Oh, J.W., 2007. Biochemical characterization of a recombinant Japanese encephalitis virus RNA-dependent RNA polymerase. BMC Mol Biol 8, 59.

Knipe, D., Howley, P., Griffin, D., Martin, M., Lamb, R., Roizman, B., and Straus, S., 2007. Fields Virology, 5 ed. Lippincott Williams & Wilkins.

Kolb, E., Laine, E., Strehler, D., Staeheli, P., 1992. Resistance to influenza virus infection of Mx transgenic mice expressing Mx protein under the control of two constitutive promoters. J Virol 66, 1709-1716.

Koonin, E.V., 1991. The phylogeny of RNA-dependent RNA polymerases of positive-strand RNA viruses. J Gen Virol 72 (Pt 9), 2197-2206.

Koonin, E.V., 1993. Computer-assisted identification of a putative methyltransferase domain in NS5 protein of flaviviruses and lambda 2 protein of reovirus. J Gen Virol 74 (Pt 4), 733-740.

Kowanetz, K., Crosetto, N., Haglund, K., Schmidt, M.H., Heldin, C.H., Dikic, I., 2004. Suppressors of T-cell receptor signaling Sts-1 and Sts-2 bind to Cbl and inhibit endocytosis of receptor tyrosine kinases. J Biol Chem 279, 32786-32795.

Kuhn, R.J., Zhang, W., Rossmann, M.G., Pletnev, S.V., Corver, J., Lenches, E., Jones, C.T., Mukhopadhyay, S., Chipman, P.R., Strauss, E.G., Baker, T.S., Strauss, J.H., 2002. Structure of dengue virus: implications for flavivirus organization, maturation, and fusion. Cell 108, 717-725.

Kummerer, B.M., Rice, C.M., 2002. Mutations in the yellow fever virus nonstructural protein NS2A selectively block production of infectious particles. J Virol 76, 4773-4784.

Lanciotti, R.S., Ebel, G.D., Deubel, V., Kerst, A.J., Murri, S., Meyer, R., Bowen, M., McKinney, N., Morrill, W.E., Crabtree, M.B., Kramer, L.D., Roehrig, J.T., 2002. Complete genome sequences and phylogenetic analysis of West Nile virus strains isolated from the United States, Europe, and the Middle East. Virology 298, 96-105.

Lee, S.H., Dimock, K., Gray, D.A., Beauchemin, N., Holmes, K.V., Belouchi, M., Realson, J., Vidal, S.M., 2003. Maneuvering for advantage: the genetics of mouse susceptibility to virus infection. Trends Genet 19, 447-457.

Lee, S.H., Girard, S., Macina, D., Busa, M., Zafer, A., Belouchi, A., Gros, P., Vidal, S.M., 2001. Susceptibility to mouse cytomegalovirus is associated with deletion of an activating natural killer cell receptor of the C-type lectin superfamily. Nat Genet 28, 42-45.

Legros, S., Boxus, M., Gatot, J.S., Van Lint, C., Kruys, V., Kettmann, R., Twizere, J.C., Dequiedt, F., 2011. The HTLV-1 Tax protein inhibits formation of stress granules by interacting with histone deacetylase 6. Oncogene.

Lehto, M., Laitinen, S., Chinetti, G., Johansson, M., Ehnholm, C., Staels, B., Ikonen, E., Olkkonen, V.M., 2001. The OSBP-related protein family in humans. J Lipid Res 42, 1203-1213.

Lehto, M., Olkkonen, V.M., 2003. The OSBP-related proteins: a novel protein family involved in vesicle transport, cellular lipid metabolism, and cell signalling. Biochim Biophys Acta 1631, 1-11.

Li, H.W., Ding, S.W., 2005. Antiviral silencing in animals. FEBS Lett 579, 5965-5973.

Li, W., Li, Y., Kedersha, N., Anderson, P., Emara, M., Swiderek, K.M., Moreno, G.T., Brinton, M.A., 2002. Cell proteins TIA-1 and TIAR interact with the 3' stem-loop of the West Nile virus complementary minus-strand RNA and facilitate virus replication. J Virol 76, 11989-12000.

Liang, S.H., Zhang, W., McGrath, B.C., Zhang, P., Cavener, D.R., 2006. PERK (eIF2alpha kinase) is required to activate the stress-activated MAPKs and induce the expression of immediate-early genes upon disruption of ER calcium homoeostasis. Biochem J 393, 201-209.

Lindenbach, B.D., Rice, C.M., 1997. trans-Complementation of yellow fever virus NS1 reveals a role in early RNA replication. J Virol 71, 9608-9617.

Lindenbach, B.D., Rice, C.M., 1999. Genetic interaction of flavivirus nonstructural proteins NS1 and NS4A as a determinant of replicase function. J Virol 73, 4611-4621.

Lindenbach, B.D., Thiel, H.J., Rice, C.M., 2007. *Flaviviridae*: The Viruses and Their Replication, Fields Virology, 5 ed. Lippincott Williams & Wilkins, pp. 1101-1152.

Lindquist, M.E., Lifland, A.W., Utley, T.J., Santangelo, P.J., Crowe, J.E., Jr., 2011a. Respiratory syncytial virus induces host RNA stress granules to facilitate viral replication. J Virol 84, 12274-12284.

Lindquist, M.E., Mainou, B.A., Dermody, T.S., Crowe, J.E., Jr., 2011b. Activation of protein kinase R is required for induction of stress granules by respiratory syncytial virus but dispensable for viral replication. Virology 413, 103-110.

Linton, K.J., Higgins, C.F., 2007. Structure and function of ABC transporters: the ATP switch provides flexible control. Pflugers Arch 453, 555-567.

Liu, R., Paxton, W.A., Choe, S., Ceradini, D., Martin, S.R., Horuk, R., MacDonald, M.E., Stuhlmann, H., Koup, R.A., Landau, N.R., 1996. Homozygous defect in HIV-1 coreceptor accounts for resistance of some multiply-exposed individuals to HIV-1 infection. Cell 86, 367-377.

Lobigs, M., Arthur, C.E., Mullbacher, A., Blanden, R.V., 1994. The flavivirus nonstructural protein NS3 is a dominant source of cytotoxic T cell peptide determinants. Virology 202, 195-201.

Locher, K.P., 2009. Review. Structure and mechanism of ATP-binding cassette transporters. Philos Trans R Soc Lond B Biol Sci 364, 239-245.

Lu, Y.E., Cassese, T., Kielian, M., 1999. The cholesterol requirement for sindbis virus entry and exit and characterization of a spike protein region involved in cholesterol dependence. J Virol 73, 4272-4278.

Macdonald, J., Tonry, J., Hall, R.A., Williams, B., Palacios, G., Ashok, M.S., Jabado, O., Clark, D., Tesh, R.B., Briese, T., Lipkin, W.I., 2005. NS1 protein secretion during the acute phase of West Nile virus infection. J Virol 79, 13924-13933.

Mackenzie, J.M., Jones, M.K., Young, P.R., 1996. Immunolocalization of the dengue virus nonstructural glycoprotein NS1 suggests a role in viral RNA replication. Virology 220, 232-240.

Mackenzie, J.M., Khromykh, A.A., Jones, M.K., Westaway, E.G., 1998. Subcellular localization and some biochemical properties of the flavivirus Kunjin nonstructural proteins NS2A and NS4A. Virology 245, 203-215.

Malet, H., Egloff, M.P., Selisko, B., Butcher, R.E., Wright, P.J., Roberts, M., Gruez, A., Sulzenbacher, G., Vonrhein, C., Bricogne, G., Mackenzie, J.M., Khromykh, A.A.,

Davidson, A.D., Canard, B., 2007. Crystal structure of the RNA polymerase domain of the West Nile virus non-structural protein 5. J Biol Chem 282, 10678-10689.

Martinand, C., Montavon, C., Salehzada, T., Silhol, M., Lebleu, B., Bisbal, C., 1999. RNase L inhibitor is induced during human immunodeficiency virus type 1 infection and down regulates the 2-5A/RNase L pathway in human T cells. J Virol 73, 290-296.

Mashimo, T., Lucas, M., Simon-Chazottes, D., Frenkiel, M.P., Montagutelli, X., Ceccaldi, P.E., Deubel, V., Guenet, J.L., Despres, P., 2002. A nonsense mutation in the gene encoding 2'-5'-oligoadenylate synthetase/L1 isoform is associated with West Nile virus susceptibility in laboratory mice. Proc Natl Acad Sci U S A 99, 11311-11316.

Matusan, A.E., Pryor, M.J., Davidson, A.D., Wright, P.J., 2001. Mutagenesis of the Dengue virus type 2 NS3 protein within and outside helicase motifs: effects on enzyme activity and virus replication. J Virol 75, 9633-9643.

Mazroui, R., Di Marco, S., Kaufman, R.J., Gallouzi, I.E., 2007. Inhibition of the ubiquitin-proteasome system induces stress granule formation. Mol Biol Cell 18, 2603-2618.

Mazroui, R., Sukarieh, R., Bordeleau, M.E., Kaufman, R.J., Northcote, P., Tanaka, J., Gallouzi, I., Pelletier, J., 2006. Inhibition of ribosome recruitment induces stress granule formation independently of eukaryotic initiation factor 2alpha phosphorylation. Mol Biol Cell 17, 4212-4219.

McInerney, G.M., Kedersha, N.L., Kaufman, R.J., Anderson, P., Liljestrom, P., 2005. Importance of eIF2alpha phosphorylation and stress granule assembly in alphavirus translation regulation. Mol Biol Cell 16, 3753-3763.

Medigeshi, G.R., Hirsch, A.J., Streblow, D.N., Nikolich-Zugich, J., Nelson, J.A., 2008. West Nile virus entry requires cholesterol-rich membrane microdomains and is independent of alphavbeta3 integrin. J Virol 82, 5212-5219.

Melian, E.B., Hinzman, E., Nagasaki, T., Firth, A.E., Wills, N.M., Nouwens, A.S., Blitvich, B.J., Leung, J., Funk, A., Atkins, J.F., Hall, R., Khromykh, A.A., 2010. NS1' of flaviviruses in the Japanese encephalitis virus serogroup is a product of ribosomal frameshifting and plays a role in viral neuroinvasiveness. J Virol 84, 1641-1647.

Mertens, E., Kajaste-Rudnitski, A., Torres, S., Funk, A., Frenkiel, M.P., Iteman, I., Khromykh, A.A., Despres, P., 2010. Viral determinants in the NS3 helicase and 2K peptide that promote West Nile virus resistance to antiviral action of 2',5'-oligoadenylate synthetase 1b. Virology 399, 176-185.

Miller, S., Kastner, S., Krijnse-Locker, J., Buhler, S., Bartenschlager, R., 2007. The non-structural protein 4A of dengue virus is an integral membrane protein inducing membrane alterations in a 2K-regulated manner. J Biol Chem 282, 8873-8882.

Miller, S., Sparacio, S., Bartenschlager, R., 2006. Subcellular localization and membrane topology of the Dengue virus type 2 Non-structural protein 4B. J Biol Chem 281, 8854-8863.

Montero, H., Rojas, M., Arias, C.F., Lopez, S., 2008. Rotavirus infection induces the phosphorylation of eIF2alpha but prevents the formation of stress granules. J Virol 82, 1496-1504.

Munoz-Jordan, J.L., Laurent-Rolle, M., Ashour, J., Martinez-Sobrido, L., Ashok, M., Lipkin, W.I., Garcia-Sastre, A., 2005. Inhibition of alpha/beta interferon signaling by the NS4B protein of flaviviruses. J Virol 79, 8004-8013.

Munoz-Jordan, J.L., Sanchez-Burgos, G.G., Laurent-Rolle, M., Garcia-Sastre, A., 2003. Inhibition of interferon signaling by dengue virus. Proc Natl Acad Sci U S A 100, 14333-14338.

Muylaert, I.R., Chambers, T.J., Galler, R., Rice, C.M., 1996. Mutagenesis of the N-linked glycosylation sites of the yellow fever virus NS1 protein: effects on virus replication and mouse neurovirulence. Virology 222, 159-168.

Nestorowicz, A., Chambers, T.J., Rice, C.M., 1994. Mutagenesis of the yellow fever virus NS2A/2B cleavage site: effects on proteolytic processing, viral replication, and evidence for alternative processing of the NS2A protein. Virology 199, 114-123.

Ohtsuka, N., Yamada, Y.K., Taguchi, F., 1996. Difference in virus-binding activity of two distinct receptor proteins for mouse hepatitis virus. J Gen Virol 77 (Pt 8), 1683-1692.

Olkkonen, V.M., Hynynen, R., 2009. Interactions of oxysterols with membranes and proteins. Mol Aspects Med 30, 123-133.

Olkkonen, V.M., Johansson, M., Suchanek, M., Yan, D., Hynynen, R., Ehnholm, C., Jauhiainen, M., Thiele, C., Lehto, M., 2006. The OSBP-related proteins (ORPs): global sterol sensors for co-ordination of cellular lipid metabolism, membrane trafficking and signalling processes? Biochem Soc Trans 34, 389-391.

Overby, A.K., Popov, V.L., Niedrig, M., Weber, F., 2010. Tick-borne encephalitis virus delays interferon induction and hides its double-stranded RNA in intracellular membrane vesicles. J Virol 84, 8470-8483.

Paytubi, S., Morrice, N.A., Boudeau, J., Proud, C.G., 2008. The N-terminal region of ABC50 interacts with eukaryotic initiation factor eIF2 and is a target for regulatory phosphorylation by CK2. Biochem J 409, 223-231.

Perelygin, A.A., Scherbik, S.V., Zhulin, I.B., Stockman, B.M., Li, Y., Brinton, M.A., 2002. Positional cloning of the murine flavivirus resistance gene. Proceedings of the National Academy of Sciences of the United States of America 99, 9322-9327.

Pestova, T.V., Kolupaeva, V.G., Lomakin, I.B., Pilipenko, E.V., Shatsky, I.N., Agol, V.I., Hellen, C.U., 2001. Molecular mechanisms of translation initiation in eukaryotes. Proc Natl Acad Sci U S A 98, 7029-7036.

Piotrowska, J., Hansen, S.J., Park, N., Jamka, K., Sarnow, P., Gustin, K.E., 2010. Stable formation of compositionally unique stress granules in virus-infected cells. J Virol 84, 3654-3665.

Plevka, P., Battisti, A.J., Junjhon, J., Winkler, D.C., Holdaway, H.A., Keelapang, P., Sittisombut, N., Kuhn, R.J., Steven, A.C., Rossmann, M.G., 2011. Maturation of flaviviruses starts from one or more icosahedrally independent nucleation centres. EMBO Rep 12, 602-606.

Prilipov, A.G., Kinney, R.M., Samokhvalov, E.I., Savage, H.M., Al'khovskii, S.V., Tsuchiya, K.R., Gromashevskii, V.L., Sadykova, G.K., Shatalov, A.G., Vyshemirskii, O.I., Usachev, E.V., Mokhonov, V.V., Voronina, A.G., Butenko, A.M., Larichev, V.F., Zhukov, A.N., Kovtunov, A.I., Gubler, D.J., L'Vov D, K., 2002. [Analysis of new variants of West Nile fever virus]. Vopr Virusol 47, 36-41.

Pryor, M.J., Rawlinson, S.M., Butcher, R.E., Barton, C.L., Waterhouse, T.A., Vasudevan, S.G., Bardin, P.G., Wright, P.J., Jans, D.A., Davidson, A.D., 2007. Nuclear localization of dengue virus nonstructural protein 5 through its importin alpha/beta-recognized nuclear localization sequences is integral to viral infection. Traffic 8, 795-807.

Querec, T.D., Akondy, R.S., Lee, E.K., Cao, W., Nakaya, H.I., Teuwen, D., Pirani, A., Gernert, K., Deng, J., Marzolf, B., Kennedy, K., Wu, H., Bennouna, S., Oluoch, H., Miller, J., Vencio, R.Z., Mulligan, M., Aderem, A., Ahmed, R., Pulendran, B., 2009. Systems biology approach predicts immunogenicity of the yellow fever vaccine in humans. Nat Immunol 10, 116-125.

Ramanathan, M.P., Chambers, J.A., Pankhong, P., Chattergoon, M., Attatippaholkun, W., Dang, K., Shah, N., Weiner, D.B., 2006. Host cell killing by the West Nile Virus NS2B-NS3 proteolytic complex: NS3 alone is sufficient to recruit caspase-8-based apoptotic pathway. Virology 345, 56-72.

Rao, P.V., Kumari, S., Gallagher, T.M., 1997. Identification of a contiguous 6-residue determinant in the MHV receptor that controls the level of virion binding to cells. Virology 229, 336-348.

Rice, C.M., Lenches, E.M., Eddy, S.R., Shin, S.J., Sheets, R.L., Strauss, J.H., 1985. Nucleotide sequence of yellow fever virus: implications for flavivirus gene expression and evolution. Science 229, 726-733.

Robert, F., Kapp, L.D., Khan, S.N., Acker, M.G., Kolitz, S., Kazemi, S., Kaufman, R.J., Merrick, W.C., Koromilas, A.E., Lorsch, J.R., Pelletier, J., 2006. Initiation of protein synthesis by hepatitis C virus is refractory to reduced eIF2.GTP.Met-tRNA(i)(Met) ternary complex availability. Mol Biol Cell 17, 4632-4644.

Rocha, N., Kuijl, C., van der Kant, R., Janssen, L., Houben, D., Janssen, H., Zwart, W., Neefjes, J., 2009. Cholesterol sensor ORP1L contacts the ER protein VAP to control Rab7-RILP-p150 Glued and late endosome positioning. J Cell Biol 185, 1209-1225.

Rojas, M., Arias, C.F., Lopez, S., 2010. Protein kinase R is responsible for the phosphorylation of eIF2alpha in rotavirus infection. J Virol 84, 10457-10466.

Roosendaal, J., Westaway, E.G., Khromykh, A., Mackenzie, J.M., 2006. Regulated cleavages at the West Nile virus NS4A-2K-NS4B junctions play a major role in rearranging cytoplasmic membranes and Golgi trafficking of the NS4A protein. J Virol 80, 4623-4632.

Sabin, A.B., 1952. Genetic, hormonal and age factors in natural resistance to certain viruses. Ann N Y Acad Sci 54, 936-944.

Samson, M., Libert, F., Doranz, B.J., Rucker, J., Liesnard, C., Farber, C.M., Saragosti, S., Lapoumeroulie, C., Cognaux, J., Forceille, C., Muyldermans, G., Verhofstede, C., Burtonboy, G., Georges, M., Imai, T., Rana, S., Yi, Y., Smyth, R.J., Collman, R.G., Doms, R.W., Vassart, G., Parmentier, M., 1996. Resistance to HIV-1 infection in caucasian individuals bearing mutant alleles of the CCR-5 chemokine receptor gene. Nature 382, 722-725.

Sanchez-Vargas, I., Scott, J.C., Poole-Smith, B.K., Franz, A.W., Barbosa-Solomieu, V., Wilusz, J., Olson, K.E., Blair, C.D., 2009. Dengue virus type 2 infections of Aedes aegypti are modulated by the mosquito's RNA interference pathway. PLoS Pathog 5, e1000299.

Sangster, M.Y., Heliams, D.B., MacKenzie, J.S., Shellam, G.R., 1993. Genetic studies of flavivirus resistance in inbred strains derived from wild mice: evidence for a new resistance allele at the flavivirus resistance locus (Flv). J Virol 67, 340-347.

Sangster, M.Y., Shellam, G.R., 1986. Genetically controlled resistance to flaviviruses within the house mouse complex of species. Curr Top Microbiol Immunol 127, 313-318.

Sarkar, S.N., Sen, G.C., 2004. Novel functions of proteins encoded by viral stress-inducible genes. Pharmacology & therapeutics 103, 245-259.

Scalzo, A.A., Fitzgerald, N.A., Simmons, A., La Vista, A.B., Shellam, G.R., 1990. Cmv-1, a genetic locus that controls murine cytomegalovirus replication in the spleen. J Exp Med 171, 1469-1483.

Scherbik, S.V., Kluetzman, K., Perelygin, A.A., Brinton, M.A., 2007a. Knock-in of the Oas1b(r) allele into a flavivirus-induced disease susceptible mouse generates the resistant phenotype. Virology 368, 232-237.

Scherbik, S.V., Paranjape, J.M., Stockman, B.M., Silverman, R.H., Brinton, M.A., 2006. RNase L plays a role in the antiviral response to West Nile virus. J Virol 80, 2987-2999.

Scherbik, S.V., Stockman, B.M., Brinton, M.A., 2007b. Differential expression of interferon (IFN) regulatory factors and IFN-stimulated genes at early times after West Nile virus infection of mouse embryo fibroblasts. J Virol 81, 12005-12018.

Schriml, L.M., Dean, M., 2000. Identification of 18 mouse ABC genes and characterization of the ABC superfamily in Mus musculus. Genomics 64, 24-31.

Schweizer, M., Peterhans, E., 1999. Oxidative stress in cells infected with bovine viral diarrhoea virus: a crucial step in the induction of apoptosis. J Gen Virol 80 (Pt 5), 1147-1155.

Sejvar, J.J., 2007. The long-term outcomes of human West Nile virus infection. Clin Infect Dis 44, 1617-1624.

Sheth, U., Parker, R., 2003. Decapping and decay of messenger RNA occur in cytoplasmic processing bodies. Science 300, 805-808.

Silverman, R.H., 2007. Viral encounters with 2',5'-oligoadenylate synthetase and RNase L during the interferon antiviral response. J Virol 81, 12720-12729.

Simpson-Holley, M., Kedersha, N., Dower, K., Rubins, K.H., Anderson, P., Hensley, L.E., Connor, J.H., 2011. Formation of antiviral cytoplasmic granules during orthopoxvirus infection. J Virol 85, 1581-1593.

Smirnova, E.V., Collingwood, T.S., Bisbal, C., Tsygankova, O.M., Bogush, M., Meinkoth, J.L., Henderson, E.E., Annan, R.S., Tsygankov, A.Y., 2008. TULA proteins bind to ABCE-1, a host factor of HIV-1 assembly, and inhibit HIV-1 biogenesis in a UBA-dependent fashion. Virology 372, 10-23.

Smith, G.W., Wright, P.J., 1985. Synthesis of proteins and glycoproteins in dengue type 2 virus-infected vero and Aedes albopictus cells. J Gen Virol 66 (Pt 3), 559-571.

Smith, J.A., Schmechel, S.C., Raghavan, A., Abelson, M., Reilly, C., Katze, M.G., Kaufman, R.J., Bohjanen, P.R., Schiff, L.A., 2006. Reovirus induces and benefits from an integrated cellular stress response. J Virol 80, 2019-2033.

Somnuke, P., Hauhart, R.E., Atkinson, J.P., Diamond, M.S., Avirutnan, P., 2011. N-linked glycosylation of dengue virus NS1 protein modulates secretion, cell-surface expression, hexamer stability, and interactions with human complement. Virology 413, 253-264.

Staeheli, P., Grob, R., Meier, E., Sutcliffe, J.G., Haller, O., 1988. Influenza virus-susceptible mice carry Mx genes with a large deletion or a nonsense mutation. Mol Cell Biol 8, 4518-4523.

Stranden, A.M., Staeheli, P., Pavlovic, J., 1993. Function of the mouse Mx1 protein is inhibited by overexpression of the PB2 protein of influenza virus. Virology 197, 642-651.

Sturm, A., Cunningham, P., Dean, M., 2009. The ABC transporter gene family of Daphnia pulex. BMC Genomics 10, 170.

Su, Q., Wang, S., Baltzis, D., Qu, L.K., Wong, A.H., Koromilas, A.E., 2006. Tyrosine phosphorylation acts as a molecular switch to full-scale activation of the eIF2alpha RNA-dependent protein kinase. Proc Natl Acad Sci U S A 103, 63-68.

Superti, F., Seganti, L., Ruggeri, F.M., Tinari, A., Donelli, G., Orsi, N., 1987. Entry pathway of vesicular stomatitis virus into different host cells. J Gen Virol 68 (Pt 2), 387-399.

Suzuki, T., Kitao, S., Matsushime, H., Yoshida, M., 1996. HTLV-1 Tax protein interacts with cyclin-dependent kinase inhibitor p16INK4A and counteracts its inhibitory activity towards CDK4. EMBO J 15, 1607-1614.

Takahashi, H., Ohtaki, N., Maeda-Sato, M., Tanaka, M., Tanaka, K., Sawa, H., Ishikawa, T., Takamizawa, A., Takasaki, T., Hasegawa, H., Sata, T., Hall, W.W., Kurata, T., Kojima, A., 2009. Effects of the number of amino acid residues in the signal segment upstream or downstream of the NS2B-3 cleavage site on production and secretion of prM/M-E virus-like particles of West Nile virus. Microbes Infect 11, 1019-1028.

Tan, K., Zelus, B.D., Meijers, R., Liu, J.H., Bergelson, J.M., Duke, N., Zhang, R., Joachimiak, A., Holmes, K.V., Wang, J.H., 2002. Crystal structure of murine sCEACAM1a[1,4]: a coronavirus receptor in the CEA family. EMBO J 21, 2076-2086.

Tardif, K.D., Waris, G., Siddiqui, A., 2005. Hepatitis C virus, ER stress, and oxidative stress. Trends Microbiol 13, 159-163.

Teixeira, D., Sheth, U., Valencia-Sanchez, M.A., Brengues, M., Parker, R., 2005. Processing bodies require RNA for assembly and contain nontranslating mRNAs. RNA 11, 371-382.

Tyzack, J.K., Wang, X., Belsham, G.J., Proud, C.G., 2000. ABC50 interacts with eukaryotic initiation factor 2 and associates with the ribosome in an ATP-dependent manner. J Biol Chem 275, 34131-34139.

Urosevic, N., Silvia, O.J., Sangster, M.Y., Mansfield, J.P., Hodgetts, S.I., Shellam, G.R., 1999. Development and characterization of new flavivirus-resistant mouse strains bearing Flv(r)-like and Flv(mr) alleles from wild or wild-derived mice. J Gen Virol 80 (Pt 4), 897-906.

Vaheri, A., Sedwick, W.D., Plotkin, S.A., Maes, R., 1965. Cytopathic effect of rubella virus in RHK21 cells and growth to high titers in suspension culture. Virology 27, 239-241.

van Hemert, M.J., van den Worm, S.H., Knoops, K., Mommaas, A.M., Gorbalenya, A.E., Snijder, E.J., 2008. SARS-coronavirus replication/transcription complexes are membrane-protected and need a host factor for activity in vitro. PLoS Pathog 4, e1000054.

Vattem, K.M., Wek, R.C., 2004. Reinitiation involving upstream ORFs regulates ATF4 mRNA translation in mammalian cells. Proc Natl Acad Sci U S A 101, 11269-11274.

Venticinque, L., Meruelo, D., 2010. Sindbis viral vector induced apoptosis requires translational inhibition and signaling through Mcl-1 and Bak. Mol Cancer 9, 37.

Vihervaara, T., Uronen, R.L., Wohlfahrt, G., Bjorkhem, I., Ikonen, E., Olkkonen, V.M., 2011. Sterol binding by OSBP-related protein 1L regulates late endosome motility and function. Cell Mol Life Sci 68, 537-551.

Wattenhofer, M., Shibuya, K., Kudoh, J., Lyle, R., Michaud, J., Rossier, C., Kawasaki, K., Asakawa, S., Minoshima, S., Berry, A., Bonne-Tamir, B., Shimizu, N., Antonarakis, S.E., Scott, H.S., 2001. Isolation and characterization of the UBASH3A gene on 21q22.3 encoding a potential nuclear protein with a novel combination of domains. Hum Genet 108, 140-147.

Webster, L.T., Clow, A.D., 1936. Experimental Encephalitis (St. Louis Type) in Mice with High Inborn Resistance : A Chronic Subclinical Infection. J Exp Med 63, 827-845.

Webster, L.T., Johnson, M.S., 1941. Comparative Virulence of St. Louis Encephalitis Virus Cultured with Brain Tissue from Innately Susceptible and Innately Resistant Mice. J Exp Med 74, 489-494.

Welsch, S., Miller, S., Romero-Brey, I., Merz, A., Bleck, C.K., Walther, P., Fuller, S.D., Antony, C., Krijnse-Locker, J., Bartenschlager, R., 2009. Composition and three-dimensional architecture of the dengue virus replication and assembly sites. Cell Host Microbe 5, 365-375.

Wengler, G., 1991. The carboxy-terminal part of the NS 3 protein of the West Nile flavivirus can be isolated as a soluble protein after proteolytic cleavage and represents an RNA-stimulated NTPase. Virology 184, 707-715.

Wengler, G., 1993. The NS 3 nonstructural protein of flaviviruses contains an RNA triphosphatase activity. Virology 197, 265-273.

White, J.P., Cardenas, A.M., Marissen, W.E., Lloyd, R.E., 2007. Inhibition of cytoplasmic mRNA stress granule formation by a viral proteinase. Cell Host Microbe 2, 295-305.

Wilson, J.R., de Sessions, P.F., Leon, M.A., Scholle, F., 2008. West Nile virus nonstructural protein 1 inhibits TLR3 signal transduction. J Virol 82, 8262-8271.

Xu, Y., Liu, Y., Ridgway, N.D., McMaster, C.R., 2001. Novel members of the human oxysterol-binding protein family bind phospholipids and regulate vesicle transport. J Biol Chem 276, 18407-18414.

Yamshchikov, G., Borisevich, V., Seregin, A., Chaporgina, E., Mishina, M., Mishin, V., Kwok, C.W., Yamshchikov, V., 2004. An attenuated West Nile prototype virus is highly

immunogenic and protects against the deadly NY99 strain: a candidate for live WN vaccine development. Virology 330, 304-312.

Yamshchikov, V.F., Wengler, G., Perelygin, A.A., Brinton, M.A., Compans, R.W., 2001. An infectious clone of the West Nile flavivirus. Virology 281, 294-304.

Yan, D., Jauhiainen, M., Hildebrand, R.B., Willems van Dijk, K., Van Berkel, T.J., Ehnholm, C., Van Eck, M., Olkkonen, V.M., 2007a. Expression of human OSBP-related protein 1L in macrophages enhances atherosclerotic lesion development in LDL receptor-deficient mice. Arterioscler Thromb Vasc Biol 27, 1618-1624.

Yan, D., Lehto, M., Rasilainen, L., Metso, J., Ehnholm, C., Yla-Herttuala, S., Jauhiainen, M., Olkkonen, V.M., 2007b. Oxysterol binding protein induces upregulation of SREBP-1c and enhances hepatic lipogenesis. Arterioscler Thromb Vasc Biol 27, 1108-1114.

Yang, Y.L., Reis, L.F., Pavlovic, J., Aguzzi, A., Schafer, R., Kumar, A., Williams, B.R., Aguet, M., Weissmann, C., 1995. Deficient signaling in mice devoid of double-stranded RNA-dependent protein kinase. EMBO J 14, 6095-6106.

Zaitseva, E., Yang, S.T., Melikov, K., Pourmal, S., Chernomordik, L.V., 2010. Dengue virus ensures its fusion in late endosomes using compartment-specific lipids. PLoS Pathog 6, e1001131.

Zhang, B., Dong, H., Stein, D.A., Iversen, P.L., Shi, P.Y., 2008. West Nile virus genome cyclization and RNA replication require two pairs of long-distance RNA interactions. Virology 373, 1-13.

Zimmerman, P.A., Buckler-White, A., Alkhatib, G., Spalding, T., Kubofcik, J., Combadiere, C., Weissman, D., Cohen, O., Rubbert, A., Lam, G., Vaccarezza, M., Kennedy, P.E., Kumaraswami, V., Giorgi, J.V., Detels, R., Hunter, J., Chopek, M., Berger, E.A., Fauci, A.S., Nutman, T.B., Murphy, P.M., 1997. Inherited resistance to HIV-1 conferred by an inactivating mutation in CC chemokine receptor 5: studies in populations with contrasting clinical phenotypes, defined racial background, and quantified risk. Mol Med 3, 23-36.

Zou, G., Puig-Basagoiti, F., Zhang, B., Qing, M., Chen, L., Pankiewicz, K.W., Felczak, K., Yuan, Z., Shi, P.Y., 2009. A single-amino acid substitution in West Nile virus 2K peptide between NS4A and NS4B confers resistance to lycorine, a flavivirus inhibitor. Virology 384, 242-252.